Hydrocarbon conversion of long-chain paraffins
Role of metal (Pt, Ru, Ni) & influence of acid sites, structures and textural properties of solid catalysts

Master's Thesis

Taimoor Ahmad Kaka Khel

Supervisors:

Professor Dmitry Yu. Murzin, Associate Professor
Päivi Mäki-Arvela & Docent Narendra Kumar

Johan Gadolin
Process Chemistry Centre

Laboratory of Industrial Chemistry and Reaction Engineering

Faculty of Science and Engineering

Åbo Akademi University

Finland, 2019

Abstract

Taimoor Ahmad Kaka Khel

Hydrocarbon conversion of long-chain paraffins, role of metal (Pt, Ru, Ni) & influence of acid sites, structures and textural properties of solid catalysts.

The work was carried out under the supervision of Professor Dmitry Murzin, Associate Professor Päivi Mäki-Arvela and Docent Narendra Kumar in the Laboratory of Industrial Chemistry and Reaction Engineering at Åbo Akademi University, Finland.

Keywords Hexadecane, methyl-pentadecane, hydroisomerization, hydrocracking, Beta zeolite, Y-zeolite, Brønsted acid sites, Lewis acid sites, platinum-beta bifunctional catalysts, ruthenium beta bifunctional catalysts, nickel beta bifunctional catalysts, ruthenium Y-zeolite bifunctional catalysts.

Hydroisomerization of long-chain hydrocarbons for the production of high-quality branched fuel was studied due to their vast availability and product versatility. Most of these long paraffins are cracked to obtain lower molecular weights fuel fraction. However, substantial efforts are made globally to transform these long-chain hydrocarbons to branched hydrocarbons and improve their fuel properties. The main objectives in this work were to explore suitable catalysts for hydroisomerization of hexadecane, a model compound for long-chain hydrocarbons. Transformation of hexadecane was carried over bifunctional platinum, ruthenium and nickel catalysts also comprising beta catalysts. As a comparison with ruthenium beta zeolites, ruthenium-Y-zeolite was also studied. The experiments were performed at 210 °C and 40 bar of overall pressure. The gas phase analysis of the products in the hydroisomerization of hexadecane indicated the presence of low molecular weight hydrocarbons, mainly methane. Each catalyst formed methyl-pentadecane and cracking products, which included lower molecular weight and long-chain

hydrocarbons, and alkylated hexadecane. The fresh and spent catalysts were characterized using several physico-chemical methods. Fresh catalysts were characterized for specific area and pore size, Brønsted and Lewis acid sites, surface morphology and active metal cluster size. All catalysts exhibited deactivation by severe coking except platinum beta zeolites. The catalyst coking was confirmed by thermogravimetric analysis, organic elemental analysis and size exclusion chromatography. Among all catalysts, nickel beta zeolites formed the most gas-phase hydrocarbons with abundant cracked hydrocarbons. Ruthenium beta zeolites allowed higher isomerization selectivity compared to the parent zeolite possessing, however, low conversion. The ruthenium Y-zeolite produced the lowest amount of gas-phase hydrocarbons and exhibited relatively higher isomerization selectivity, even if large amounts of cracking products were also formed. All catalysts exhibited higher than 80 % mass balance except TR-10 (H-Beta-300). The best results were shown by the platinum beta zeolite (2 wt.% Pt/H-Beta-25), which formed lower amounts of the gas-phase and cracked hydrocarbons and a high yield of methyl-pentadecane. Temperature and pressure dependence were elucidated in kinetic experiments with a bifunctional ruthenium beta zeolite, which indicated an increase in the yield of methylpentadecane and improved selectivity towards hydroisomerization.

Referat

Taimoor Ahmad Kaka Khel

Omvandling av lång kedjade kolväten, rollen av metall (Pt, Ru, Ni), inverkan av sura säten, strukturer och ytegenskaper av fasta katalysatorer.

Detta arbete har gjorts under ledning av professor Dmitry Murzin, biträdande professor Päivi Mäki-Arvela, professor Dmitry Murzin, och docent Narendra Kumar vid Laboratoriet för Teknisk Kemi och Reaktionsteknik vid Åbo Akademi, Finland.

Nyckelord

Hexadekan, metylpentadekan, väteisomericering, vätekrackning, Beta zeolit, Y-zeolit, Brønsted sura säten, Lewis sura säten, platinum, ruthenium beta, nickel, beta zeolit, Y zeolite, bifunktionella katalysatorer.

Väteisomericering av långkedjade kolväten för framställning av högkvalitets förgrenade kolväten, bränsle undersöktes därför att dessa kolväten är lätt tillgängliga och olika produkter kan syntetiseras av dem. Största delen av dessa lång-kedjade paraffiner skall spjälkas för att producera bränslekomponenter med lägre molekylmassa. Mycket forskning har redan gjorts i världen att omvandla dessa lång-kedjade kolväten till förgrenade kolväten med avsikt att förbättra deras bränsleegenskaper. Huvudmålsättning i detta arbete var att utreda lämpliga katalysatorer för väteisomericering av hexadekan, en modellkomponent av långkedjade kolväten. Omvandling av hexadekan undersöktes på beta zeoliter samt på bifunktionella platina, rutenium och nickel katalysatorer. Som jämförelse testades också rutenium på beta och Y zeoliter. Experimenten utfördes vid 210 °C under 40 bar totalt tryck.

Resultaten av gasfasanalyser från väteisomericering visade att den lågmolekylära kolväteprodukten är huvudsakligen metan. De olika katalysatorerna producerade metylpentadekan och krackade samt alkylerade produkter. Färska och använda katalysatorer karakteriserades med hjälp av flera olika fysikalisk-kemiska metoder.

För färska katalysatorer mättes den specifika ytarean, och porstorleken, Brønsted och Lewis sura säten, ytmorfologi samt den aktiva metallens storlek. Alla katalysatorer deaktiverades, förutom platina beta zeoliterna. Koksbildning bekräftades med hjälp av termogravimetrisk analys, elementäranalys samt med strorleksexklusionskromatografi av extraherad koks. Nickel beta zeoliterna bildade största andelen gasfas kolväten och stora mängder krackade kolväten bland alla katalysatorerna. Rutenium beta zeoliterna gynnade bildning av isomericeringsprodukter med en högre selektivitet och lägre omsättningsgrad jämfört med zeoliter. Rutenium Y-zeolit producerade den lägsta mängden gasfas kolväten och hade en relativt hög isomericeringsselektivitet, trots att stora mängder krackade produkter bildades. Alla katalysatorer visade högre än 80 % mass balans, förutom H-Beta-300.

De bästa resultaten fick man med platina beta zeolit (2 vikt-% Pt/H-Beta-25), vilken producerade mindre mängder gasfas och krackade kolväten samt ett högt utbyte av metylpentadekan. Temperatur och tryckberoende studerades i kinetiska experimenten med en bifunktionell rutenium beta zeolit, och resultaten visade att ett högt utbyte av metylpentadekan och en förbättrad selektivitet kunde uppnås under optimala betingelser i väteisomericering.

Acknowledgements

I would like to express my gratitude to Prof. Dmitry Yu. Murzin for providing an opportunity to work in the Laboratory of Industrial Chemistry and Reaction Engineering and to expand my abilities and knowledge.

I would like to acknowledge Docent Päivi Mäki-Arvela and Docent Narendra Kumar for their guidance and thank them for their scientific guidance and knowledge shared during the thesis work. Their valuable comments on the thesis are warmly appreciated. Dr. Kari Eränen is acknowledged for help and technical advice related to laboratory equipment. I am grateful to Dr. Atte Aho for helping me with FTIR.

I would like to thank my classmates and great friends Jeffery, Umara and Moldir for always being supportive and encouraging. I felt lucky to be surrounded by some good friends during my stay in Finland.

Finally, I would like to dedicate this work to my family for their encouragement and freedom to pursue my Master's degree in Chemical Engineering.

It has been an amazing experience being a research assistant in the Laboratory of Industrial Chemistry and Reaction Engineering and work under Prof. Dmitry Yu. Murzin at Åbo Akademi University, Finland.

Thank you!

List of Figures

List of Tables

Table of Contents

1 Introduction

1.1 General overview of hydroconversion

Hydroconversion has been playing an essential role in the petroleum industry for decades. It is a well-explored and recognized technology that has been used in crude oil refining. Hydroconversion generally refers to three typical oil refinery processes, i.e. hydrocracking, hydroisomerization and hydrotreatment, carried out for different oil fractions in an oil refinery. These processes are carried out in the presence of hydrogen and, therefore, known as hydroconversion. In this research work, hydroisomerization of long-chain hydrocarbons was investigated using hexadecane as a model compound over different bi-functional catalysts. The selection of hexadecane as a model reactant compound in this work is a compromise between the representation of long-chained hydrocarbons and analytical work allowing simpler product identification.

Recently, long-chain hydrocarbons have attracted attention for their interesting properties. These long-chain hydrocarbons (>C_{15}) make up to 80 wt.% of the material known as wax, i.e. long straight-chained (normal) hydrocarbons.[1] Several studies have been carried out to transform value-added products from a low-grade long-chain waxy feedstock. These long-chain normal hydrocarbons improve the thermal stability and viscosity of the fuel, but they also have adverse effects on other fuel properties, such as freezing and pour point and therefore should be removed to improve the fuel quality. The branched alkanes, in contrast, have superior cold flow properties and do not compromise other properties of the fuel. [2]

The transformations of normal to branched alkanes are carried out mainly by hydroconversion, i.e. hydrocracking and hydroisomerization. In hydrocracking, the feedstock is catalytically converted to lower carbon numbers, i.e. Mobil Oil using ZSM-5 catalyst with strong acidity and a uniform pore size commercialized selective catalytic cracking of long-chain hydrocarbons in the lube dewaxing (MLDW) process.[3] In hydroisomerization, the properties of the feedstock are improved by transforming normal hydrocarbons to branched ones having the same carbon number. Selective hydroisomerization is a highly desirable reaction in an oil refinery and is used mainly in two processes, first, for improvement of the octane number for the gasoline pool (C_5-C_6) and second, by dewaxing of long-chain hydrocarbon for improvement of flow properties. In both of these processes, normal hydrocarbons are

transformed to branched alkanes exhibiting the same carbon number. [1,6,7] Selective isomerization of short-chain alkanes is easy to achieve, while it is more difficult for long-chain hydrocarbons due to their rapid cracking after the hydroisomerization step. Improving selectivity of the bifunctional catalysts for the production of isomerized middle distillates is challenging.[10] Moreover, the specification of the cold flow properties of fuels mainly depends on the geographical region where they are used, and may vary from -3 °C for tropical regions to -35 °C for cold regions. [5] In general, for high-quality long-chain products isomerization of the straight-chained wax into high-valued branched paraffins is desired in order to improve properties of the resulting fuels.

1.2 Metal-acid bifunctional catalysts

The catalysts used in hydroisomerization are bifunctional, i.e. containing a metal function along with an acidic function. In these catalysts, the metal provides the hydrogenation/dehydrogenation function, while the isomerization/cracking function is provided by an acidic support, e.g. ZSM-5, SAPO-11, MCM-41, MCM-48, Beta (BEA) and Y zeolites. Isomerization and cracking of n-alkanes can occur simultaneously or competitively for all bifunctional catalysts. Carbenium ion is a key intermediate for n-alkane transformations, as shown in Figure 1.1.[3] The reaction scheme for hydroisomerization of long-chain paraffins over bifunctional catalysts established more than five decades ago is shown in Figure 1.1.[2,3]

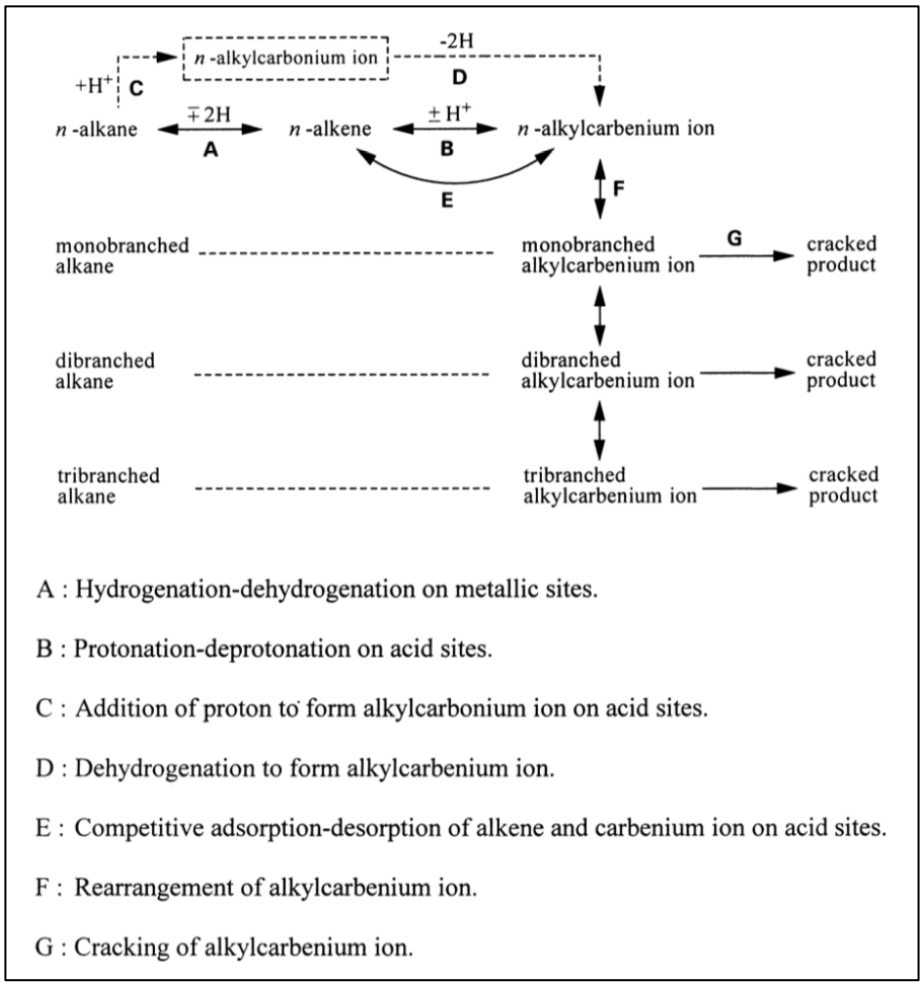

Figure 1.1: Reaction pathways for isomerization and cracking over bifunctional catalysts. [3]

The role of the metal (mostly noble ones, e.g. Pt and Pd) is to provide the hydrogenation/dehydrogenation function. The metal loading and dispersion play a key role in hydrogenation/dehydrogenation. In the case of a highly active metal, activity and selectivity of the overall process in the absence of diffusional limitations depend on the acidic function.

A suitable balance between the metal and acid functions influences the activity and selectivity of these catalysts. The acidic function in bifunctional catalysts is more important, and a correct density and strength of the acidic sites are of great significance.[4] More acidic catalysts are prone to excessive cracking resulting in yield loss, while less acidic catalysts do not catalyze the reaction or allow only insufficient isomerization, resulting in the formation of low octane number long-branched products with low volatility. Catalyst acidity determines the extent of isomerization/cracking reactions, and a decrease in acidity decreases cracking. [4,9,10,11]

It is generally understood that long-chain hydrocarbons are more reactive than short-chain hydrocarbons and their acidity requirements increase inversely with the chain length.[3] Moreover, both hydroisomerization and hydrocracking are acid catalyzed reactions proceeding on the acid sites, i.e. Brønsted acid sites. After isomerization, cracking can also proceed on the same sites. Therefore, the selectivity of these bifunctional catalysts for isomerization is expected to depend on the balance between the metal and acid functions.

In the case of zeolites, the pore structure of the zeolites also influences the activity and selectivity of bifunctional catalysts.[8] In the literature, for platinum and palladium exchanged medium pore size zeolites, such as ZSM-22 and ZSM-23, high selectivity for isomerization was obtained due to the small channels allowing isomerization and cracking. The small pore size restrains multi-branched iso-alkanes from cracking at inner acidic sites and, in this way, the isomerization selectivity can be increased. [4]

An ideal hydroisomerization catalyst should achieve high isomerization selectivity for long-chain hydrocarbons resulting in a high liquid yield with lower amounts of cracking products.

1.3 Hydroisomerization of hexadecane in batch and continuous reactors

Hydrocarbons have been intensively investigated for hydroisomerization of long-chain hydrocarbons.[2,3,4,5,7,9] In batch conditions, only a few studies on hydroisomerization can be found.[3] Most of the studies were carried out in continuous reactors with a variety of different model compounds ranging from C_{12} to C_{24}. In this section, an overview is presented for hexadecane as a model compound for isomerization of long-chain hydrocarbons. [2,4,5]

1.3.1 Hydroisomerization of hexadecane in the batch mode

Hydroisomerization of hexadecane with bifunctional catalysts containing 0.5 wt.% platinum with ZSM-5, ZSM-22, SAPO-11, Al-MCM-41, H-Y, H-β as catalyst supports was investigated by Park et al.[3] Conversion of hexadecane and selectivity over bifunctional catalysts at 103 bar and 350 °C are shown in Table 1.1.[3] The catalytic activities decreased for hexadecane conversion in the following order: Pt/ZSM-5>Pt/H-β>Pt/ZSM-22>>Pt/Al-MCM-41>Pt/H-Y>Pt/SAPO-11. The highest hexadecane conversion was achieved for Pt/ZSM-5, Pt/H-β and Pt/ZSM-22, which is due to their strong Brønsted acidity compared to other catalysts. Pt/ZSM-5, Pt/ZSM-

22 and Pt/SAPO-11 are medium pore sizes zeolite. The lowest activity among these materials was exhibited by Pt/SAPO-11, related to weak Brønsted acidity. Pt/H-β and Pt/H-Y have the same metal dispersion and pore size, with Pt/H-β displaying high activity. Alkenes formed during hydroisomerization were hydrogenated due to a high total pressure (103 bar) and were not found in the product mixture. It is expected that a high metal dispersion favors hydroisomerization over hydrocracking. The cracking selectivity increased with conversion for Pt/H-β, Pt/ZSM-5 and Pt/ZSM-22, while it remained constant for Pt/SAPO-11, Pt/H-Y and Pt/Al-MCM-41. Some bi-branched products were found in Pt/H-Y and Pt/H-β and tri-branched products in Pt/ZSM-5, Pt/ZSM-22 and Pt/SAPO-11. The product distributions were different for each catalyst. Pt/ZSM-5 generated more lighter alkanes, i.e. C_5-C_6, while other catalysts gave alkanes higher than C_7. The maximum amount of isoalkanes was formed over Pt/H-β, while other catalysts also formed n-alkanes. [3]

Table 1.1: Hydroisomerization of hexadecane over bifunctional platinum/zeolites.[a] [3]

Catalysts	Pt/ZSM-5	Pt/ZSM-22	Pt/SAPO-11	Pt/Al-MCM-41	Pt/H-Y	Pt/H-β
Conversion (%)	37.1	41.3	44.0	44.7	39.2	42.5
B-C_{16} selectivity (wt.%)	15.6	31.2	66.6	88.9	75.7	50.7
Mono-C_{16} (CH_3–C_{15})	14.2 (13.9)	29.3 (29.2)	61.8 (61.0)	63.6 (55.8)	55.3 (15.3)	22.6 (19.4)
Di-C_{16}	1.4	1.9	4.5	20.8	15.3	17.5
Tri-C_{16}	0.0	0.0	0.3	4.6	5.1	10.6
Hydrocracking selectivity for $C_{\leq 15}$ (wt.%)	84.4	68.8	33.4	11.1	24.3	49.3

[a] CH_3–C_{15}=methylpentadecane, mono-C_{16}=monobranched isohexadecanes, di-C_{16}=dibranched isohexadecanes, tri-C_{16}=tribranched isohexadecanes, B-C_{16}=branched isohexadecanes.

From Table 1.1, it is evident that in the conversion range of 35-50%, Pt/Al-MCM-41 has the highest selectivity of 89 wt.% for the isomerization products and has the least cracking selectivity. The least isomerization and the highest cracking activity were displayed by Pt/ZSM-5. Lube oil quality is related to the presence of methylpentadecane (CH_3-C_{15}). In this context, the highest activity for methylpentadecane was shown by Pt/Al-MCM-41 and Pt/SAPO-11. It was concluded that Pt/Al-MCM-41 exhibits high selectivity towards methylpentadecane and has high dewaxing capabilities.[3]

A detailed overview of hydroisomerization in a batch mode ranging from catalyst preparation to catalytic results is presented in Appendix A1.1.

1.3.2 Hydroisomerization of hexadecane in a continuous mode

1.3.2.1 Hydroisomerization of hexadecane over Pt/H-Beta catalyst

Batalha et al. [2] carried out hydroisomerization of n-hexadecane over three series of bifunctional Pt/H-Beta and Pt/Al_2O_3 catalysts (Appendix 1.2, Table 3).[2] In series 1, the catalysts were prepared by ion-exchange platinum giving metal loading from 0.2 to 1.5 wt.%. The remaining two sets of catalysts were prepared by mixing different amounts of the zeolite and 2 wt.% Pt alumina sample by the incipient wetness technique. Catalysts in the series-1 were calcined at 450 °C while the other series were calcined at a higher temperature of 500 °C. Hydroisomerization of hexadecane was carried out in a fixed-bed stainless steel reactor with 0.3 g of the catalyst exhibiting the particle size between 0.2-0.4 mm mixed in 1.7 grams of carborundum of the particle size 0.25 mm under the following condition: 220 °C, 30 bar, H_2/n-C_{16} molar ratio 20, and WHSV 2-100 h^{-1}.

The pure Beta catalysts and Pt alumina catalysts were inactive in hexadecane hydroisomerization at reacting conditions, while their bifunctional counter parts catalyzed the reaction under operating conditions. The lowest conversion was observed for 0.7Pt/(H-Beta/alumina) catalyst, while other catalysts exhibited relatively high conversion (Appendix 1.2, Figure 4). It was noted that isomerization activity increases at a lower ratio of platinum to the protons (C_{Pt}/C_{H+}) and then remained constant for all catalysts with a low C_{Pt}/C_{H+}. Mono-branched, bi and multi-branched products were formed for each bifunctional catalyst with their product distribution depending on the catalyst type and conversion. For all catalysts, the cracked products ranged from C_3-C_{13} having both linear and branched products with a low yield of the cracked product. Methane and ethane were not present in the products.

The reaction pathways for the products were n-C_{16} ⇄ M ⇄ B → C, where, ‘M’ are the mono-branched, and ‘B’ are the bi and multi-branched isomerized products, which are formed and then successively cracked ‘C’ in the following reactions. It was concluded that for the simplified scheme (n-C_{16} ⇄ M ⇄ B → C), two conditions should be fulfilled, a) high C_{Pt}/C_{H+} values and b) a high degree of intimacy between hydrogenating and acid function.

1.3.2.2 Hydroisomerization of long-chain alkanes over Pt/zeolite catalyst

Hydroisomerization of n-decane, n-tetradecane and n-hexadecane was carried out over three types of bifunctional catalysts, i.e. Pt/H-Beta, Pt/MCM-22 and Pt/ZSM-5 by Soualah et al.[4] All catalysts contained 1 wt.% platinum having 80% dispersion for H-Beta, 65% for MCM-22 and 70% for ZSM-5. All experimental work was carried in a fixed-bed stainless steel reactor under the following conditions: 220 °C, 30 bar, H_2/n-alkane molar ratio of 20, WHSV = 2-100 h^{-1}.

All catalysts were active for hydroisomerization of hexadecane under operating conditions. However, the activity of the catalysts decreased for Pt/HMCM-22 and Pt/HZSM-5 when the alkane chain length was increased. On the other hand, for Pt/H-Beta, the activity was independent of the alkane chain length and remained constant. Pt/H-Beta was the most active catalyst exhibiting the highest turn-over frequency (TOF) which was significantly higher than for Pt/HMCM-22 and Pt/HZSM-5. For all alkanes, the decreasing order of activity was Pt/H-Beta >> Pt/HMCM-22 > Pt/HZSM-5.

The products formed were categorized into three groups, i.e. isomerized products (I), mono-branched (M), multi-branched (B) and cracking products (C). The main products were methyl-substituted ones for each reactant, e.g. methyl-nonane for n-decane, methyl-tridecane for n-tetradecane, and methyl-pentadecane for n-hexadecane. The best product distribution was shown by Pt/H-Beta catalyst, having significant amounts of C_{13}-C_{15} with no formation of lighter gases, e.g. methane, ethane and propane. For some catalysts, ethyl substituted products were also found. The cracking products were formed with light gaseous products. For each catalyst, three groups of products were formed in which Pt/H-Beta gave mono-branched hydrocarbons as primary products for n-hexadecane. Therefore, it can be concluded that Pt/H-Beta shows the highest activity and selectivity for hydroisomerization of alkanes.

1.4 Objectives and scope

Hydroisomerization of long-chain hydrocarbons had gathered a lot of interest, as it is a gateway for production of sustainable and excessive long-chain hydrocarbons with many superior properties compared to their normal chain counterparts. The aim of this work was to select a stable and active catalyst with an optimum metal to acidity ratio for hydroisomerization of long-chain hydrocarbons using hexadecane as a model

compound. In this work, hydroisomerization of hexadecane was investigated with different types of supports, i.e. Al_2O_3, Beta and Y zeolites modified with metals, such as platinum, nickel, and ruthenium.

The following objectives were set for hydroisomerization of long-chain hydrocarbons.

- Characterization of the fresh and spent catalysts used in the reaction, e.g. by measuring specific surface area, acidity, applying scanning electron microscopy and energy dispersive X-ray microanalysis (SEM-EDX), transmission electron microscopy (TEM), thermogravimetric analysis (TGA), coke extraction and size exclusion chromatography (SEC), organic elemental analysis (CHNS) and dissolution of zeolites in hydrofluoric acid (HF) and GC-MS analysis.
- Performing preliminary experiments with hexadecane under the operating conditions, identification of possible products and their calibration for possible product analysis.
- Determination of the gas-phase and liquid-phase products with their identification and categorization.
- Comparison of different metals supported on acidic zeolites.
- Determination of the influence of catalyst structure, pore dimensions and crystalline structure of the acidic support.
- Investigation of the temperature dependence of selectivity and product distribution over different catalysts.
- Selection of catalyst for hydroisomerization of hexadecane.
- Elucidation of possible reaction mechanisms and pathways for hydroisomerization of hexadecane.

2 Catalyst supports, methods of catalyst characterization, catalyst deactivation and reaction mixture analysis

2.1 Zeolite type alumino-silicate material

There are two types of zeolites used in this research work, namely Beta and Y zeolite, which is discussed below addressing their molecular arrangement and structure.

2.1.1 Beta zeolite (BEA)

Beta zeolite is a large pore material having 3-dimensional structures with 12-membered (number of T atoms) inter-connected rings. The pore size of Beta zeolites is between 0.64 and 0.76 nm. [12] The basic unit of Beta zeolite is tetragonal in its structure and was first produced in 1967 by Camblor and Pérez-Pariente. [13] Beta zeolites are primarily used in refineries worldwide due to their unique properties, such as a) high specific surface area and a unique pore size, b) high Brønsted acidity and c) high chemical and thermal stability.[15] The framework of Beta zeolite and its 12-ring channel framework are shown in Figure 2.1(a) and Figure 2.1(b), respectively. [14] Morphology of the proton form of H-Beta-25 zeolite (H-BEA-25) is shown in scanning electron microscopy (SEM) image (Figure 2.2).

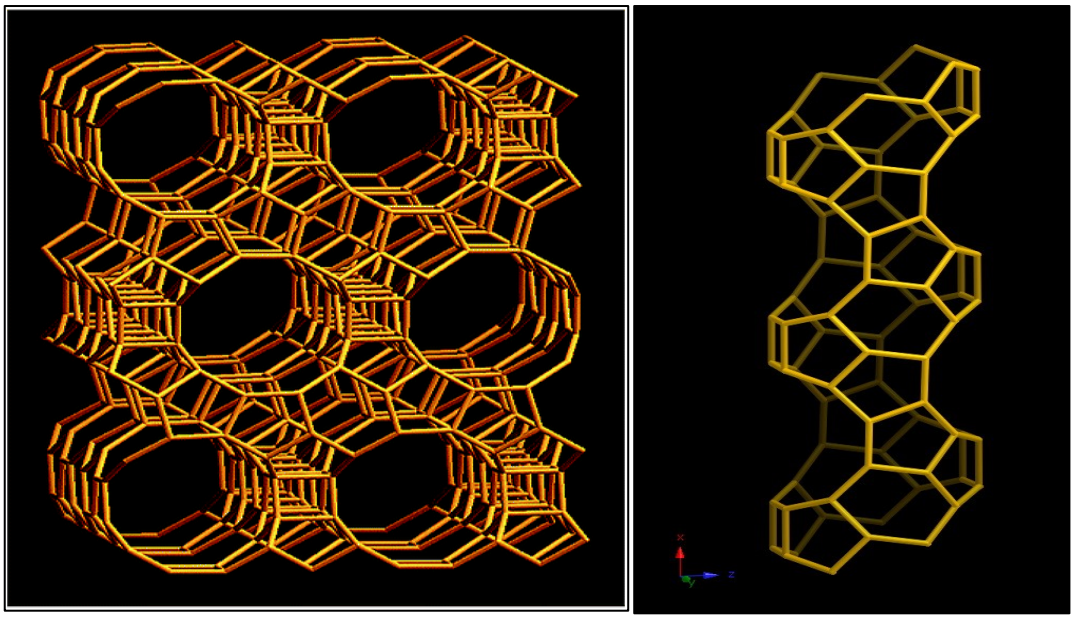

Figure 2.1 (L-R): a. The framework of Beta zeolite, b. 12-ring channel in Beta zeolite framework. [14]

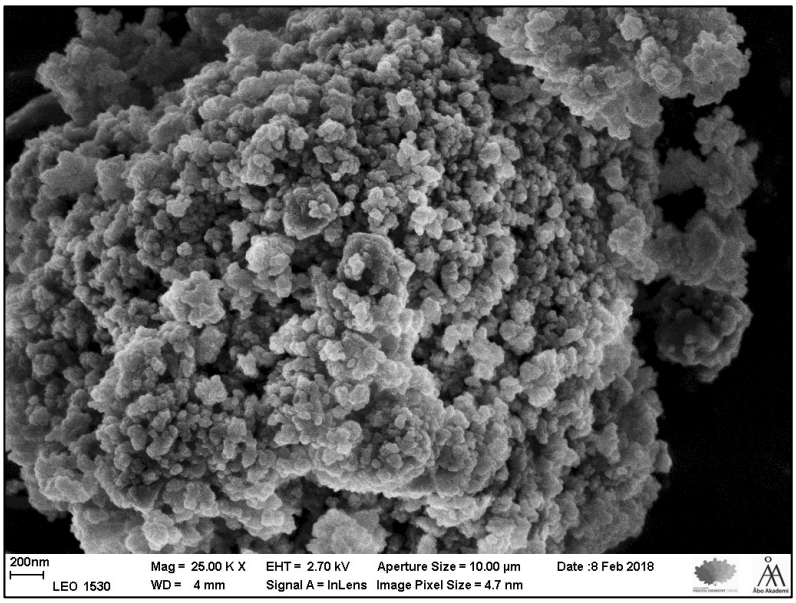

Figure 2.2: Scanning electron micrograph of H-Beta-25 zeolite catalyst.

2.1.2 Ultra-stable Y-zeolite (USY)

Y zeolite is a large pore material with a 3-dimensional structure containing 12-membered rings (number of T atoms) and having a uniform pore size of 0.74 nm. [15] The basic unit of Y zeolite is cubic in structure. Y zeolite has a vital role in oil refining especially as fluid catalytic cracking (FCC) catalysts due to a) high surface area and large pore size, b) high Brønsted acidity and c) high chemical and thermal stability.[15] Although Y zeolites have been used for decades, their drawback is the presence of micropores. The molecules in fluid catalytic cracking (FCC) feedstock are either too large or have prolonged diffusion rates into the micropores of Y zeolite. [16] To avoid this situation, there have been attempts to transform these micropores into mesopores by post synthesis techniques, including steaming at high temperature and acidic leaching.[16] With these post synthesis methods, aluminum (Al) is removed from the framework transforming a microporous material into a mesoporous one and increasing the pore size. [16] The steaming method is used for the synthesis of ultra-stable solid acid USY zeolite catalyst with uniform pore size.[16] This technique modifies its thermal and hydrothermal stability and increases the inter-crystalline diffusion. [16]

The framework of Y zeolite with a 12-membered ring channel framework and cavities is shown in Figure 2.3. [14]

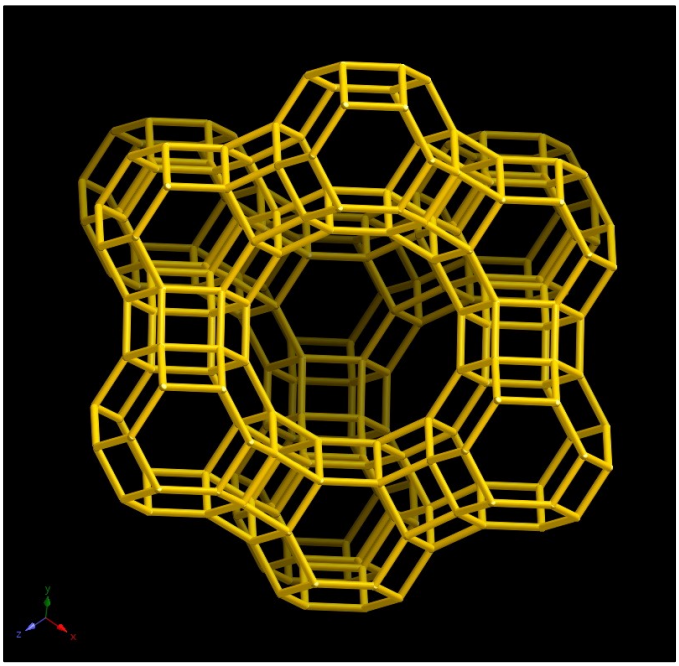

Figure 2.3: Framework of Y zeolite. [14]

2.2 Methods of physico-chemical characterization

The following techniques were used for physico-chemical characterization of the catalysts. The results obtained from the physico-chemical characterization were used to explain the catalytic properties of materials studied in hydroisomerization of hexadecane. These characterization methods include nitrogen physisorption, FTIR with pyridine as a probe molecule, scanning electron microscopy and energy dispersive X-ray microanalysis (SEM-EDX), transmission electron microscopy (TEM), thermogravimetric analysis (TGA), coke extraction with heptane and size exclusive chromatography (SEC), organic elemental analysis (CHNS), zeolites coke analysis with dichloromethane and GC-MS analysis. These techniques are shortly discussed below.

2.2.1 Nitrogen physisorption

The catalysts in this study are heterogeneous porous solids exhibiting high specific surface area.[17] The increase in the surface area surges dispersion of the active metals on the catalysts surface while a large number of pores with high porosity enables an increase in the internal surface area. [17] Moreover, an increase in the number and size of the pores also provides easier reactant diffusion into the pores towards the active sites, e.g. in case of this study, reactants from the outer surface of Beta catalysts to the acid sites, and diffusion of the products to the bulk fluid after the reaction. Here, it is

important to mention that the reactants can isomerize/crack and the size of the molecules may increase as the reaction proceeds (transformation of linear to branched products). In this case, the size of the pores is significant because the pores can be blocked if the pore size is smaller than the product sizes. This results in the pore blockage causing catalysts deactivation.

Therefore, it is of utmost importance to optimize the specific surface area and specific pore volume of these materials in order to utilize their catalytic properties maximally, i.e. specific surface area and pore accessibility to the active sites. To find out these properties, nitrogen physisorption was performed to determine the specific surface area and specific pore volume. With respect to the size and diameter of pores, the catalysts are classified into three categories;[17]

1. Microporous (<2 nm)
2. Mesoporous (2-50 nm)
3. Macroporous (>50 nm)

The nitrogen physisorption method was developed in the 1940s by Brunauer, Emmett and Teller, and thus known as a BET method for surface area measurement. [17] This method is performed at the boiling temperature of liquid nitrogen, i.e. -196 °C (77 K) to record adsorption isotherms, which give information about the specific surface area and porosity of the catalyst determined from desorption at the same temperature.[17] Despite apparent drawbacks, this method is still widely used for the specific surface area determination.[17]

For microporous materials, Beta and Y zeolite, the Dubinin-Radushkevich method was applied. It relates the adsorbate volume and monolayer volume using the following equation 1;[17]

$$V = V_m \exp\left[-B\,(RT^2/\beta^2)^2 * \ln^2(P_0/P)\right]$$

where, B and β are constants and T is temperature. Equation 1 displays a linear relationship between lnV and $\ln^2(p_0/p)$. The curve bends at low values of $\log^2(p_0/p)$, but extrapolation to zero can provide the values for V_m. [17]

For the mesoporous materials, e.g. alumina (Al_2O_3), the BET model is utilized providing the monolayer volume and specific surface area. In the BET method the following assumptions were used; [17]

1. The surface is uniform for adsorption and molecules in cross linkages can be ignored (assuming a constant monolayer heat of adsorption).
2. For multilayer adsorption, an adsorbed molecules act as new adsorption sites.
3. The heats of adsorption and condensation are equal, except for the first layer.

The BET method allows determination of the monolayer volume, which can be further used to calculate the specific surface area;

$$A_s = (V_m/22414) * A_m * N_a$$

Where:

A_s - the specific surface area, m^2/g;

V_m - monolayer volume of the adsorbate, cm^3/g;

A_m - area occupied by one molecule, m^2/molecule;

N_a - Avogadro's number, $6.023*10^{23}$ molecules/mol.

2.2.2 Fourier-transform infrared spectroscopy (FTIR) with pyridine as a probe molecule

The strength and amounts of acid sites of the catalysts were analyzed by FTIR using pyridine as a probe molecule. This technique enables to determine the amounts and strength of the Brønsted and Lewis acids sites. [18] These acid sites are vital for the activity of the solid catalysts and strongly influence the reaction.

In this technique, an infrared beam is generated and transmitted into an interferometer and then split by a beam-splitter. These beams are transmitted into two mirrors: a stationary and a moving mirror. These two beams are then collected and recorded as an interferogram. This makes a set point for the sample called background. The same procedure is then repeated with the light transmitted through the sample in the sample compartment, and the beams are collected, and a detector perceives all the wavelengths absorbed. The mathematical calculations are preceded using Fourier transform that generates a spectrum from the light interferences.[18] The background readings are then subtracted from the sample readings.

The selection of the probe molecule is also an important factor in this characterization. These probe molecules range from strong bases, i.e. ammonia and pyridine to weak bases, i.e. carbon monoxide. An advantage of pyridine is in weaker basicity compared to ammonia giving better resolution. Pyridine adsorption distinguishes between the Brønsted acid sites and Lewis acid sites exhibiting the

adsorption bands of 1545 cm^{-1} and 1455 cm^{-1}, respectively. [18] Weak, medium and strong acid sites correspond to amounts of pyridine retained at 250 °C, 350 °C and 450 °C, respectively. A total of six reading are taken at each temperature, and an average value is calculated using the Emeis extinction factor for pyridine. [35]

2.2.3 Scanning electron microscope and Energy dispersive X-ray microanalysis (SEM-EDX)

Scanning electron microscopy is an important tool for characterization of the surface morphology and chemical composition of the materials. It utilizes a focused beam of a highly energized electron to produce signals to the sample surface. The sample is coated with carbon to make it conductive in order to collect electrons during analysis. The derived signals from the samples provide information about the sample texture, chemical composition, and crystalline structure with the orientation of components comprising the sample. SEM has the magnification ranging from micrometers (μm) to nanometers (nm) and can analyze the microstructure of the solid materials in focus and with good resolution. The magnification of SEM ranges from 1 cm to 5 microns with a spatial magnification up to 50 nm on a two dimensional image. The quantitative analysis reveals the crystalline structure and crystal orientation. In the semi-qualitative analysis with the help of energy dispersive X-ray spectrometer (EDX), generally highly focused electron beams are focusing on a specific area showing its chemical composition.[19]

2.2.4 Transmission electron microscopy (TEM)

Transmission electron microscopy (TEM) is used to determine the metal particle size, pore dimensions, structure and periodicity of pores in different materials. The results from TEM images are sharper with a resolution higher in comparison with scanning electron microscopy (SEM) due to better a penetration of its higher energy electron beam of 100-300 keV. It allows creating an image of the specimen in the range of nanometers. [20]

The sample is placed on a grid as shown in Figure 2.4(a), which is kept in the vacuum chamber inside a transmission electron microscope (TEM) shown in Figure 2.4(b). The sample is covered by a thin graphite layer for electric conductivity and kept inside a vacuum chamber. A high voltage electron beam of 100-300 keV is emitted from an electron gun, which is enhanced by an anode. These electrons pass through

the sample; a part of these electrons is transparent to electrons while the other scatter out the beam. The image is formed by different lateral absorption of the beam in which heavier atoms exhibit a dark color while lighter atoms are exhibiting soft colors as shown in Figure 2.5. Any noise coming from the gas molecule is avoided by using 10^{-7} Torr low pressure, giving a high resolution. [20]

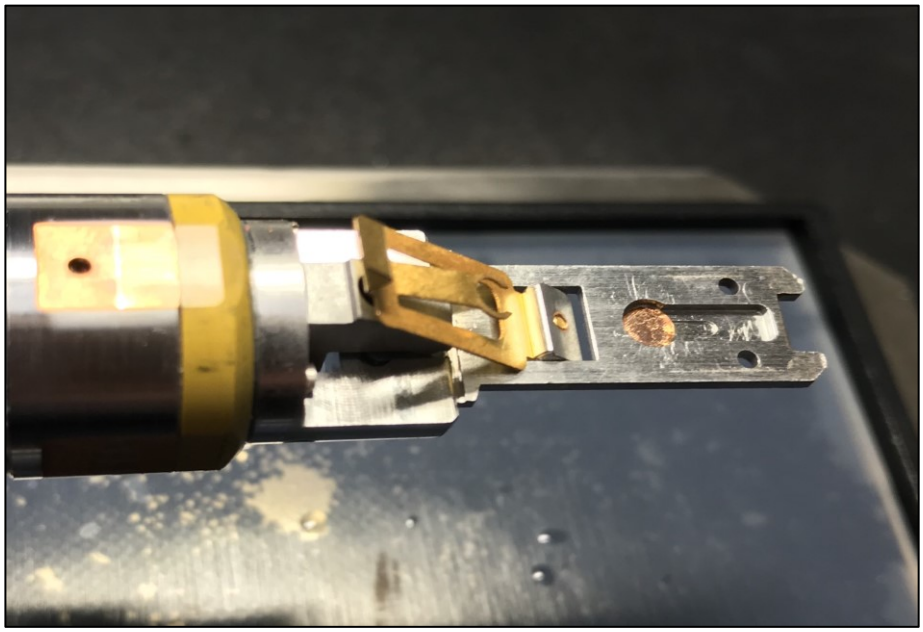

Figure 2.4(a): A sample grid of Transmission Electron Microscopy (TEM).

Figure 2.4(b): Transmission Electron Microscopy (TEM) instrument.

Materials with different phases are preferred for analysis due to better contrast. It is also beneficial to have phases with different d-spacing and shapes. Moreover, a specimen with a metallic phase is easier to be distinguished than oxide supports. If the contrast is of good quality, the support and the supported phase can be determined as shown in Figure 2.5 for ruthenium on ultra-stable Y (USY) zeolite.

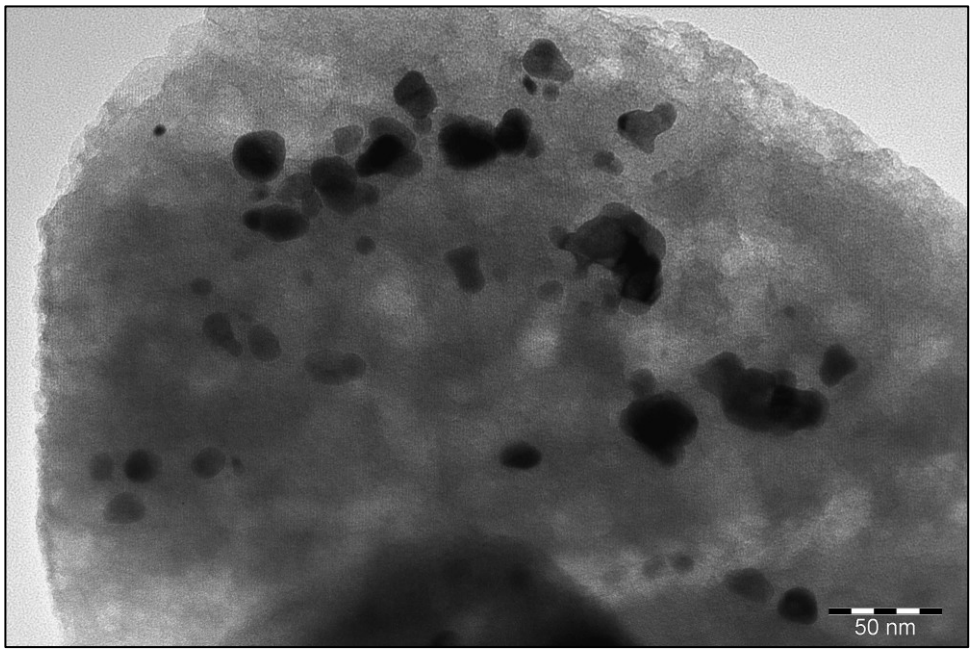

Figure 2.5: A TEM image is showing ruthenium on ultra-stable Y (USY) zeolite support.

2.2.5 Thermogravimetric analysis (TGA)

In thermal analysis weight changes of the sample are recorded when the temperature is changing with time.[21]

In this analysis, the temperature ramp (°C/min) is kept constant, and the physical characteristics of the sample are recorded. The samples can be analyzed in a powder form or as grains when the interior temperature is close to the outside environment. [21] This technique can be used for a number of samples ranging from organic or inorganic ones, metals, polymers, and plastics to composite materials. The temperature ranges from 25 °C as the initial temperature to a final temperature of 900 °C in conventional analysis. In modern instruments, the final temperatures can be up to 1500 °C if required. [21]

In this work, two sets of samples were analyzed namely fresh and spent catalysts. Typically air, helium and nitrogen are used in TGA, which can also be done under vacuum. The gas atmosphere is set according to the sample requirements.[21] In carbon containing samples, a nitrogen atmosphere is used to avoid any carbon oxide or carbon dioxide production and emissions, while air is applied for other samples. In this study, nitrogen was used due to coke deposition on the spent catalyst surface.

2.2.6 Coke extraction with heptane and size exclusion chromatography (SEC)

Out of several problems in oil refining regarding catalysts, catalyst deactivation is one of the main concerns whilst developing a new catalyst. Catalyst deactivation in hydroconversion is a common problem due to the formation of carbon deposits, sintering and poisoning of metals due to such impurities in the hydrocarbon feed as, S, N, and P. Coke is complex in nature comprising heavy aromatic hydrocarbons and hydrogen-deficient carbonaceous deposits. Coke forms a cluster as the reaction proceeds and a rapid loss of catalytic activity can occur towards the end of an experiment due to severe catalyst deactivation. This activity loss is due to blocking of pores by the coke and metals deposition. [22]

A limiting factor in the identification of different components in coke is its complexity. In order to investigate the constituents of coke, it has to be extracted from the spent catalyst. The amount of soluble coke obtained by extraction depends on the selection of the solvent, extraction technique, the feedstock and the catalyst type. The commonly used solvents are hexane, toluene, tetrahydrofuran (THF), pyridine, methanol and dichloromethane. Several extraction techniques have been applied, such as solvent extraction, soxhlet extraction and accelerated solvent extraction (ASE). [22]

Size exclusion chromatography (SEC) was developed in the 1970s by Halász and Martin.[36] Porosity can be determined by SEC combined with high performance liquid chromatography (HPLC). The solvent polarity is usually kept between water and tetrahydrofuran (THF) in the mobile phase.[23] The catalyst is dissolved in a solvent and introduced into the column of known pore size. [38] The same solvent is also used in the mobile phase. [38] When molecules move into the pores larger molecules are eluted through the column voids,[38] while smaller molecules move through the pores and are eluted. Heavy molecules are eluted first followed by smaller molecules.[38] The respective molecules movement across the pores determine the retention times which are higher for smaller molecules and lower for heavier ones.[23] Since SEC is a relative and not an absolute molecular weight technique; the column must be calibrated with standards of a known molecular weight. For detection, a differential refractometer is widely used.[38]

2.2.7 Organic elemental analysis (CHNS)

Organic elemental analysis was performed to identify and quantify contents of carbon, hydrogen, nitrogen and sulfur in the spent catalysts. Organic elemental analyzers are capable of handling a variety of sample types including solids, liquids, volatile and viscous materials. [24]

In this analysis, combustion is carried out at high temperature in an oxygen rich environment based on the Pregl-Dumas method.[36] Pure oxygen and inert gas (helium) are connected to the instrument. Such analysis can be carried out in static conditions, i.e. in an initial fixed amount of oxygen or dynamic conditions, i.e. a constant flow of oxygen through the combustion. Moreover, additives are also added to aid combustion and increase conversion.

The combustion temperatures are kept at 1000 °C, and all the combustible organic materials are converted to their oxides while carbon is transformed to carbon dioxide (CO_2), hydrogen to water (H_2O), nitrogen to nitrogen oxide (NO_2) and sulfur to sulfur oxide (SO_2). If other elements are present in the sample, they are converted and detected, e.g. chlorine is converted to hydrogen chloride. The combustion products are swept off the chamber by an inert gas (helium) and passed through (pure) copper at 600 °C. The latter is needed to oxidize any unreacted nitrogen that is trapped through absorbents. These absorbents trap all other gases except carbon dioxide, water, nitrogen and sulfur dioxide for their detection. Detection can be carried out in different ways, e.g. first the gases are separated and detected by a thermal conductivity detector, and second, a series of infrared and thermal conductivity cells are used for individual gas detection. [24] Both of these methods can detect carbon, hydrogen, nitrogen and sulfur by gas chromatography (GC).

2.3 Catalyst deactivation

A loss in activity and/or selectivity of the catalyst over reaction time is termed as catalyst deactivation. In chemical industries, processes are well optimized to achieve high production efficiency and prolong catalyst activity. Moreover, a demand for high value added products, i.e. gasoline, middle distillate and lube oil is in a surge. [30]

This trend motivates researchers to study the heavy oil fraction that can be transformed into lighter oil fractions mainly by hydroconversion, i.e. hydrotreating and hydrocracking. [30] Catalyst lifetime depends on the chemical process, feed stock and operating conditions.[30] The catalyst lifetime ranges from a few seconds, e.g. in

fluid catalytic cracking (FCC) in oil refineries to 10-20 years, e.g. in ammonia synthesis. Moreover, the same catalyst can respond to different feed for the same process differently due to local quality changes in the feedstock, e.g. sulfur-containing feed in ammonia process influences catalytic stability. [31]

Activity/selectivity decline with time-on-stream is slow in mature processes, such as hydrotreating and hydrocracking. The amount of impurities (e.g. sulfur, nitrogen and vanadium etc.) in these fractions has, however, adverse effects on these catalysts.[30] Additionally, any sudden change in operational parameters can have a drastic effect on the catalysts, e.g. exceeding the critical points in temperatures or steam/hydrogen-to-hydrocarbons ratios can lead to catalyst deactivation in a short time interval. On one hand, catalyst deactivation is an industrial reality, on the other hand, catalyst deactivation can be delayed, avoided and catalysts can be efficiently regenerated. Significant research efforts are devoted to a) prevention or retardation deactivation and b) regeneration and reactivation to enhance catalytic activity and selectivity.[31] Coking is one of the main reason of zeolite deactivation, and in most industrial processes, the costs related to catalyst deactivation are very high. Mastering the catalyst stability has become as important as controlling activity and selectivity of zeolite catalysts.[46,47]

Coke formation in zeolites depends on the pore structure and reaction temperature. The coke formation starts inside the micropores, which grows to block the pore, thus causing catalyst deactivation. Formation of coke in acidic catalysts depends mainly on, a. the characteristics of acid sites and pore structure and b. the nature of feed along with operating conditions (temperature, pressure).[43,44,46] It is now established that the reaction involved in coke formation and the origin of coke retention highly depends on the reaction temperature.[45] Guisnet et al.[46] also reported an increase of coking with increased reactant pressure.[46] Deactivation of zeolite catalysts is due to retention of heavy secondary products within the pores and on the outer surface of the catalyst.[43] Furthermore, alkenes cause rapid coking in acidic catalysts due to their rapid transformation through oligomerization, cyclization, alkylation and hydrogen transfer.[43,44,45] Coke molecules can be found inside the channels, the cavities, the channel intersections and on the surface of the zeolites.[45] Deactivation in zeolites can proceed in two ways, a. one active site per coke molecule is deactivated and b. several actives sites are deactivated.[43,44]

2.3.1 Deactivation mechanisms

There are many deactivation mechanisms, explaining losses in the catalyst activity and selectivity. Some of these factors are listed below: [31]

1. **Fouling/Coke formation**: Deposition and blockage due to diffusion of organic molecules of carbonaceous materials from the liquid bulk into pores.
2. **Sintering**: Loss of catalytic activity due to agglomeration of metal nano-particles at elevated temperature.
3. **Poisoning**: Adsorption of any impurity/contaminants in the feed that leads to losses in catalyst activity/selectivity.
4. **Vapor formation**: Changes of the catalyst active phases in the presence of reactive gases in a feed.
5. **Attrition**: Loss of catalytic material/surface area due to crushing or any mechanical force.

In this study, we will focus on the first three more important reasons for catalyst deactivation. These deactivation mechanisms are briefly discussed below.

2.3.1.1 Fouling/Coke formation

Fouling or coke formation is a physical deposition of metallic or carbonaceous material from the liquid bulk to the catalyst surface. The deposition blocks the catalyst surface and pores decreasing catalytic activity. The pore blockage inhibits the use of the internal surface area and active sites, which results in the major activity losses. In excessive fouling, the catalyst can even disintegrate, and breakdown is possible. It is important to define and differentiate between carbon and coke material. Carbon is a result of carbon monoxide disproportion while coke is the result of condensation/decomposition of hydrocarbons on catalyst surfaces forming heavy polymerized hydrocarbons. In the literature, it is mentioned that catalysts can tolerate 6-10 wt.% coke with a major activity loss if the deposition is on the support surface and not directly on the catalyst active sites.[30] However, when the coke deposition continues to ca. 15-25 wt.% major activity losses are observed in a short time. [32] Tamm et al. have shown the monolayer coke formation on the catalyst surface is a result of coke deposition, which starts from the outer surface continuing in the pores as the reaction proceeds. [33] The chemical structure of coke is very complex and depends on the time scale and temperature of the reaction. Menon et al. classified

coke-forming reactions broadly into two categories, i.e. coke-sensitive and coke-insensitive.[34] The unreacted coke is deposited on the catalyst surface in coke-sensitive processes, e.g. catalytic cracking. In coke-insensitive processes, the coke formed is removed by hydrogen (or other gases), e.g. in Fischer-Tropsch synthesis and catalytic reforming.[31]

Coke formation can be minimized by a) higher C/H ratios, b) tuning acidity in zeolites to optimize coke formation and c) purifying feedstock by removing the polynuclear aromatics that are likely to form coke. [31]

2.3.1.2 Thermal degradation/sintering

The thermal degradation of catalysts occurs mainly due to two reasons:[31]

1. Loss of activity due to the crystalline growth of the catalytically active phase (sintering).
2. Loss of activity due to mechanical support failure and pore blockage.

Generally, sintering takes place at the elevated temperature being accelerated by the presence of water vapors. The deactivation mechanism in sintering includes a) migration of the crystalline structure in the catalyst, b) atomic migrations, and c) vapor migrations at elevated temperatures. In atomic migration, the metallic atoms are detached and recombine as agglomerates decreasing the active surface area, metal dispersion and catalytic activity. Temperature is an important parameter in sintering as sintering increases exponentially at elevated temperatures. Moreover, sintering also depends on the catalyst supports and the environment. Namely, the rate for noble metal migration is increased in the presence of oxygen and is relatively suppressed in hydrogen. Sintering can effect structure-sensitive reactions positively or negatively depending on the type of catalytically active sites (edges and corners etc.). In structure-insensitive reactions, sintering does not have any effect on the specific activity. Generally, sintering processes are slow and can easily be prevented at low temperatures.[31]

2.3.1.3 Poisoning

Poisoning is related to strong chemisorption of any reactant/impurity on the catalyst active sites. The poisoning phenomena can be easily understood by sulfur poisoning on nickel surfaces in ethylene hydrogenation. A two-dimensional image illustrates the sulfur atom on the surface of nickel (Figure 2.6). [31]

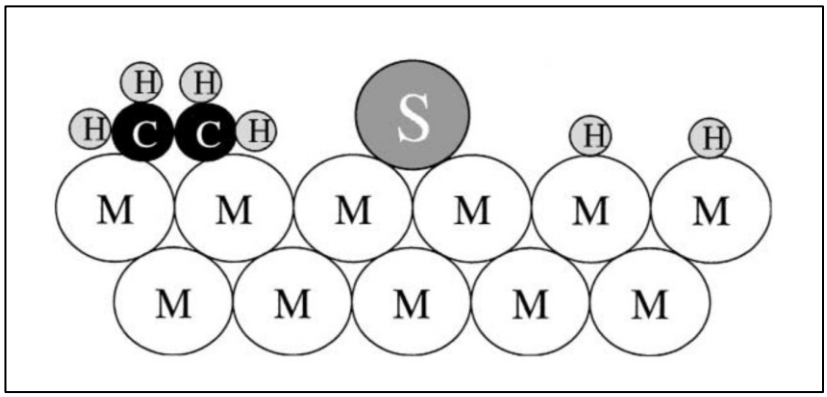

Figure 2.6: Conceptual image of sulfur poisoning of nickel in ethylene hydrogenation.[31]

First, 3-4 adsorption sites on the metallic surface are blocked by the strong sulfur adsorption in the three-dimensional surface. Second, the sulfur atom has also an adverse effect of electronically modifying neighboring atoms due to its strong chemical affection with surface nickel atoms altering the ability of the later to adsorb reactants. Third, surface restructuring by sulfur causes adverse catalytic properties of the nickel surface. [31]

Other examples of metallic poisoning include metallic compounds by poisoning of the automotive catalysts, e.g. Ni, Pb and Zn. Sulfur and arsenic compounds are poisons for metals in hydro/dehydrogenation and steam reforming reactions. Apart from poisoning by chemical elements, different compounds can also act as poisons for different catalysts, e.g. organic bases like ammonia/amines are poisons for acidic catalysts, i.e. zeolites in hydrocracking reaction and acetylene is a poison for hydrotreating of residual petroleum fraction. [31]

2.4 Reaction mixture analysis

2.4.1 Gas chromatography (GC)

Gas chromatography refers to a variety of analytical separation techniques for volatile components in the gas phase. Gas chromatography is a powerful tool, which can be used for analysis of the gases and liquids. In the later case, the sample is dissolved in a solvent (toluene/ethanol in this research) and is vaporized to separate its components from the solvent by two phases, i.e. stationary phase and mobile phase. The stationary phase is generally a solid adsorbent while an inert gas (hydrogen, helium) acts as a mobile phase. [26] Capillary columns are widely used in gas chromatography for efficient separation.

A basic gas chromatography apparatus has the following parts: [26]

- An injector
- A column, usually a metal tubing with a solid coating
- A flow control equipment (for carrier gas constant flow)
- A flame ionization detector (FID)
- An oven/heater for temperature controls
- An integrator.

2.4.2 Gas chromatography and mass spectrometry (GC-MS)

Gas chromatography with mass spectrometry is a very useful tool for the identification of various mixtures. In GC-MS, the components can be identified not only by their retention times as in gas chromatography (GC), but also analyzed with their unique mass spectra.[27] With this technique, different isomers of chemical components with the same carbon number can also be qualitatively identified. [27]
The spectrum generated for a certain compound is unique and is collected during analysis. The gas chromatography (GC) separates the mixture into its individual compounds. These compounds are then exposed to an electron beam known as electron impact (EI) where the molecules are ionized with an average energy of 50-70 eV. By taking electrons from the molecules, charged molecules are produced. The charged molecules are further excited by the electrons and are disintegrated into fractions. The mass analyzer detects molecular fragments that give a unique mass spectrum. The results from GC-MS are highly reproducible if a similar energy source is provided. In this manner, libraries of compounds have been generated and can be used for identification.[28] In integrated GC-MS, the data are displayed as a total ions current (TIC) chromatogram. Such chromatogram relates the sum of signals, forming the mass spectrum, with the retention time from the gas chromatography (GC) column. Additionally, a bar graph displays the mass spectrum which relates the mass intensity with the respective mass to charge ratio.[29]

2.4.3 Definitions

The mass balance in the experimental work was calculated as follows:

$$\text{Hexadecane}_{\text{ before experiment}} = 46.38 \text{ g [60 ml]}$$

$\text{Hexadecane}_{\text{ after experiment}}$= Reactant left in reactor + samples + waste samples + coke, g

$$\text{Mass balance (\%)} = \frac{\text{Hexadecane after experiment}}{\text{Hexadecane before experiment}} * 100$$

Conversion of the reactant was calculated using the following equation:

$$X_t = \frac{C_0 - C_i}{C_0} * 100$$

X_t – conversion of reactant at time t, %;

C_0 - initial molar concentration of the reactant (mol/l);

C_t - molar concentration of the reactant at time t (mol/l).

Selectivity was calculated according to:

$$S_{a,z} = \frac{C_{a,z}}{\sum C_{a+b+c+\cdots,z}} * 100$$

$S_{a,z}$ – selectivity to product *a* at certain conversion (%);

$C_{a,z}$ – molar concentration of the product *a* at a particular conversion (mol/l);

$C_{a+b+c+\ldots,\, z}$ – molar concentration sum of all products at the same conversion (mol/l).

3 Experimental part

3.1 Materials

The list of chemicals used in this research is shown in Table 3.1. The chemicals were used without any purification. The properties of the reactant, hexadecane (n-C_{16}), are listed in Table 3.2.

Table 3.1: List of chemicals

Serial no.	Chemical	Manufacturer	Purity (%)	CAS Number	Chemical formula
1	**Toluene**	Sigma-Aldrich	99.8	108-88-3	$C_6H_5CH_3$
2	**Ethanol**	Sigma-Aldrich	99	64-17-5	CH_3CH_2OH
3	**Pyridine**	Sigma-Aldrich	≥99	110-86-1	C_5H_5N
4	**2-methyl-pentane**	Sigma-Aldrich	Analytical standard	107-83-5	C_6H_{14}
5	**Hexane**	Sigma-Aldrich	Analytical standard	110-54-3	C_6H_{14}
6	**2-methyl-heptane**	Sigma-Aldrich	98	592-27-8	C_8H_{18}
7	**Octane**	Sigma-Aldrich	≥99	111-65-9	C_8H_{18}
8	**2,5-dimethyl-hexane**	Sigma-Aldrich	99	592-13-2	C_8H_{18}
9	**Nonane**	Sigma-Aldrich	≥99	111-84-2	C_9H_{20}
10	**2,6-dimethyl-octane**	Sigma-Aldrich	99	2051-30-1	$C_{10}H_{22}$
11	**2-methyl-nonane**	Sigma-Aldrich	≥98.5	871-83-0	$C_{10}H_{22}$
12	**Decane**	Sigma-Aldrich	≥99	124-18-5	$C_{10}H_{22}$
13	**Undecane**	Sigma-Aldrich	99+	112-21-4	$C_{11}H_{24}$
14	**Dodecane**	Sigma-Aldrich	≥99	112-40-3	$C_{12}H_{26}$
15	**Pentadecane**	Acros-Organics	99	629-62-9	$C_{15}H_{32}$
16	**Hexadecane**	Sigma-Aldrich	99	6765-39-5	$C_{16}H_{34}$
17	**Heptadecane**	Acros-organics	>95	629-78-7	$C_{17}H_{36}$
18	**Octadecane**	Sigma-Aldrich	99	593-45-3	$C_{18}H_{38}$
19	**Heneicosane**	Acros-organics	98	629-94-7	$C_{21}H_{44}$
20	**Tetracosane**	Aldrich	99	646-31-1	$C_{24}H_{50}$

Table 3.2: Properties of the reactant, hexadecane.

Chemical	Formula	Structure	Molar mass (g/mol)	MP (°C)	BP (°C)	Density (g/cm^3)
Hexadecane	$C_{16}H_{34}$	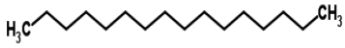	226.45	18	287	0.773

3.2 Catalyst preparation

For simplicity and reference in writing, the catalysts used in this work can be divided into seven series based on metal modification. They are listed in Table 3.3.

Table 3.3: List of the catalyst series.

Series number	Catalyst
Series 1	H-Beta-25, 150 and 300
Series 2	Desilicated H-Beta-150, 300
Series 3	2 wt.% Pt/H-Beta-25, 150 and 300
Series 4	5 wt.% Ni/H-Beta-25, 150 and 300
Series 5	5 wt.% Pt/Al_2O_3: H-Beta-25, 300
Series 6	1 wt.% Ru/H-Beta-150
Series 7	2.5 wt.% Ru/USY-15, 30

3.2.1 Synthesis of proton form catalysts

The catalysts in series 1 were purchased from Zeolyst International as NH_4-Beta-25, NH_4-Beta-150 and NH_4-Beta-300 in a powder form. These Beta zeolites were transformed from ammonium to proton forms, i.e. H-Beta-25, H-Beta-150 and H-Beta-300 by step calcination procedure in a muffle oven. The step calcination temperature program is given in Table 3.4. These calcined proton forms of Beta zeolites were tested and also used for modification with metals, i.e. platinum, nickel and ruthenium or for desilication to obtain larger pore size Beta catalyst.

3.2.2 Synthesis of desilicated catalysts

The pore size modification of H-Beta-150 and 300 for series-2 catalysts was done with desilication using 0.1 NaOH solution. These microporous materials were modified into mesopores ones to study the influence of pore size distribution. The desilicated Beta zeolites were then calcined in a muffle oven by the step calcination procedure as series 1.

Table 3.4: Stepwise calcination procedure for catalysts.

Catalyst		Time (min)	Temperature (°C)
Series 1, 2 H-Beta-25, 150, 300		60	250
	Dwell	40	250
		70	400
	Dwell	240	400
		100	25
Series 3 2 wt. % Pt/H-Beta-25, 150, 300		75	250
	Dwell	50	250
		65	400
	Dwell	180	400
		100	25
Series 4 5 wt. % Ni/H-Beta-25, 150, 300		75	250
	Dwell	50	250
		60	400
	Dwell	120	400
		100	25
Series 6 1 wt. % Ru/H-Beta-150		75	250
	Dwell	60	250
		50	400
	Dwell	180	400
		100	25

3.2.3 Synthesis of metal modified catalysts

3.2.3.1 Synthesis of platinum modified catalysts

The proton H-Beta catalysts were modified with platinum for series-3 using hexachloroplatinic acid, (H_2PtCl_6, Sigma-Aldrich) as a metal precursor by the evaporation impregnation method and dried overnight. The resulting 2 wt.% Pt/H-Beta-25, and 300 catalysts were calcined through a step calcination procedure in a muffle oven, mentioned in Table 3.4.

3.2.3.2 Synthesis of nickel modified catalysts

The proton H-Beta catalysts were modified with nickel for series-4. The proton H-Beta-25, 150 and 300 catalysts were modified with nickel using nickel nitrate $Ni(NO_3)_2$ as a metal precursor by the evaporation impregnation method and then dried overnight. The resulting 5 wt.% Ni/H-Beta-25, 150 and 300 catalysts were calcined through a step calcination procedure in a muffle oven (Table 3.4).

3.2.3.3 Synthesis of a mechanical mixture of H-Beta-300 and Pt/Al_2O_3

The 5 wt.% Pt/Al_2O_3 catalyst of series-5 was purchased from Sigma-Aldrich. This catalyst was mechanically mixed with calcined Beta-300 zeolite catalyst with a 1:1 mass ratio and used in the experimental work.

3.2.3.4 Synthesis of ruthenium modified catalysts

The proton H-Beta catalysts were modified with ruthenium for series-6 using ruthenium chloride ($RuCl_3$) as a metal precursor by the ion exchange method. The resulting 1 wt.% Ru/H-Beta-150 catalyst was dried overnight for complete removal of moisture and then calcined (Table 3.4). Catalysts reduction is described in section 3.4.3.

3.2.3.5 Ruthenium/USY catalysts

The catalysts of series-7 were provided by ETH, Zürich, Switzerland.

3.3 Physico-chemical characterizations of catalysts

Information on the physico-chemical properties of the catalysts is of great importance for the explanation of the catalyst behavior. The catalysts mentioned in Table 3.4 were characterized by the following methods;

1. Nitrogen physisorption.
2. FTIR spectroscopy with pyridine as a probe molecule.

3. Scanning electron microscopy and energy dispersive X-ray microanalysis (SEM-EDX).
4. Transmission electron microscopy (TEM).
5. Thermogravimetric analysis (TGA).
6. Coke extraction and size exclusion chromatography (SEC).
7. Organic elemental analysis (CHNS).
8. Dissolution on zeolites in hydrofluoric acid (HF) and GC-MS analysis.

3.3.1 Nitrogen physisorption

Nitrogen physisorption was applied for the specific surface area and pore volume using Sorptometer 1900 (Carlo Erba Instruments) device. There are different programs used for different textures. In this diploma work, there are two types of support materials used, i.e. microporous Beta zeolite and mesoporous alumina support (in case of platinum catalyst) BET for mesoporous and Dubinin-Radushkevich for microporous materials, were respectively applied. The equipment for analysis is shown in Figure 3.1.

For a typical experiment, a catalyst was dried overnight and ca. 0.25 g catalyst was weighed. An empty burette was outgassed, and then the catalyst was placed inside the burette. The burette was outgassed and heated to 150 °C under pressure lower than 8 mbar for three hours. This procedure was carried out for removal of any entrapped air or water molecule inside the burette, as zeolitic materials contain 10-15% moisture. The outgassed burette was then connected to the instrument for analysis as shown in Figure 3.1b and Figure 3.1c.

a. b. c.

Figure 3.1: (L-R) a. Equipment for degassing of the catalyst, b. Burette connection for analysis, c. Burette setup for analysis in liquid nitrogen and liquid nitrogen flasks.

3.3.2 Fourier-transform infrared spectroscopy (FTIR) with pyridine adsorption/desorption

The FTIR analysis using ATI Mattson FTIR was applied for determination of the Brønsted and Lewis acid sites with pyridine (Sigma-Aldrich) as a probe molecule.

For a typical experimental procedure, a thin self-supported catalyst wafer of around 10-20 mg was pressed and placed in the FTIR cell. The cell was evacuated, and the temperature was raised under vacuum to 450 °C for one hour. The temperature was decreased to 100 °C, and a background spectrum of the sample was recorded. Pyridine was absorbed on the sample for 30 min at 100 °C followed by desorption at 250 °C, 350 °C and 450 °C for one hour with spectra recording between every temperature ramp. The scanning was performed under vacuum at 100 °C. Spectral bands at 1545 cm^{-1} and at 1450 cm^{-1} were used to quantify Brønsted acid and Lewis acid sites, respectively. The extinction coefficient of Emeis was used for calculations.[35]

3.3.3 Scanning electron microscopy and energy disruptive X-ray microanalysis (SEM-EDX)

The scanning electron microscopy was used for characterization of surface morphology, size, shape and distribution of crystals along with its elemental

composition. The elemental analysis of the fresh and spent catalysts was carried out using energy disruptive X-ray analysis. All measurements were done with Leo Gemini 1530 microscope combined with secondary electron and back-scattered electron detectors.

For the analysis, about 10-15 mg of the catalyst was placed on a thin film and coated with carbon to enhance conductivity for a high quality of resulting images.

3.3.4 Transmission electron microscopy (TEM)

The transmission electron microscopy was used for the metal particle size, structure of pores, channels, and periodicity of pores. For characterization JEOL JEM1400 PLUS, JOEL ltd. Japan device available at Laboratory of Electron Microscopy University of Turku was utilized. The ImageJ software was used for determination of the metal particle size from TEM images. The TEM images can be found in Appendix 3.

3.3.5 Thermogravimetric analysis (TGA)

Thermogravimetric analysis was used for both fresh and spent catalysts using SDT Q600, V20.9 Build 20 equipment. For this work, the characterization was carried out in synthetic air. About 10-20 mg of the catalyst was placed onto an aluminum oxide support pan with a reference empty pan and heated from room temperature to 1000 °C with a ramp of 10 °C/min. The volumetric airflow rate used was 100 ml/min.

3.3.6 Organic elemental analysis (CHNS)

Organic elemental analysis was used for determination of carbon, hydrogen, nitrogen and sulfur content in the spent catalysts. ThermoFisher Scientific Flash 2000-Combustion CHNS/O analyzer was used. One of each series of catalysts was selected for this characterization.

3.3.7 Coke extraction and size exclusion chromatography (SEC)

SEC analysis was carried for identification of oligomers/alkylated hexadecane on the catalyst surfaces. For extraction of the oligomer materials, heptane was used as a solvent.[22] About 10-20 mg of the spent catalyst was placed in a round bottom flask (25 ml) with a magnetic stirrer, reflux condenser and 20 ml of heptane (Sigma

Aldrich) was then added to the flask. The round bottom flask was kept in an oil bath, placed on a heater with a magnetic stirrer. The extraction set point was 4 hours at the boiling point of heptane, i.e. 98.4 °C. The stirring rate was kept at around 400 rpm. The condenser temperature was kept at ca. 0-0.5 °C. The volumetric flow rate of the inert gas (5% Ar in 95% N_2) was maintained at 80-100 ml/min.

The resulting solution after 4 hours was then kept on a heater for complete evaporation of heptane at 40 °C with an inert gas (~5% Ar in 95% N_2) flushing the surface of the liquid. Afterwards, the organic residue was dissolved in 10 ml of tetrahydrofuran (THF). The solution was then filtered and placed in bottles for SEC analysis. The concentration of the resulting organic residue was ca. 1-2 mg/ml.

The resulting sample was then placed in GC-vials for analysis. The samples were filtered with 0.2 mm membrane filter PTFE and analyzed by SEC-HPLC that was supplied with two columns, i.e. Jordi Gel DVB 500A (300x7.8 mm) and Guard column (50x7.8 mm). The flow rate was kept at 0.8 ml/min, the temperature at 40°C, while the air pressure was maintained at 3.5 bars.

3.4 Experimental procedures

3.4.1 Reactor system

The experimental work was carried in a batch reactor. The purpose of the experimental part was to study the effect of different catalysts in hydroisomerization of long-chain paraffins. Hexadecane was used as a model compound. Second, the focus was on the selective synthesis of mono-branched products.

The experiments were carried out with seven different types of catalysts mentioned in Table 3.3 at 210 °C and 40 bars for 4 hours. Neat hexadecane was used without any solvent. The catalysts used in the experimental work were sieved to the fraction below 63 μm to avoid the internal mass transfer limitations. The catalyst amounts of 0.5 or 1 gram were used in the experimental work. High stirring speed of 900 rpm was applied to suppress the external mass transfer limitations.

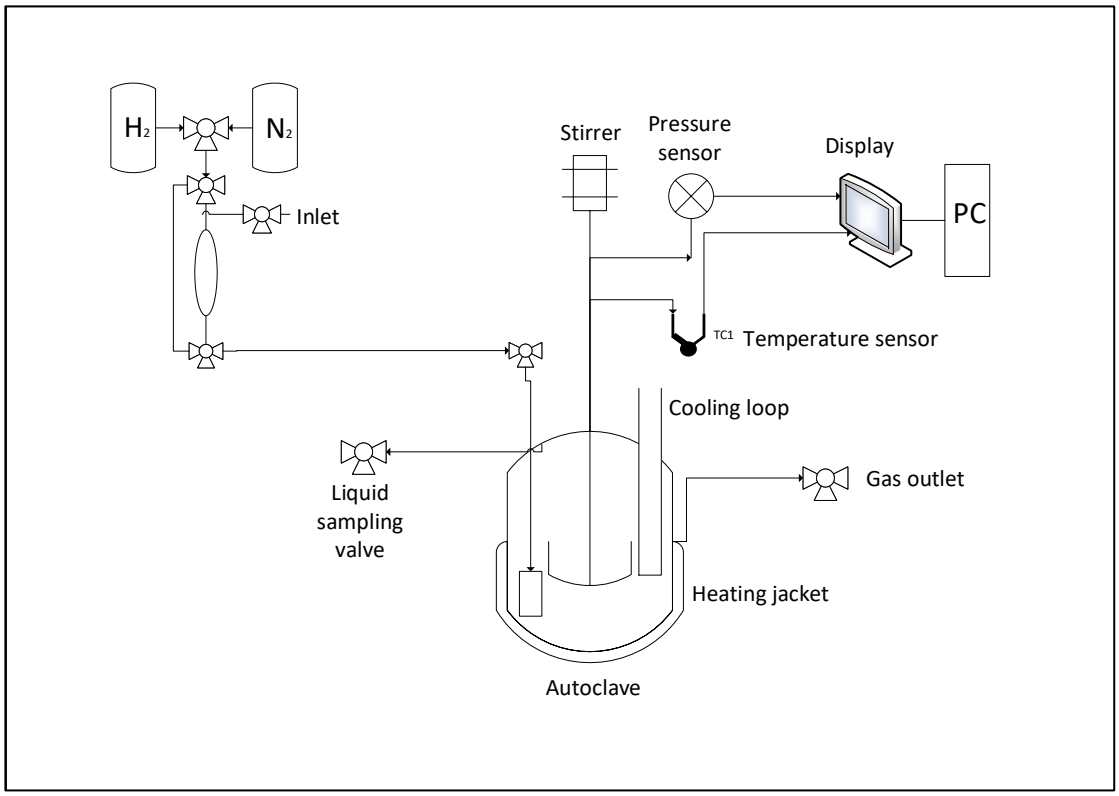

Figure 3.2: Reactor setup.

The reactor (Figure 3.2) was placed in a fume hood for safety purposes. The reactor setup with all controlling systems for pressure, temperature and stirring is shown in Figure 3.2 and visualized in Figure 3.3.

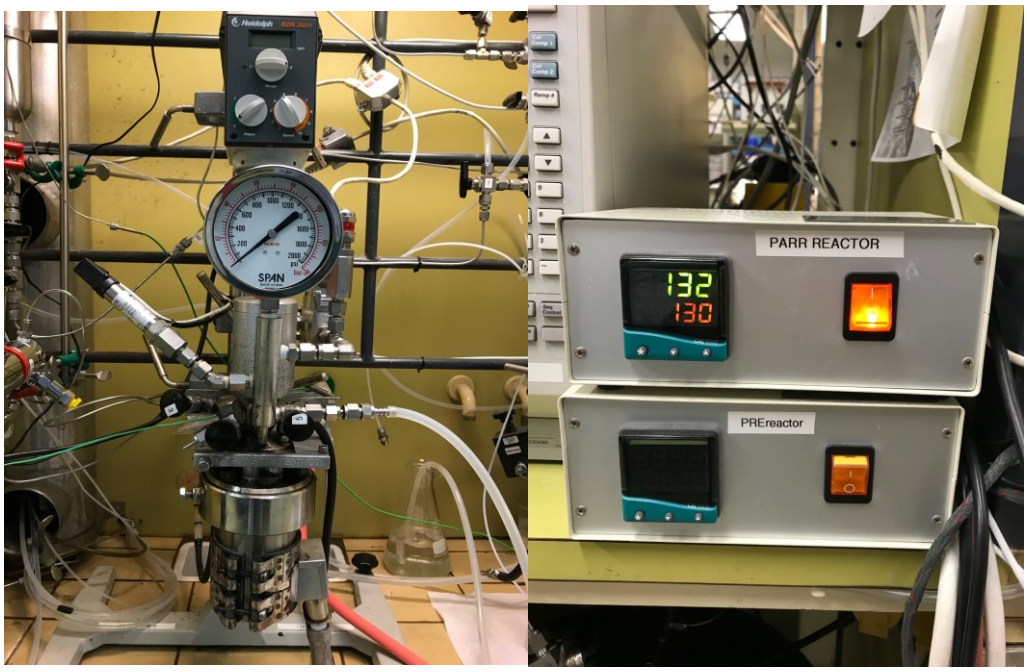

a b

Figure 3.3: Reactor setup, a. Parr autoclave, b. Temperature display.

Isomerization of hexadecane was carried out in a batch reactor (Parr autoclave, 300 ml) equipped with a pressure gauge, a temperature probe, a stirrer, a cooling-water line, a baffle inside the reactor with the liquid and gas sampling lines. For control, a manometer was used for pressure detection. A heating system surrounding the reactor was for heating with a thermocouple placed inside the reactor for temperature readings. A baffle inside the reactor aided a stirrer with curved blades/propellers for the axial flow. The reactor was equipped with a liquid phase sampling valve, and finally, a rubber mounted gas phase sampling valves.

3.4.2 Experimental procedure for hydroisomerization of hexadecane

In a typical experiment, a weighed amount of the catalyst (0.5 or 1 g) and 60 ml of hexadecane were put into the reactor, which was then bolted and checked for any leakages. The reactor was flushed with a small amount of an inert gas (≅95% N_2, ≅5% Ar, AGA) for 10 minutes for complete removal of air and water from the reactor system. This step was important for safety as it removes all oxygen from the reactive environment. The reactor was then flushed with hydrogen (99.99%, AGA) for 10 min for the removal of the inert gas.

After flushing with H_2, the reactor was pressurized slowly to 25 bar. Subsequently, the reactor was heated stepwise to the reaction temperature of 210 °C by 10 °C/min. The stirrer was turned on when the desired pressure and temperature were reached and slowly increased to the final speed of 900 rpm. At this point, the clock was started, and the first gas and liquid phase samples were taken. The reaction conditions were monitored throughout the reaction; a manometer and a stirrer above the reactor showed the pressure and stirring speed while a console besides the reactor setup displayed the reactor temperature.

The gas phase samples were taken at 4 h after the liquid samples to analyze the gas phase products. The gas phase samples were taken in a syringe from the rubber mounted gas phase sampling valve. The liquid phase samples were taken in a glass bottle at six different intervals during the reaction. Three of the first samples were taken at 30 min interval, i.e. 0, 30, 60 min and the last three samples, i.e. 120, 180, 240 min were taken after an hour. A waste sample of ~0.5 ml was taken every time before the actual sampling for purging the leftover of any previous sampling. The liquid phase sample volume was ca. ~0.5-1.0 ml. The last samples were taken at 4

hours (240 min) from the start of the reaction. The bottles for the liquid samples were weighed before and after sampling for calculation of the total mass of liquid samples taken during the reaction, and for calculation of the mass balances.

The reactor was stopped after the last samples, and the cooling water circulation was increased for a gradual decrease in temperature in the reactor. After the temperature was dropped to the room temperature, the reactor was gradually depressurized to atmospheric conditions. The reactor was then opened, and the reaction mixture was collected from the reactor for quantitative analysis. The reactor and stirrer were washed with acetone, and finally, the reactor was cleaned with acetone under stirring.

3.4.3 Catalyst reduction

The catalyst was reduced prior to the reaction in a glass tube in pure hydrogen flow (~40 ml/min) (99.99%, AGA) at different temperatures, depending on the metal on the zeolite i.e. 350, 400 and 450 °C for ruthenium, platinum and nickel for 2 hours, respectively. Prior to this, the heating rate was kept at 10 °C/min. The glass tube containing the catalyst was air-cooled to the room temperature followed by flushing with an inert gas (≅95% N_2, ≅5% Ar) for 10 minutes to remove hydrogen. Ca. ~10 ml of the reactant was added to the catalyst at room temperature to avoid any catalyst oxidation. The ex-situ reduced catalyst was kept overnight under hydrogen and the solvent in the glass tube for the experimental work the following day.

3.4.4 Catalyst regeneration

The spent catalysts from each series were regenerated after the experiments. The spent catalysts were weighed, dried overnight and calcined using the same procedure as for the fresh catalysts (Table 3.4) to remove moisture and coke. After regeneration activity, selectivity and stability of the regenerated catalyst were evaluated.

3.5 Analysis of the reaction products

The samples were analyzed by gas chromatography for analysis of the reaction products and also with gas chromatography equipped with mass spectrometry for identification of the reaction products.

3.5.1 Gas chromatography

The quantitative analyses of the samples were carried by a gas chromatograph (GC) using Agilent QO4+MS6 60 m column for the gas phase and Agilent 123-506E DB-5 (60 m x 328 μm x 0.50 μm column) for the liquid phase samples.

For the gas phase analysis, the gas samples of 0.5 ml were taken directly from the reactor system and injected to the GC. One gas phase samples was taken in the reaction run, before taking the last sample at 4 hours. Hexadecane conversion was determined by diluting the samples to 1-2 mg/ml with respect to hexadecane using a toluene/ethanol mixture as a solvent.

The temperature profile was updated with time as the research progressed for better peak separation for the reaction products. Slow temperature rise was kept at the beginning of the GC temperature program separation of lower boiling point products. Then the temperature elevation was allowed to be slightly higher leading to a better separation of the peaks for higher carbon number products. The column was kept at 300 °C for 10 minutes for the removal of any residues from the samples. The temperature programs for the gas phase (serial number-I) and the liquid phase (serial number-II) samples are presented in Table 3.5-3.7.

3.5.2 Gas chromatography calibration

Calibration for the gas chromatography was done with two GCs. The gas phase GC was calibrated with methane, ethane, ethylene, propane, n-butane and iso-butane. For the liquid phase GC calibration, a test run was conducted, and the reaction products were analyzed and detected with GC-MS. These reaction products, 17 for the liquid phase, were then calibrated for identification of their retention times and calibration curves. The temperature program for the gas and liquid phases are shown in Table 3.5.

Table 3.5: Temperature programs for GC analysis.

Serial Number	Column	Temperature program			
		Column temperature (°C)	Temperature ramp (°C/min)	Final temperature (°C)	Hold (Min)
1	Agilent QO4+MS6 60m			35	8
			20	150	35
			Post run	35	-
2	Agilent 123-506E DB-5 60m*328µm*0.5µm column	80	3	140	-
		-	6	270	-
		-	15	300	10

The retention times for the gas phase products are presented in Table 3.6 and the liquid phase products in Table 3.7.

Table 3.6: Retention times for gas phase products.

Serial number	Gas phase products	Chemical formula	Retention time (min)
1	Methane	CH_4	2
2	Carbon dioxide	CO_2	2.5
3	Ethylene	C_2H_4	3.6
4	Ethane	C_2H_6	4.5
5	Propane	C_3H_8	12.01
6	Iso-butane	C_4H_{10}	14.60
7	n-butane	C_4H_{10}	15.17

Table 3.7: Retention times for liquid phase products.

Serial number	Liquid phase products	Chemical formula	Retention time (min)
1	2-methylpentane	C_6H_{14}	2.6
2	Hexane	C_6H_{14}	2.7
3	2,5-dimethylhexane	C_8H_{18}	3.33
4	Octane	C_8H_{18}	4.0
5	2-methylheptane	C_8H_{18}	5.0
6	Nonane	C_9H_{20}	5.4
7	Toluene	$C_6H_5CH_3$	5.53
8	2,6-dimethyloctane	$C_{10}H_{22}$	6.1
9	2-methylnonane	$C_{10}H_{22}$	6.78
10	Decane	$C_{10}H_{22}$	7.71
11	Undecane	$C_{11}H_{24}$	10.93
12	Dodecane	$C_{12}H_{26}$	14.8
13	Pentadecane	$C_{15}H_{32}$	26.2
14	Hexadecane	$C_{16}H_{34}$	28.85
15	Heptadecane	$C_{17}H_{36}$	31.2
16	Octadecane	$C_{18}H_{38}$	33.3
17	Heneicosane	$C_{21}H_{44}$	37.1
18	Tetracosane	$C_{24}H_{50}$	43.3

3.5.3 Determination of the response factors as a function of the carbon number

Response factors as a function of carbon number for the calibrated compounds were determined. The products were categorized in three groups of products, i.e. linear, mono-branched and bi-branched products. The response factor for unidentified products was interpolated using the response factors of these calibrated products and grouped with their respective groups, shown in Figure 3.4.

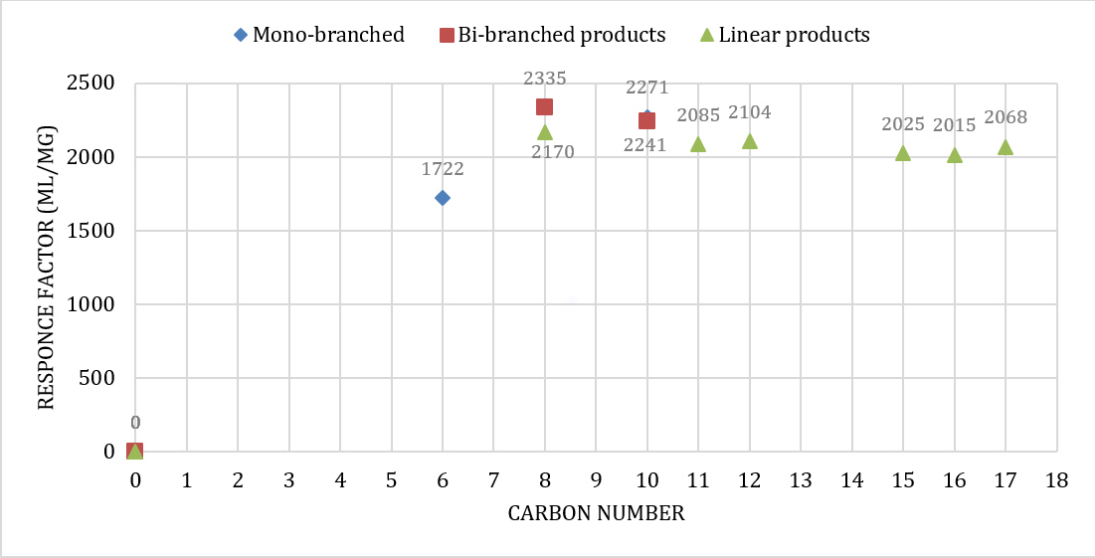

Figure 3.4: Response factors for the calibrated products with respect to carbon number.

4 Results and discussion

4.1 Physico-chemical characterization

4.1.1 Nitrogen physisorption

The specific surface areas of fresh and spent catalysts used in this work are summarized in Table 4.1. Series-1 catalysts showed the highest specific surface area, i.e. beta zeolite, H-Beta-25, H-Beta-150 and H-Beta-300 having values 807, 664 and 805 m^2/g_{cat}, respectively. It has also been reported that the parent H-Beta-150 has a smaller specific surface area than H-Beta-25 and H-Beta-300.[40] There might be two reasons for the lower specific surface area of H-Beta-150 compared to H-Beta-25 and H-Beta 300. First, commercial zeolites were used, and the samples can be taken from different batches and second, calcination temperature can influence specific surface area of the catalysts.

Series-2 catalyst, desilicated H-Beta-150 displayed higher specific surface areas than the parent material, H-Beta-150, i.e. 771 m^2/g_{cat} while the desilicated H-Beta-300 exhibits a lower value of 476 m^2/g_{cat}. Moreover, the desilicated H-Beta-150 had a larger pore size compared to H-Beta-300 with the pore volumes of 0.27 and 0.16 cm^3/g_{cat}, respectively. An increase in the specific surface area of the desilicated H-Beta-150 was due to an increase in pore size and extraction of the framework silicon.[102] Thus, the internal pores were made more accessible with a more exposed surface area. A decrease in the specific surface area of the H-Beta-300 and the decreased pore size could be explained with the higher extraction of silica and alumina from the framework, and much of these elements could be dissolved into the liquid phase. The results from the pore size of H-Beta-300 reveal that the desilication method was not as effective as for H-Beta-150, and the pore size modification was not efficiently achieved.

Series-3 catalysts, platinum exchanged beta zeolites were prepared by evaporation impregnation method and exhibited a reduced specific surface area compared to the parent Beta zeolite material. These catalysts showed specific surface areas of 592, 621 and 686 m^2/g_{cat} for 2 wt.% Pt/H-Beta-25, 2 wt.% Pt/H-Beta-150 and 2 wt.% Pt/H-Beta-300 with pore volumes of 0.21, 0.22 and 0.24 cm^3/g_{cat}, respectively. Among platinum exchanged catalysts the specific surface area decreases as Pt/H-Beta-300> Pt/H-Beta-150> Pt/H-Beta-25. The surface area decreased in the same order as for

parent zeolites. The specific surface area of Pt/H-Beta-25 has decreased more than for other catalysts due to smaller crystals since impregnation of platinum blocks the pores of the zeolite eventually resulting in a lower surface area.[42]

Nickel exchanged beta zeolite (series-4) was prepared by evaporation impregnation method. The specific surface area measurement was only performed for 5 wt.% Ni-H-Beta-150 since it was efficient in hydroisomerization. The specific surface area and pore volume of this catalyst are 629 m^2/g_{cat} and 0.22 cm^3/g_{cat}, respectively.

In series-5, a mechanical mixture of 5 wt.% Pt/Al_2O_3 and H-Beta-300 (1:1 mass ratio) was used, and these mechanical mixtures possessed a low specific surface area of 202.5 m^2/g_{cat} and the lowest pore volume among bifunctional catalysts, 0.017 cm^3/g_{cat}.

Ruthenium exchanged H-Beta-150 (series-6) was prepared by the ion-exchange method and displayed a specific surface area comparable with platinum catalysts. 1 wt.% Ru/H-Beta-150 exhibits a specific surface area of 667 m^2/g_{cat} with the pore volume of 0.23 cm^3/g_{cat}. It can be seen that Pt, Ni and Ru impregnated H-Beta-150 catalysts exhibit comparable specific surface areas and pore volumes.

Ruthenium exchanged ultra-stable Y-zeolite (series-7) showed the lowest specific surface area among all bifunctional catalysts, 104 and 118 m^2/g_{cat} for 5 wt.% Ru/USY-15 and 2.5 wt.% Ru/USY-30, respectively. The pore volumes for these catalysts were comparable to the volumes of beta zeolite, 0.27 and 0.31 cm^3/g_{cat}.

Series-8 in this list contains the spent catalysts. The specific surface area of the spent catalysts had severely decreased after hydroisomerization of hexadecane at 210 °C and 40 bar. The specific surface areas of H-Beta-25 and H-Beta-300 have decreased to 74 and 22.5 m^2/g_{cat}, respectively. Such a severe decrease of the specific surface area of the spent catalysts can be correlated to excessive coking after the hydroisomerization reaction blocking pores of the catalyst, and resulting in a decreased catalyst activity. The coke accumulation on the catalysts was also confirmed by thermogravimetric analysis, size exclusion chromatography and organic elemental analysis (Section 4.1.5, 4.1.6, 4.1.7).

The bifunctional metal beta zeolites exhibited the highest specific surface areas while the bifunctional ruthenium Y-zeolites exhibited the lowest specific surface area among all catalysts.

Table 4.1: Specific surface area and pore volume for catalysts.

Catalysts series.	Catalyst	Specific surface area (m^2/g_{cat})	Pore volume (cm^3/g_{cat})	Ref.
Fresh catalysts				
1	**H-Beta-25**	807	n.a.	39
	H-Beta-150	664	n.a.	
	H-Beta-300	805	n.a.	
2	**H-Beta-150 (Desilicated)**	771	0.27	a
	H-Beta-300 (Desilicated)	476	0.16	
3	**2 wt.% Pt/H-Beta-25**	592	0.21	
	2 wt.% Pt/H-Beta-150	621	0.22	
	2 wt.% Pt/H-Beta-300	686	0.24	
4	**5 w.% Ni/H-Beta-150**	629	0.22	
5	**5 w.% Pt/Al_2O_3 : H-Beta-300 (1:1)**	202	0.017	
6	**1 wt.% Ru/H-Beta-150**	667	0.23	
7	**5 wt.% Ru/USY-15**	104	0.27	
	2.5 wt.% Ru/USY-30	118	0.31	
Spent catalysts				
8	**H-Beta-25**	74	0.026	a
	H-Beta-300	22	0.008	

a. Experimentally found.

4.1.2 Fourier-transform infrared spectroscopy (FTIR) with pyridine adsorption/desorption

Pyridine adsorption desorption with FTIR spectroscopy showed the presence of both Brønsted and Lewis acid sites in all catalysts (Table 4.2). Series 1 Beta zeolite had high Brønsted acid sites. Overall, the Brønsted acid sites decreases as expected in the following order: H-Beta-25> H-Beta-150>> H-Beta-300. The series 2 desilicated H-Beta catalysts and series 3,4,6,7 bifunctional catalysts exhibit less the weak and medium Brønsted acid sites and no strong acid sites except the desilicated H-Beta-150, 5 wt.% Ni/H-Beta-25 and 5 wt.% Ru/USY-15. The same trend was shown in for Lewis acid sites. H-Beta-150 showed a significantly higher acidity than H-Beta-300 similar to their parent materials.

Series 3 and 4, bifunctional catalysts showed the same trend except for 2 wt.% Pt/H-Beta-25, which contained a high amount of weak Brønsted acid sites. Series 3, 2 wt.% Pt/H-Beta-25 catalyst and Series 7, 5 wt.% Ru/USY-15 catalyst had the highest

Brønsted acid sites in all catalysts. However, series 6, the ruthenium exchanged H-Beta-150 showed much higher Brønsted acid sites than 2 wt.% Pt/H-Beta-150. Moreover, series 7, Ru/USY-15 and 30 also displayed high Brønsted acid sites. The Brønsted acid sites on Ru/USY catalysts were higher than in other catalysts. However, according to Park et al., Brønsted acid sites in Y-zeolites are weaker than beta zeolites.[3] The results for series 5, a mechanical mixture of H-Beta and Pt/alumina catalysts could not be obtained.

It was reported in the literature that with metal addition, the acidity of zeolites decreases[2] and this trend was shown by all catalysts except 2 wt.% Pt/H-Beta-25 and 1 wt.% Ru/H-Beta-150. Metal crystals blocking the pore openings and interactions of the metal crystals and acid sites can cause a decrease of acidity after metal impregnation. In addition, Kubička et al.[51] reported that the concentration of strong acid sites is decreasing after impregnation of zeolites with the metal precursor, which can be related to changes in acidity during impregnation upon exposure to the metal precursor solution.

The 2 wt.% Pt/H-Beta-25 showed higher Brønsted acid sites compared to the parent H-Beta-25. The modification of Brønsted acid sites in 2 wt.% Pt/H-Beta-25 was caused by metal precursor hexachloroplatinic acid (H_2PtCl_6), during impregnation by aluminum leaching from the framework or extra framework. This process is known as dealumination, and it can increase the amount of Brønsted acid sites in 2 wt.% Pt/H-Beta-25.[51]

Table 4.2: Brønsted and Lewis acid sites determined by FTIR spectroscopy.

Catalyst	**Brønsted acid sites ($\mu mole/g_{cat}$)**			**Lewis acid sites ($\mu mole/g_{cat}$)**			**Ref.**
	250 °C	**350 °C**	**450 °C**	**250 °C**	**350 °C**	**450 °C**	
Series 1							
H-Beta-25	219	187	125	82	43	25	39
H-Beta-150	176	161	72	43	23	10	
H-Beta-300	54	49	23	28	9	4	
Series 2							

H-Beta-150 (Desilicated)	155	131	96	69	30	9	
H-Beta-300 (Desilicated)	25	20	0	33	20	0	
Series 3							
2 wt.% Pt/H-Beta-25	300	16	0	88	2	0	
2 wt.% Pt/H-Beta-150	69	3	0	17	9	3	
2 wt.% Pt/H-Beta-300	33	2	0	12	5	0	
Series 4							a
5 wt.% Ni/H-Beta-25	110	95	54	191	113	64	
5 wt.% Ni/H-Beta-150	74	60	0	137	89	0	
Series 6							
1 wt.% Ru/H-Beta-150	200	31	0	25	2	0	
Series 7							
5 wt.% Ru/USY-15	321	7	4	42	3	1	
2.5 wt.% Ru/USY-30	207	7	0	39	5	0	

(a) Experimentally found in this work.

4.1.3 Scanning electron microscope and energy dispersive X-ray microanalysis (SEM-EDX)

Relevant SEM micrographs are presented here while other micrographs are given in Appendix 2. All micrographs presented are on the scale of 200 nm with 25000 magnification.

SEM micrographs for H-Beta-25, 150 and 300 show uniform round shaped particles with well-defined structures having average sizes of 60-140 nm, 80-190 nm and 0.4-1.0 μm respectively, as was reported by Liu et al.[48] The desilicated H-beta-150 and 300 possess the same zeolite structure as the parent materials (Appendix 2, Figure A2.2).

The fresh and spent SEM micrographs for Pt/H-Beta-25 catalysts (Figure 4.1) do not show any change in the size and shape of the zeolite after hydroisomerization. It can be concluded from Table 4.4 that leaching of platinum occurred from Pt/H-Beta-25 during hydroisomerization, although Si/Al remained nearly the same. Analogous spherical shape and structure can be seen in 1 wt.% Ru-H-Beta-150 catalyst (Figure 4.2).

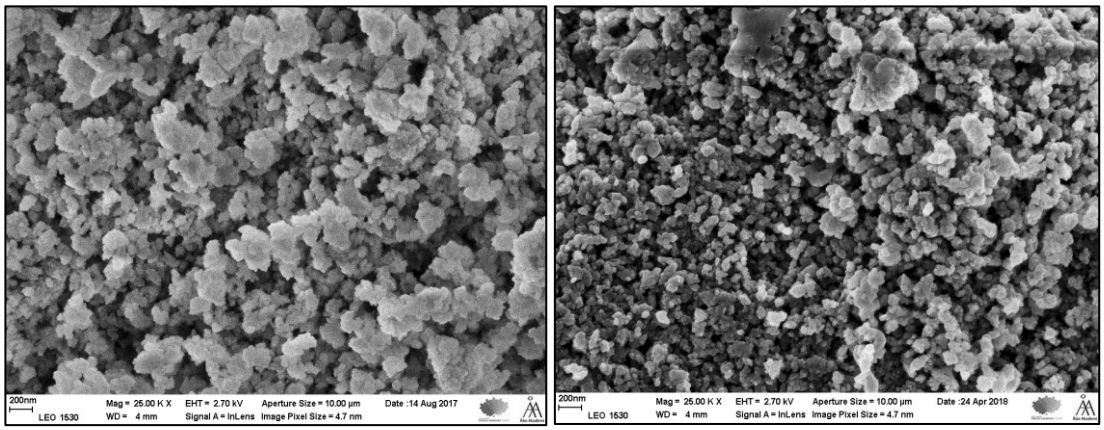

a b

Figure 4.1: SEM images for a) the fresh and b) the spent Pt/-H-Beta-25.

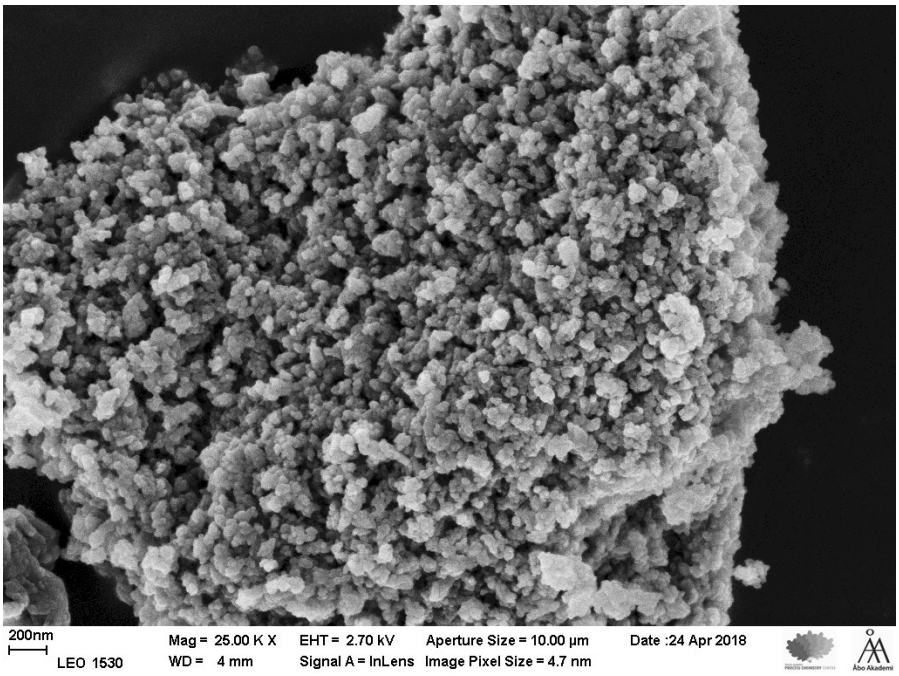

Figure 4.2: SEM image for the fresh 1 wt.% Ru/H-Beta-150 catalyst.

The SEM micrograph for the regenerated 5 wt.% Pt/alumina and H-Beta-300 mechanical mixture shows spherical structures with some elongated structure, which can be originated from the alumina particles in the mixture. However, other possibilities still exist due to the complexity of the reaction mixture.

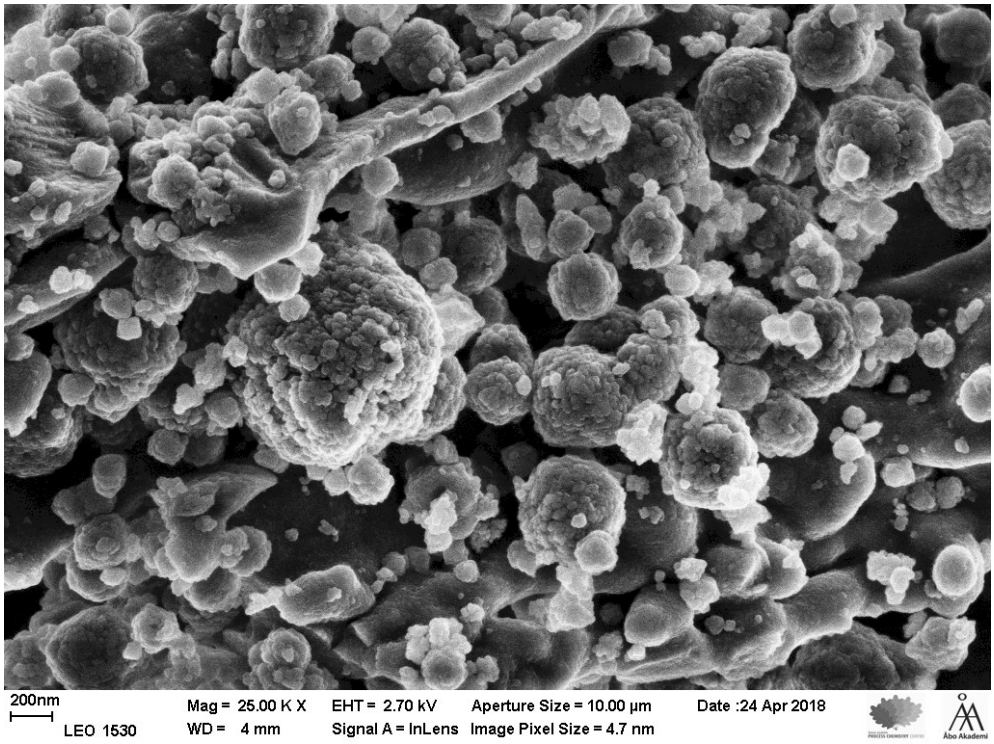

Figure 4.3: SEM micrograph of regenerated 5 wt.% Pt/Al_2O_3: H-Beta-300 mixture.

The elemental composition of some of the catalysts analyzed by SEM-EDX, metal-to-metal ratios in the bifunctional catalysts along other metals is displayed in Table 4.3. The EDX results show a higher platinum loading for 2 wt.% Pt/H-Beta-25 and 300 while a lower metal loading was achieved for the ruthenium catalyst. Sodium was found in the desilicated H-Beta-150 catalyst while it was absent in desilicated H-Beta-300. This could be due to desilication performed in 0.1M NaOH solution, and careful washing was not carried out.

Table 4.3: Results from EDX analysis from the bifunctional catalysts. The amounts of different elements are given in wt.%.

Catalyst	**O**	**Al**	**Si**	**Other elements**	**Si/Al**	**Si/Pt, Si/Ru**
Desilicated H-Beta-150	52.6	3.7	43.1	Na=0.5	11.6	n.a.
Desilicated H-Beta-300	53.0	1.4	45.5	n.a.	32.5	n.a.
2 wt.% Pt/H-Beta-25	51.5	3.4	42.6	Pt=2.5	12.5	17
2 wt.% Pt/H-Beta-300	52.1	0.73	45.1	Pt=1.98	61.7	22.7
1 wt.% Ru/H-Beta-150	52.7	1.5	44.8	Ru=0.81	29.8	55.3

Mechanical mixture (1:1) 5 wt.% Pt/alumina: H-Beta-300 (Regenerated)	43.7	47.7	0.7	Pt=4.8, F=2.5, S=0.3	0.014	0.14
Spent 2 wt.% Pt/H-Beta-25	51.8	3.3	42.9	Pt=1.9	13	22.5

n.a. Not available.

4.1.4 Transmission electron microscopy (TEM)

Transmission electron microscopy allows to analyze the catalyst structure and determine active metal cluster size (Table 4.4). It should be mentioned that this characterization was not carried out for all catalysts used in the experimental work, but for the best catalysts with respect to hexadecane conversion, i.e. one of each catalyst series was selected and characterized.

Table 4.4. Metal particle size determined from TEM images.

S. No.	Catalyst	Size max. (nm)	Size min. (nm)	Av. particle size (nm)	Dispersion* (%)
1	**2 wt.% Pt-H-Beta-25**	8.5	1.28	3.3	30.3
2	**2 wt.% Pt-H-Beta-300**	42.0	4.1	14.8	6.75
3	**5 wt.% Ni-H-Beta-25**	22.3	4.0	9.38	10.6
4	**1 wt.% Ru-H-Beta-150**	24.4	3.6	8.83	11.3
5	**5 wt.% Ru-H-USY-15**	31.6	4.2	15.05	6.64

*Dispersion calculated by 100/average particle size.

For TEM characterization the catalysts were pre-reduced similarly as for the hydroisomerization. It was observed that the zeolite crystal size has a direct impact on the active metal particle size (Table 4.4). For 2 wt.% Pt/H-Beta-25 with a smaller crystal size, the metal particle size was the smallest, i.e. 3.3 nm, while 4.95 nm was reported for 2 wt.% Pt/H-Beta-150 and 14.8 nm for 2 wt.% Pt/H-Beta-300. In general, the particle size of different metals on the same support material can have a different particle size. For example, the average particle size for 5 wt.% Ni/H-Beta-25, 1 wt.% Ru/H-Beta-150 and 5 wt.% Ru/USY-15 was 9.38, 8.83 and 15.05, respectively. TEM characterization for the spent catalyst was not performed.

The average particle size from Table 4.4 suggests that all metal crystals were larger than the pore opening of the supports. Thus, it can be concluded that large fractions of

metal crystals were located on the external surface of the supports, since, the pore volume of Beta zeolites and Y-zeolites are 7.4 Å and 5.6 x 6.5 Å, respectively.[3]

The TEM image for 2 wt.% Pt/H-Beta-25 along with the average particle size histogram is presented in Figure 4.4, while other histograms with their average particle size histogram are given in Appendix 3.

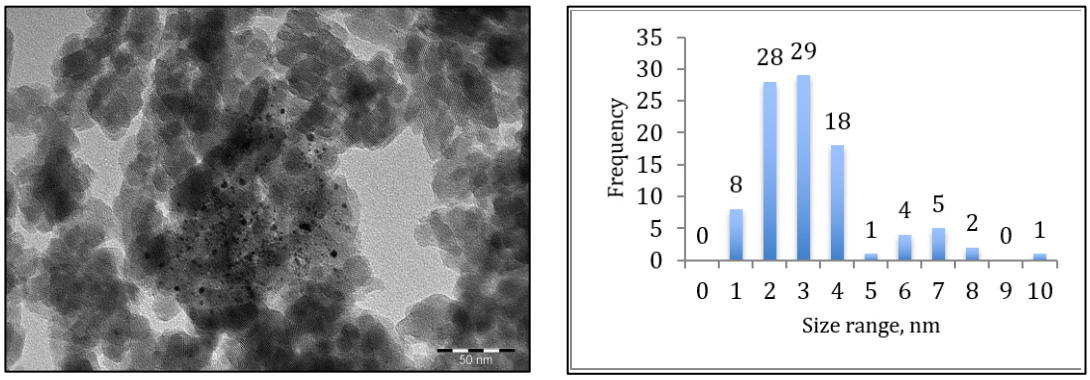

a b

Figure 4.4 (a): TEM image and
(b) Average particle size histogram for 2 wt.% Pt/H-Beta-25.

4.1.5 Thermogravimetric analysis (TGA)

Thermogravimetric analysis (TGA) was carried out for the fresh and spent catalysts to determine coke deposition on the catalyst surface during hydroisomerization of hexadecane, performed at 210 °C, 40 bar. The TGA analysis was performed to determine the amount of organic residue on the spent catalyst due to paraffinic compounds and include that into the GC-determined mass balance.

The TGA results revealed that 2 wt.% Pt/H-Beta-25 exhibited the lowest coke content, i.e. 7 wt.% and the highest was shown by 5 wt.% Ni/H-Beta-25, i.e. 54 wt.%. 1 wt.% Ru/H-Beta-150 exhibited 43 wt.% of coke which was much higher than in the platinum catalyst. The amount of coke in 1 wt.% Ru/H-Beta-150 was close to the one observed in 5 wt.% Ni/H-Beta-150 catalyst. The fresh catalysts peaks are present in lines while the spent catalyst result is given in dotted lines in derivative temperature difference (DTD).

A typical TGA Derivative temperature difference (DTD) shows four main regions based on temperature. The first region is below 150 °C in which moisture is removed with another solvent (if present in samples) and desorption of gases entrapped in the samples. The second region (150-250 °C), indicates the loss of lower molecular

weight decomposition products. The third region of (250-500 °C), shows the onset thermal decomposition of higher molecular weight products. The last region above 500 °C implies carbonization of hydro-carbonated compounds which pyrolysed with no volatiles formation related.

Table 4.5: Coke content in different catalysts based on thermogravimetric analysis data.

Catalyst series	Spent catalyst	Organic coke content in nitrogen (wt.%)*
3	**2 wt.% Pt/H-Beta-25**	7
4	**5 wt.% Ni/H-Beta-25**	54
6	**1 wt.% Ru/H-Beta-150**	43

*Coke analysis in nitrogen environment using the corresponding spent catalysts used in hydroisomerization of hexadecane at 210 °C and 40 bar.

The Derivative temperature difference (DTD) for 2 wt.% Pt/H-Beta-25 is presented in Figure 4.5, showing the results for the fresh and spent catalysts. The weight loss in the fresh catalyst was 13% corresponding to the moisture content in the catalyst and thermal decomposition of the catalyst. Temperature changes were consistent with the weight loss and showed a uniform peak in the temperature range of 150-250 °C. The weight loss for the spent catalysts shows three distinct descent peaks. The first descend refers to the moisture removal of 3.8 wt.% of the total weight for the spent catalysts from start to 150 °C with a gradual increase in the temperature peak. The second descend demonstrates the loss of lower molecular weight reaction products, i.e. 9.2 wt.% of the total weight that was adhered to the catalysts in the temperature range of 150-225 °C. An increase in the temperature peak of 25 °C shows the thermal decomposition of these products. A significant endothermic peak can be seen at 200 °C. The third descend shows the decomposition of the higher molecular weight organic coke material of 6.5 wt.% of the total weight with a slight increase of 1 °C in the temperature peak in range of 200-350°C. A small descend in the temperature peak shows a minor coke amount adhered to the spent catalysts.

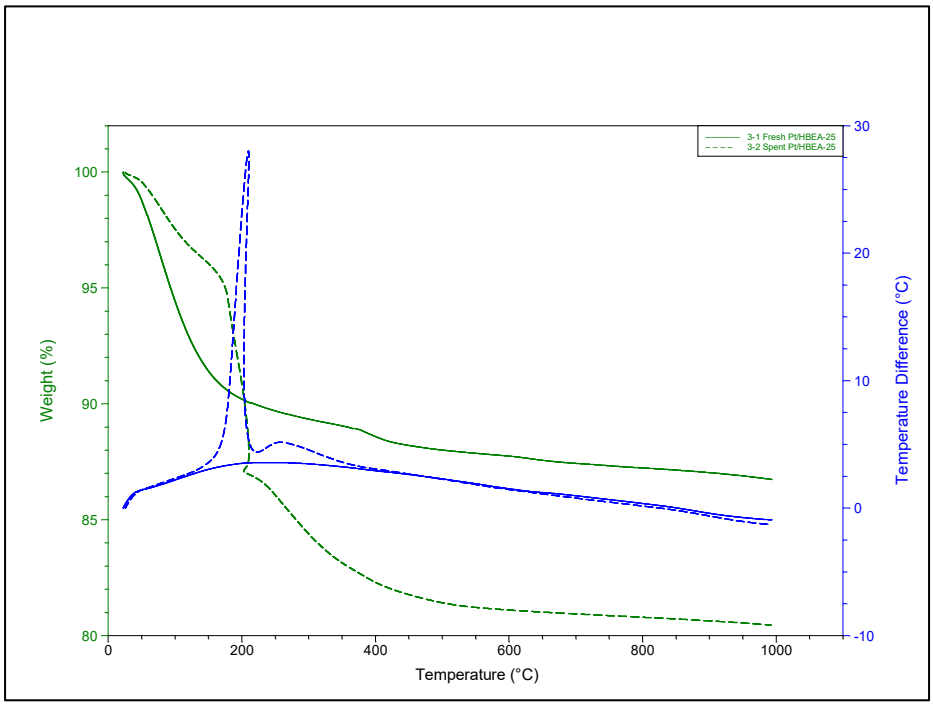

Figure 4.5: Derivative temperature difference (DTD) and weight loss for the fresh (solid line) and the spent (dotted line) 2 wt.% Pt/H-Beta-25 catalysts.

The DTD for 5 wt.% Ni/H-Beta-25 (Appendix 4) shows the results for the fresh and the spent catalysts. This catalyst exhibits the highest amount of coke deposition on the spent catalysts as shown by the TGA results. The fresh catalyst has shown 12 wt.% of the total weight loss, including both moisture removal and later thermal decomposition of the catalyst. The TGA of the spent catalyst displays two distinct slopes, which can be correlated to nickel. The first slope shows the removal of moisture and volatile lower molecular weight compounds in the spent catalyst from the start until 220 °C. The main weight loss was incorporated at 220 °C, i.e. 60 wt.% of the total weight. The second descent was almost linear with the temperature ramp with only 6 wt.% loss of the total weight and a high temperature peak, which was related with a high heat release for higher molecular weight organic coke. A major endothermic peak can be seen at 250-600 °C.

The DTD for 1 wt.% Ru/H-Beta-150 (Appendix 4) displays the results for the fresh and the spent catalysts. This catalyst had a much higher coke content than the platinum catalysts and being marginally lower than in the spent nickel catalyst. The fresh catalyst has a different weight loss curve than other catalysts analyzed by TGA. In other catalysts, the highest weight loss occurred in the volatile region, where moisture was removed, but the actual decomposition of the catalyst material was not

significant. In 1 wt.% Ru/H-Beta-150 catalyst, a weight loss was initially, i.e. 6 wt.% between 50 and 250 °C. The largest weight loss, i.e. 12 wt.% occurred at elevated temperature, where decomposition of the material occurred, and a major endothermic peak can be seen at 250-400 °C. The TGA of the spent catalyst shows an analogous pattern with two peaks similar to nickel catalysts. A slight change in the TGA curve was, however, visible in the elevated temperature range. The first peak shows the removal of moisture and volatile low molecular weight components where the main total weight loss occurred, i.e. 58 wt.%. The second peak was interesting, as the temperature ramp gradually increases, the temperature peak increases, but at ~311 °C, a sudden rise in temperature can be seen without sudden a decrease in the catalyst total weight loss. It can be deduced that the higher molecular weight organic coke was decomposed, i.e. 2-3 wt.%, in 325-375 °C temperature range, which resulted in a sudden temperature elevation. This behavior can also be seen in nickel catalyst, however, displaying a steady weight decrease with a very small peak in the same temperature range.

The coke content in 2 wt.% Pt/H-Beta-25 was significantly smaller than in other catalysts. This behavior was predominantly due to its superior hydrogenating ability compared to other metals, i.e. nickel and ruthenium, used in other catalysts.[50] The data from the TGA analysis of coke were in accordance with the organic elemental analysis for the platinum catalyst (Section 4.1.7).

4.1.6 Coke extraction with heptane and size exclusion chromatography (SEC)

Size exclusion chromatography was utilized to investigate alkylated hydrocarbons present in the spent catalysts The SEC results for Ru/H/Beta-150 are displayed in Table 4.6 while other results with the calibration curve and the corresponding table are shown in Appendix 5.

Identification and qualitative characterization of adsorbed organic compounds on 1 wt.% Ru/H-Beta-150 are shown in Table 4.6. In size exclusion chromatography, peaks of heavy components appear at shorter retention times followed by lighter components. The heaviest coke (i.e. 12.91 min) was not identified while other coke components were identified with respect to their retention times. SEC analysis reveals that all organic compounds were heavy hydrocarbons and only 0.5 wt.% was lighter than hexadecane, the reactant used for hydroisomerization reaction. This reveals that

alkylation reaction was also taking place together with hydroisomerization and hydrocracking.

Table 4.6: The retention times with the corresponding molecular weights of adsorbed organic compounds determined from SEC for Ru/H-Beta-150.

1 wt.% Ru-H-Beta-150		
Retention time (min)	**Molecular weight (g/mol)**	**Area (%)**
12.91	n.a.[a]	23.4
18.87	1600	2.20
19.70	1280	6.70
21.08	682	32.6
21.86	578	34.6
24.15	104.1[b]	0.50

n.a. Not available.

[a] The coke components eluted at 12.91 and 24.15 min could not be found due to sitosterol calibration limitations.

[b] This value was acquired from polystyrene calibration.

The SEC results for extracted adsorbed organic compounds from 2 wt.% Pt/H-Beta-25 are shown in Table 4.7. About 91.5 wt.% of coke is light coke while the rest is heavy coke. Even if the latter could not be identified, from the weight percentage it could be deduced that coke from the platinum catalyst, composed mainly of light compounds was unique, which is related to superior hydrogenation ability of platinum preventing coke formation or forms lighter coke components.[50]

Table 4.7: The retention times with the molecular weights of the extracted coke analyzed SEC for Pt/H-Beta-25.

2 wt.% Pt-H-Beta-25		
Ret. Time (min)	**Molecular weight (g/mol)**	**Area (%)**
13.41	n.a.[a]	0.6
18.48	n.a.[a]	1.2
19.02	n.a.[a]	1.6
19.75	1250	5.1
21.13	682	33.6
21.88	500	57.9

[a] The coke components eluted at 13.41, 18.48 and 19,02 min could not be found due to sitosterol calibration limitations.

In comparison, lighter coke (ca. 8.5 wt.%) was formed over 2 wt.% Pt/H-Beta-25 while the largest amounts of coke were formed over 5 wt.% Pt/alumina: H-Beta-300, 5 wt.% Ru/USY-15 and desilicated H-Beta-150, i.e. 55, 57 and 40 wt.%, respectively. Moreover, the other half coke was lighter with 10-13 wt.% of medium coke. 1 wt.% Ru/ H-Beta-150 and 5 wt.% Ni/H-Beta-25 formed reasonably less heavy coke, ca. 26 and 32 wt.%. In conclusion, all results were comparable as almost half coke was towards the heaviest and unknown while the other half coke was identified.

4.1.7 Organic elemental analysis (CHNS)

Organic elemental analysis shows an increase in all elements, i.e. nitrogen, carbon and hydrogen after hydroisomerization of hexadecane except sulfur at experimental conditions of 210 °C and 40 bar.

The highest carbon content of 49-51wt.% was indicated for desilicated H-Beta-150, Ni-H-Beta-25, Ru-H-Beta-150 and Ru-USY-15. The lowest carbon content was determined in Pt-H-Beta-25, i.e. 9.8 wt.%. The mechanical mixture of Pt-Al_2O_3 (Sigma-Aldrich, commercial) and H-Beta-25 showed a lower carbon content, i.e. 38 wt.%. It should, however, be noted that a low carbon content from the mechanical mixture of Pt-Al_2O_3 and H-Beta-25 is due to reduced acidity function by the Pt/alumina and only Beta zeolite contributing in coking.

These results illustrate severe coke formation on the catalysts after the reaction and explain their low catalytic activity. A lower carbon content from Pt-H-Beta-25, 9.8 wt.%, suggests a superior hydrogenating function in this case compared with other metals over the same beta type zeolite.[50] It can be seen that the non-metallic desilicated H-Beta-150 and non-platinum catalysts resulted in the same carbon content. These results suggest their low hydrogenating activity, forming more coke on the catalyst surface. Coke blocks the pores and active sites resulting thus in catalyst deactivation.

The elemental analysis shows that hydrogen is present in all spent catalysts. In hydroisomerization, the reaction proceeds in the presence of hydrogen. The amount of hydrogen is comparable in all catalysts except Pt-H-Beta-25, i.e. 7.1-9.4 wt.% and 1.8 wt.% respectively. The hydrogen to carbon molar ratio for normal alkanes is 2.0, and coke analysis confirms the absence of aromatic hydrocarbons. The low hydrogen content from Pt-H-Beta-25 is in line with the suggestion of superior hydrogenation

activity of platinum. This was also evident from the lower hydrogen content of 71 wt.% in the mechanical mixture of Pt-Al_2O_3 and H-Beta-25.

Nitrogen amount in the fresh catalysts would be zero as the catalysts were calcined and reduced before the experiment. The nitrogen amount after hydroisomerization was negligible for all spent catalysts, slightly higher for Pt-H-Beta-25 and Ni-H-Beta-25, whereas it was considerably smaller in all other catalysts. This nitrogen may have resulted from the flushing reactor with an inert gas containing nitrogen.

Sulfur was not found in any catalysts revealing no contamination and impurity traces in the spent catalysts.

Table 4.7: CHNS result of bifunctional catalysts.

Sample (Spent catalyst)	**Weight (mg)**	**N (% w/w)**	**C (% w/w)**	**H (% w/w)**	**H/C Molar ratio**
Cystine (Standard)	1.84	11.11	30.11	5.02	2.0
TR-15, H-Beta-150 (desilicated)	2.05	0.01	51.11	9.44	2.2
TR-5, 2 wt.% Pt/ H-Beta-25	1.95	0.08	9.86	1.89	2.3
TR-7, 5 wt.% Pt/Al_2O_3, H-Beta-25 (1:1)	2.26	0.01	38.62	7.15	2.2
TR-17, 5 wt.% Ni/H-Beta-25	2.27	0.07	50.48	9.41	2.2
TR-14, 1 wt.% Ru/H-Beta-150	2.01	0.03	51.31	9.45	2.2
TR-18, 5 wt.% Ru/USY-15	2.16	0.01	49.08	8.98	2.2

n.a. Not available.

The hydrogen to carbon molar ratio (Table 4.7) suggests that there were no aromatic compounds in the spent coke and only linear hydrocarbons are present in spent coke after the reaction.

Coke analysis from three techniques for the spent catalysts is listed in Table 4.8. From the table, it can be concluded that the platinum catalyst was least susceptible to coke formation and resulted in prolonged catalyst activity, which gave a higher yield of methyl-pentadecane (iso-C_{16}).

Table 4.8: Coke analysis of the spent catalysts by different techniques.

Catalyst	Coke analysis		
	SEC[a]	CHNS[b]	TGA[b]
2 wt.% Pt/H-Beta-25	1.0	9.8	7
5 wt.% Ni/H-Beta-25	0.72	50.5	54
1 wt.% Ru/H-Beta-150	3.2	51.3	43

[a] Relative amounts of heavy alkylated hexadecane in the spent catalyst.

[b] Coke content

4.2 Evaluation of catalytic properties

In this work, seven series of catalysts were studied for hydroisomerization of long-chain hydrocarbons, using hexadecane as a model compound. The most interesting results will be presented here while a detailed list with catalytic data can be found in Appendix 6.

A preliminary experiment (TR1) with H-Beta-300 was performed for 4 hours at 210 °C, 40 bar and 900 rpm of the stirring rate. The experiment was performed for evaluation of catalytic results along with possible gas and liquid phase products. Using GC-MS, these products were identified, and the liquid phase products were acquired for calibration. The gas phase calibration had been already completed prior to the current work. Furthermore, the experimental conditions were for all catalysts 210 °C, 40 bar and 900 rpm if not specified otherwise.

4.2.1 Interpretation of GC chromatograms

For gas and liquid phase samples Agilent QO4 and DB-5 columns were used. Chromatograms for each sample were obtained and interpreted for different reaction components. Figure 4.6 shows a sample chromatogram withdrawn at 4 hours after the start of the reaction.

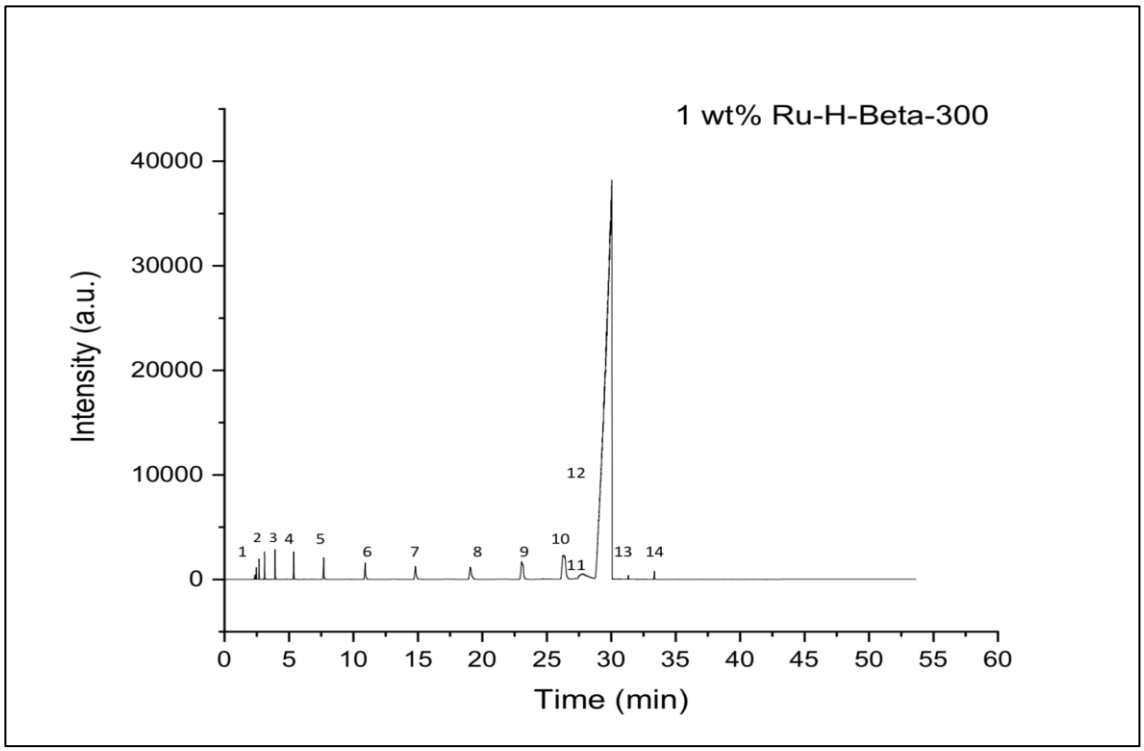

Figure 4.6: A chromatogram of a liquid phase sample at 4-hour reaction time for 1 wt.% Ru/H-Beta-300 catalyst. Notation:

1. Cracked hydrocarbons, 2. Iso-octane, 3. Octane, 4. Nonane, 5. Decane, 6. Undecane, 7. Dodecane, 8. Tridecane, 9. Tetradecane, 10. Pentadecane, 11. Methyl-pentadecane, 12. Hexadecane, 13. Heptadecane, 14. Octadecane.

The long column was calibrated using different hydrocarbons in the gas and liquid phase along with modifications in the temperature programs to obtain an effective peak separation displayed in Chapter 3, Table 3.5, 3.6 and 3.7, respectively.

4.2.2 Effect of metal and acidity on gas-phase products

Gas-phase samples were taken at 4 hours of the reaction time. The gas-phase results are normalized by the catalyst mass and the lowest value and shown for the highest gas products in each catalyst series. Figure 4.7 displays the identified gas-phase products for all series used in this work. Table 4.9 shows the total peak area and a number of unidentified gas-phase products. The most prominent results are displayed here while other results are given in Appendix 9.

The highest amounts of gas products were formed by 5 wt.% Ni/H-Beta-150 while the lowest one was measured for 2.5 wt.% Ru/USY-30, is negligible. H-Beta-25 displayed the best selectivity to gas products among all catalysts and formed the

highest amount of iso-butane. Platinum exchanged H-Beta-300 and a mechanical mixture of Pt/alumina and H-Beta-300 exhibited mainly methane with traces of other gases. The desilicated H-Beta-300 and nickel-exchanged beta-150 revealed an analogous trend in the formation of different gas-phase products. The nickel catalyst gave, however, an excessive number of unknown gaseous products heavier than the calibrated ones (Table 4.9). Ruthenium exchanged H-Beta-150 showed the same amount of gaseous products as desilicated H-Beta-300. 1 wt.% Ru/H-Beta-150 showed a higher amount of ethane and propane than iso-butane. Propane was present in all gas samples while ethane and butane were seen in only a few samples. Branched butane was present in all samples except in 2 wt.% Pt/H-Beta-300. The higher amount of isobutane was observed over highly acidic H-Beta-25 and 2 wt.% Pt/H-Beta-25.

A high gas amount obtained with the nickel catalyst is typical as nickel has a high tendency for forming gaseous products. However, a high methane content from 2 wt.% Pt/H-Beta-300 was unexpected.

Few gas-phase samples were taken at 0 min to investigate if cracking products were formed in the gas phase. In the gas phase, several products, calibrated and non-calibrated ones were formed. These products were generated directly from n-hexadecane transformations analogous to the work of Batalha et al.[2,4]

The presence of methane and lighter gas-phase products clearly indicates a hydrogenolysis reaction. This was contrary to the literature, not reporting low molecular gas-phase products.[2,3]

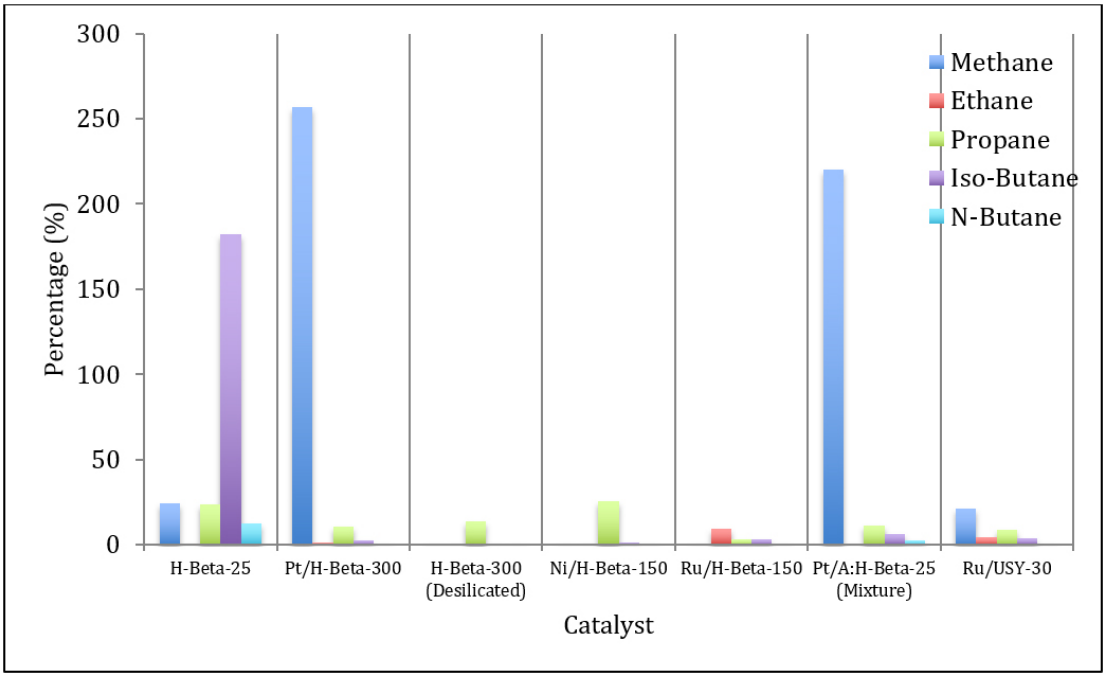

Figure 4.7: The identified gas-phase products for all catalyst series.

The unidentified gas products were present in all gas samples. 5 wt.% Ni/H-Beta-150 showed the highest number of unknown gaseous products in which most were heavy gases eluting at long retention times. These gases may be formed due to either nickel or the medium and low Brønsted acid sites present in the catalyst. H-Beta-25, 1 wt.% Ru/H-Beta-150 and desilicated H-Beta-300 displayed a high number of gaseous products. Formation of heavy gases from 5 wt.% Ni/H-Beta-150 and 1 wt.% Ru/H-Beta-150 is in line with the spent catalysts analysis, displaying the presence of heavy organic compounds. Moreover, low metal dispersion (6.7 to 11%) might also contribute to the formation of heavy gases. For comparison 2 wt.% Pt/H-Beta-25 with 30% dispersion showed very low amounts of short chain hydrocarbons in the gas phase (Appendix 9). Among these catalysts, H-Beta-25 exhibited formation of lighter gases. Ruthenium modified H-Beta-150, desilicated H-Beta-300 along with 2 wt.% Pt/H-Beta-300 and mechanical mixtures were able to produce heavy gases. Ruthenium exchanged Y-zeolite generated only low amounts of gases among all the catalysts used. Lower amounts of gaseous products over Ru/USY zeolites can result from their less low acidity, metal dispersion and specific surface area (Table 4.1. 4.2).

Table 4.9: The number of unidentified peaks and a total peak area of the gaseous products for all catalyst series.

Catalyst	Number of unidentified peaks	The total area of in the GC analysis of the formed gaseous products normalized by catalyst mass
H-Beta-25	6	18284
2 wt.% Pt/H-Beta-300	4	18424
H-Beta-300 (Desilicated)	5	24100
5 wt.% Ni/H-Beta-150	11	57241
1 wt.% Ru/H-Beta-150	5	21089
5 wt.% Pt/A: H-Beta-25 (1:1 mass ratio)	4	15704
2.5 wt.% Ru/USY-30	3	92

4.2.3 Liquid-phase hydroisomerization

4.2.3.1 Conversion of hexadecane isomerization

4.2.3.1.1 Beta zeolites

The results for hydroisomerization of hexadecane over beta zeolites are displayed in Figure 4.8. There are different masses of catalysts used in these experiments. Thus, the conversions were plotted as a function of normalized time (multiplication of time with mass) in order to compare the results (Table 4.10).

The results for H-Beta-300b and H-Beta-300c (Figure 4.8) in which two different catalysts masses were used showed clearly that with a high catalyst amount the gas liquid mass transfer limitations are present since lower conversion levels were obtained in these experiments in comparison with the ones with a small mass of catalyst. The same behavior was also seen in the metal-acid bifunctional catalyst (Figure 4.9, 4.10). Thus, it was decided to compare different catalysts using the catalysts mass of 0.5 and 1 g.

The results demonstrate that H-Beta-300b, H-Beta-300c and desilicated H-Beta-150 had the highest conversion ca. 12% at the end of experiments while H-Beta-25a and H-Beta-150a exhibited 11% conversion. H-Beta-300a had 10% conversion, and the lowest conversion was shown by desilicated H-Beta-300d by 7%.

Conversion for H-Beta-25a and H-Beta-150a is similar due to their analogous acidity and comparable crystal sizes. H-Beta-300a displayed the lowest conversion of all beta zeolites most probably due to its mild acidity. The desilicated H-Beta-150d exhibited conversion higher compared to H-Beta-150a. This increase could be correlated with an increased pore size, which enabled shape selectivity towards the branched hexadecane. Similar acidity for the desilicated material compared to H-Beta-150a contributed to an increase in the overall conversion over parent H-Beta-150a (Table 4.2). The desilicated H-Beta-300d had a lower conversion than H-Beta-300a, which can be linked to the diminished pore size and decreased acidity. Moreover, a lower conversion of H-Beta-300 catalysts and desilicated H-Beta-300 can be linked to a larger crystalline structure of zeolite, and longer diffusion paths compared to a smaller crystalline size of H-Beta-25 and H-Beta-150 (Section 4.1.3).

From Figure 4.8, it is also evident that all he catalysts were active except H-Beta-300d which deactivated completely.

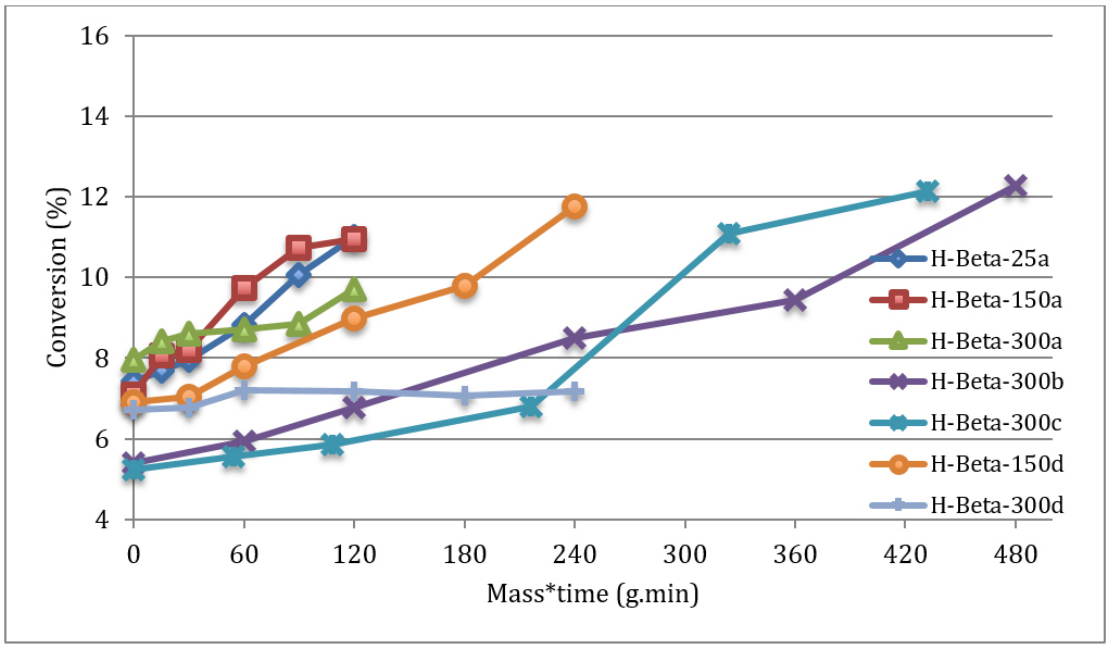

Figure 4.8: Conversion of hexadecane in hydroisomerization over different beta zeolites catalysts.

a. 0.5 g catalyst. b. 2 g catalyst, c. 1.8 g catalyst (40 ml C_{16}), d. desilicated beta zeolites (1 g).

Table 4.10: Beta catalysts conversion at 120 min.g_{cat}.

Catalyst	Conversion at 120 min.g_{cat} (%)
H-Beta-25a	11
H-Beta-150a	11
H-Beta-300a	9
H-Beta-300b	6
H-Beta-300c	5
H-Beta-150d	9
H-Beta-300d	7

a. 0.5 g catalyst. b. 2 g catalyst, c. 1.8 g catalyst (40 ml C_{16}), d. desilicated beta zeolites (1 g).

4.2.3.1.2 Platinum catalysts

Results on hydroisomerization of hexadecane over platinum catalysts are displayed in Figure 4.9, where conversion is plotted as a function of the normalized time (multiplication of time with mass) in order to compare the results with different catalyst masses (Table 4.11).

The results revealed that Pt/H-Beta-25 exhibited 10.4% conversion, which is higher than for other platinum catalysts, ca. 7%. From Figure 4.9 it is evident that platinum with high hydrogenation ability [3,50], high acidity and smaller crystalline structure of H-Beta-25 resulted in better overall conversion. The effect of acidity and crystalline structure can be seen in the case of 2 wt.% Pt/H-Beta-300, which exhibited a lower conversion in the same reaction conditions. Moreover, other catalysts showed similar conversion values except for a mechanical mixture of Pt/A: H-Beta-300, which resulted in a 7% conversion in 240 min.g_{cat} compared to 10.4% and 7% in 120 min.g_{cat}. For comparison Park et al.,[3] for hexadecane hydroisomerization over platinum-ZSM, Beta and Y-zeolites in a batch reactor at 360 °C and 103 bar total pressure, reported conversion of 42.5% and selectivity of 50% in the case of Pt/H-Beta (SiO_2/Al_2O_3=50). The current data could not be directly compared to this literature study due to much different reaction conditions.

Mechanical mixtures Pt/A: H-Beta-25 and Pt/A: H-Beta-300 were also tested. High platinum loading (5 wt.%) provided hydrogenation/dehydrogenation activity, and acidic beta zeolite was active in isomerization. Due to excessive coking in the spent catalyst (Table 4.7), deactivation was higher for Pt/A: H-Beta-25 (38.6%) than for any other catalysts. In Pt/A: H-Beta-25 a large amount of coke is due to strong Brønsted

acid sites, promoting coke formation. Conversion over Pt/A: H-Beta-300 was two fold lower than with other catalysts at the same conversion levels.

From Figure 4.9 it is also evident that Pt/H-Beta-25 was active and conversion was steadily increasing analogously Pt/A: H-Beta-300. Organic elemental analysis for Pt/H-Beta-25 also displayed the least amount of coke (9.8%) on the catalysts. Pt/H-Beta-300 and Pt/A: H-Beta-25 have been nearly completely deactivated.

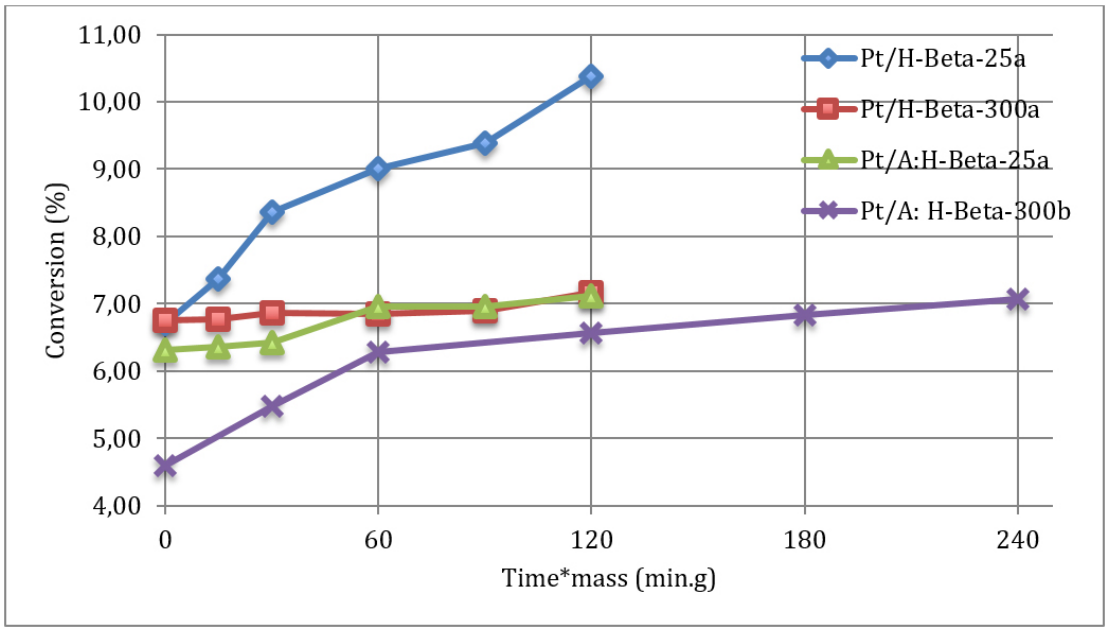

Figure 4.9: Conversion of hexadecane in hydroisomerization over platinum beta zeolites. Notation: a: 0.5 g catalyst, b. 1 g catalyst. (Pt/A: Pt/Alumina)

Table 4.11: Conversion of hexadecane over platinum catalysts at 120 min.g_{cat}.

Catalyst	**Conversion at 120 min.g_{cat} (%)**
Pt/H-Beta-25a	10
Pt/H-Beta-300a	7
Pt/A*: H-Beta-25a	7
Pt/A*: H-Beta-300b	7

*Pt/A: Pt/Alumina

a: 0.5 g catalyst, b. 1 g catalyst. (Pt/A: Pt/Alumina)

4.2.3.1.3 Nickel and ruthenium catalysts

The results from hydroisomerization of hexadecane over nickel and ruthenium catalysts are displayed in Figure 4.10. 1 g of catalyst was used in all experiments, and the results are shown as a function of the normalized time for easier comparison.

The results revealed that 5 wt.% Ru/USY-15 exhibited the highest conversion of 15%. 5 wt.% Ni/H-Beta-25 and 1 wt.% Ru/H-Beta-150 showed 9% conversion. Ni/H-Beta-150, 5 wt.% Ni/H-Beta-300 and 2.5 wt.% Ru/USY-30 displayed 8%, 7% and 6%, respectively. It was reported by Park et al.[3] that conversion depends on the strength of acid sites in the catalysts, which are identified qualitatively by the maximum peak temperature location in ammonia TPD results. The author reported more strong sites in H-Beta zeolite than H-Y zeolite.[3]

The highest conversion in this work was obtained over 5 wt.% Ru/USY-15 and 5 wt.% Ni/H-Beta-25 (250 °C) catalyst (Figure 4.10, Table 4.13). These catalysts exhibited similar metal loading of 5 wt.% however; the former one had the highest Brønsted acidity in all catalysts (Table 4.2). 1 wt.% Ru-H-Beta-150 and 5 wt.% Ni/H-Beta-25 showed the same conversion, although the nickel catalyst had a higher metal loading, ruthenium catalyst possessed higher Brønsted acidity (Table 4.2). The conversion obtained over nickel catalysts decreased by 1% for each catalyst with a higher SiO_2/Al_2O_3 ratio, i.e. Ni/H-Beta-150 and Ni/H-Beta-300 compared to Ni/H-Beta-25 showing that conversion is linearly proportional to acidity.

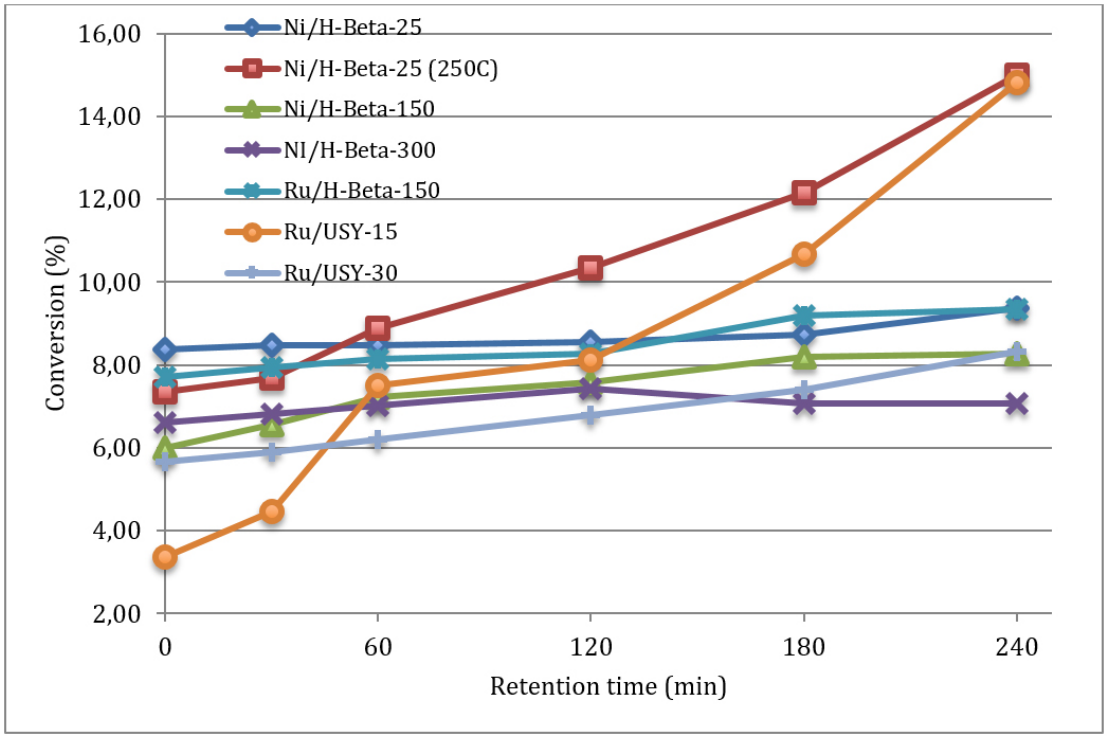

Figure 4.10: Conversion of hexadecane in hydroisomerization over nickel beta and ruthenium on beta and USY zeolites.

Table 4.12: Conversion over nickel and ruthenium catalysts at 240 min.g_{cat}.

Catalyst	**Conversion at 120 min.g_{cat} (%)**
5 wt.% Ni/H-Beta-25	9
5 wt.% Ni/H-Beta-25 (250 °C)	15
5 wt.% Ni/H-Beta-150	8
5 wt.% Ni/H-Beta-300	7
1 wt.% Ru/H-Beta-150	9
5 wt.% Ru/USY-15	15
2.5 wt.% Ru/USY-15	8

4.2.4 Mass balance

Experimental data are given in Table 4.13, showing experimental conditions, conversion and the mass balance closure.

Table 4.13: List of experimental details.

Exp. No.	Catalyst	Catalyst Amount, (g), Reactant, (ml), *	Exp. Condition T (°C), P (bar)	X, %	Mass Balance, (%)	Liquid disappearance, (%)
TR2	H-Beta-25	0.50, 60	210, 40	11.0	84	8
TR3	H-Beta -150	0.50, 60	210, 40	11	57	7
TR4	H-Beta -300	0.50, 60	210, 40	10	89	3
TR5	2 wt.% Pt/ H-Beta -25	0.54, 60	210, 40	10	91	1
TR6	2 wt.% Pt/ H-Beta -300	0.55, 60	210, 40	7	94	6
TR7	5 wt.% Pt/Al2O3, H-Beta -25 (1:1)	0.50, 60	210, 40	7	87	6
TR8	H-Beta-300	2.0, 60	210, 40	12	80	12
TR9	5 wt.% Pt/Al2O3, H-Beta -300 (1:1)	1.0, 60	210, 40	7	81	11
TR10	H-Beta -300	1.8, 40	210, 40	12	70	18
TR11	5 wt.% Ni/ H-Beta -25	1.0, 60	210, 40	9	80	11
TR12	5 wt.% Ni/ H-Beta -150	1.0, 60	210, 40	8	81	13
TR13	5 wt.% Ni/ H-Beta -300	1.0, 60	210, 40	7	85	9
TR14	1 wt.% Ru/ H-Beta -150	1.0, 60	210, 40	9	86	8
TR15	H-Beta -150 (desilicated)	1.0, 60	210, 40	11	81	12
TR16	H-Beta -300 (desilicated)	1.0, 60	210, 40	7	84	9
TR17	5 wt.% Ni/ H-Beta -25	1.0, 60	250, 45	15	88	7
TR18	5 wt.% Ru/USY-15	1.0, 60	210, 40	15	88	6
TR19	2,5 wt.% Ru/USY-30	0.46, 28	210, 40	8	86	19

* Stirring rate 900 rpm.

Hydroisomerization of hexadecane was performed at 210 °C and 40 bar. Figure 4.11 shows the conversion and mass balance in percentage for all experiments. The mass balance was calculated as the mass of hexadecane before and after the experiments.

$$\text{Hexadecane}_{\text{before experiment}} = 46.38 \text{ g (60 ml)}$$

$$\text{Hexadecane}_{\text{after experiment}} = \text{Reactant left in reactor + samples + waste samples + coke (g)}$$

The highest mass balance was displayed by 2 wt.% Pt/H-Beta-300 (TR6) while the lowest was shown by H-Beta-300 (TR10, 1.8 g, 40 ml), 94.1% and 69.7%, respectively. All the catalysts exhibited ≥80 % mass balance except H-Beta-300 (1.8 g, 40 ml). There seems to be an inverse relation between acidity (Brønsted acid sites) and mass balance, i.e. the higher is acidity of the support, the lower is the mass balance. This decrease in the mass balance can be correlated to the formation of gaseous products, which were qualitatively analyzed (Figure 4.7, Table 4.9). TR11, TR12 and TR13, exhibited conversions of 9.3%, 8.2% and 7.0% and gave the mass balance closure of 80%, 81.3% and 85%, respectively. The same trend can be seen for all beta zeolites, platinum catalysts and desilicated beta zeolites. Moreover, the mass balance closure decreased when the mass of catalysts increased from 0.5 g to 1.0 g (TR7= 0.5 g, TR9= 1.0 g). This trend cannot be seen for TR8, TR10 (Beta-300) and TR18, TR19 (Ru/USY), because different catalyst mass and amounts of reactant were used.

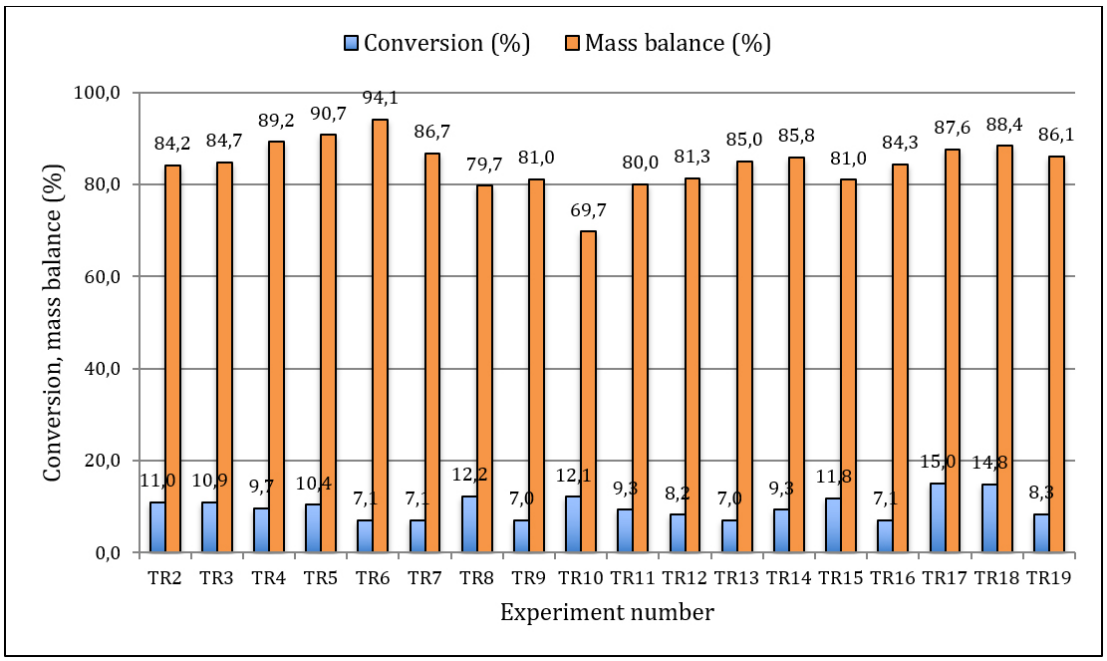

Figure 4.11: Mass balance for hydroisomerization of hexadecane at 210 °C and 40 bar for each experiment after 4 hours (TR-17 at 250°C and 45 bar).

4.2.5 Product formation in hexadecane hydroisomerization over beta zeolites

Hydroisomerization of hexadecane was tested over a variety of beta zeolites. All beta zeolite catalysts formed different products including cracked, branched and alkylated hexadecane. There were no clear trends in the products distribution due to secondary cracking reported by Park et al.[3]

4.2.5.1 Cracked hydrocarbons

There were 11 hydrocarbons (for each carbon number) varying from linear, mono-branched to di-branched one, which was calibrated for GC analysis (Table 3.1). Each catalyst formed different cracked hydrocarbons. Methylpentane was formed over all beta zeolites, displayed in Figure 4.12 apart from desilicated H-Beta-300 and rest of the cracked products are displayed in Figures 4.13a and 4.13b.

The highest concentration of methylpentane was formed over H-Beta-300 (2 g), ca. 0.027 mol/L. The absence of methylpentane in desilicated H-Beta-300 is due to its lower acidity (Table 4.2). The highest rate for formation of monobranched methylpentane was seen over H-Beta-25, which could be related to its high acidity. Moreover, desilicated H-Beta-150 showed the same concentration value being less active, and H-Beta-300 (1.8 g) it was even less active than H-Beta-25. Furthermore,

catalysts with strong acid sites produced methylpentane in larger amounts compared to lower acidic catalysts.

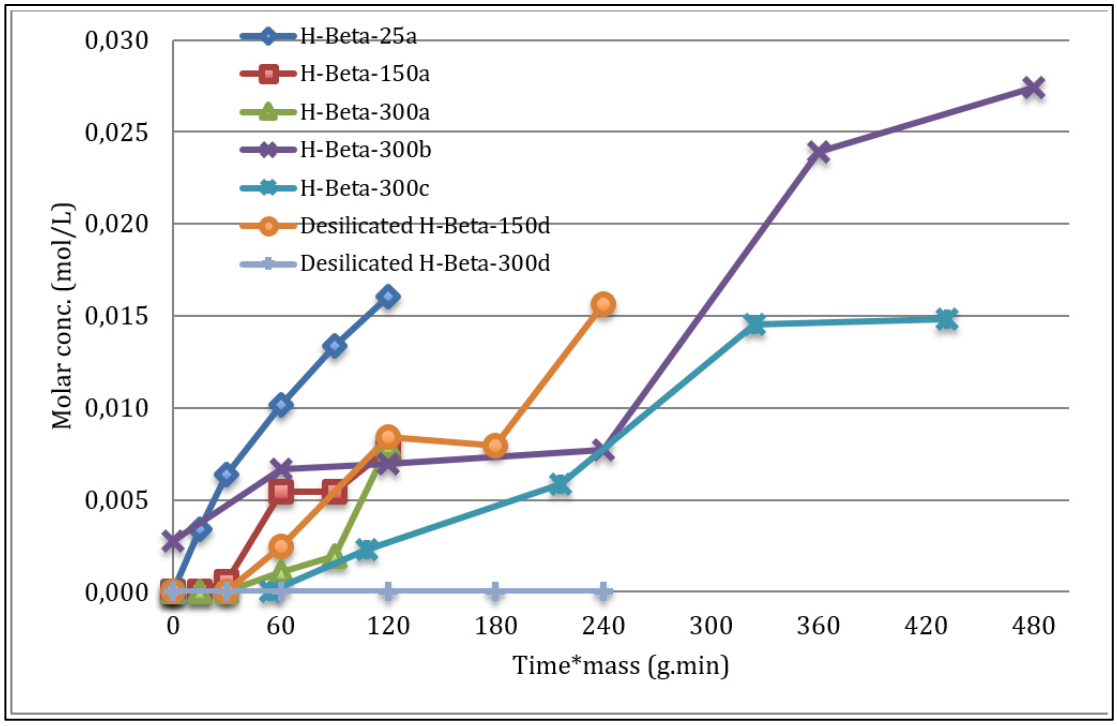

Figure 4.12: Molar concentration of 2-methylpentane over different beta zeolites.
Notation: a. 0.5 g catalyst, b, 2 g catalyst, c. 1.8 g catalyst, d. 1 g catalyst.

The cracked products for all beta zeolites except for H-Beta-300 (1.8 g and 2 g) are displayed in Figure 4.13a. On the other hand, H-Beta-25 formed a high amount of normal hexane, nonane, decane and dodecane (Figure 4.13a). H-Beta-150 formed minimal amounts of n-hexane and n-decane. H-Beta-300 did not result in any cracked products except methylpentane and hexane. This can solely be dependent on the lower acidity of the zeolite.

Desilicated H-Beta-150 showed the highest number of cracked hydrocarbons and produced branched hexane, octane and nonane together with normal decane and dodecane. The molar concentrations of this branched octane and nonane were higher than formed over any other catalysts. The concentration of normal decane was the highest, ca. 0.006 mol/L while the concentration of dodecane was small. The desilicated H-Beta-300 was the only catalyst, which did not form any cracked hydrocarbons.

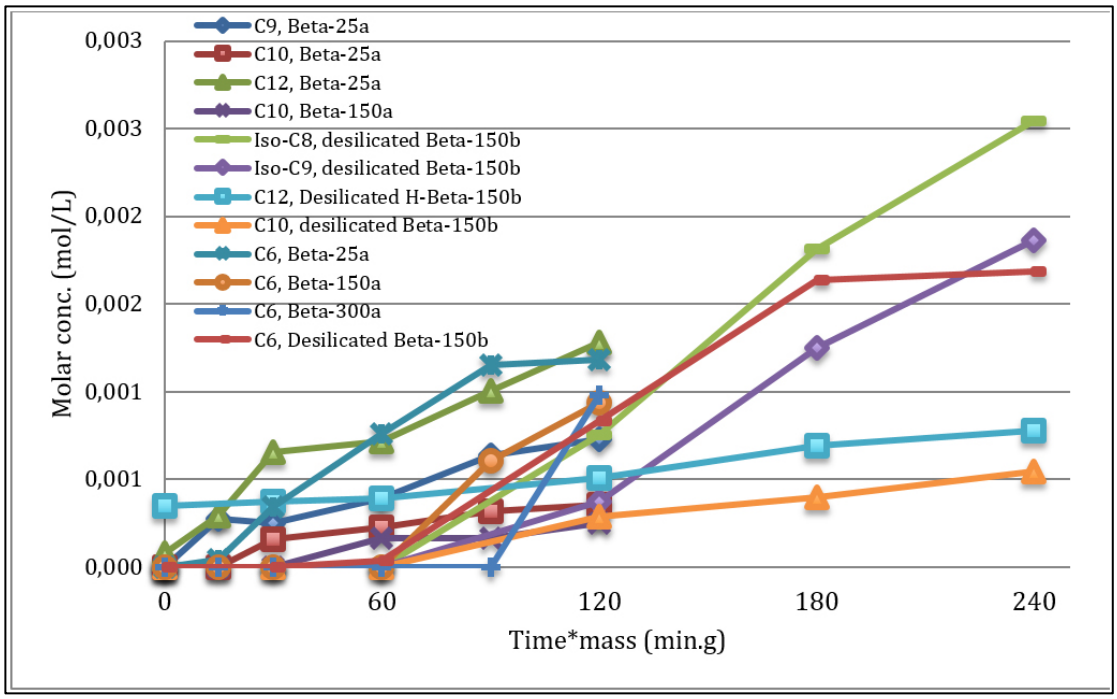

Figure 4.13a: Molar concentration of the cracked hydrocarbons over beta zeolites.

Notation: a. 0.5 g catalyst, b. 1 g catalyst.

H-Beta-300 (2 g) (Figure 4.13b) formed n-hexane, iso-octane and n-dodecane. H-Beta-300 (1.8 g) formed n-hexane, n-octane and n-dodecane (Figure 4.13b).

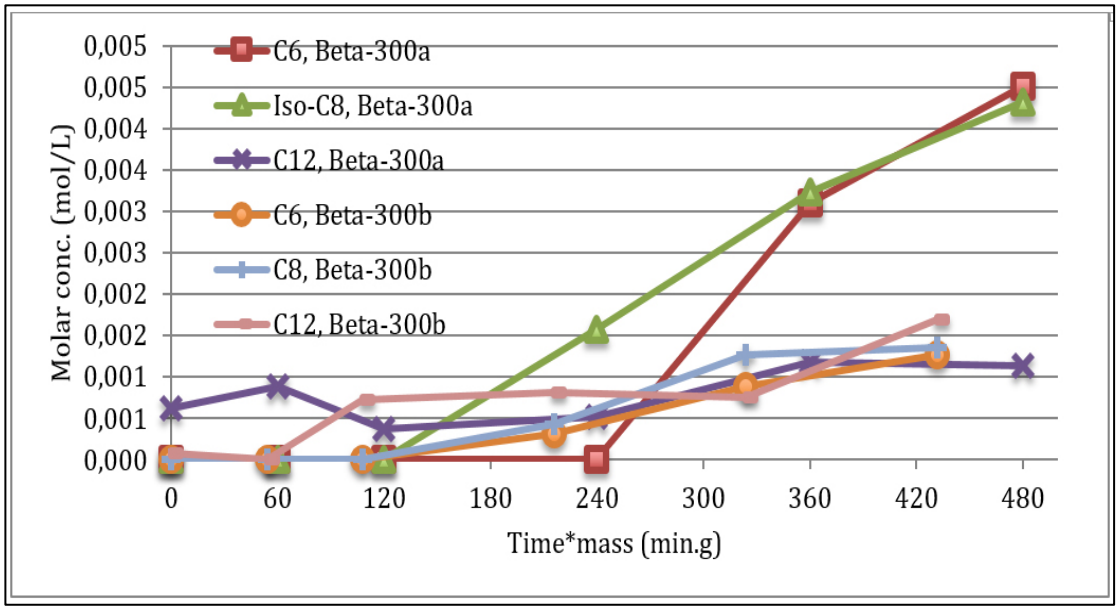

Figure 4.13b: Molar concentration of the cracked hydrocarbons over H-Beta-300 catalyst.

Notation: a. 2 g catalyst, b. 1.8 g catalyst.

4.2.5.2 Long-chain hydrocarbons

All tested catalysts formed long-chain hydrocarbons (Figure 4.14 and 4.15) comprising of tridecane, tetradecane and pentadecane. Tridecane was absent in all beta catalysts except some traces in desilicated H-Beta-150. The concentration of tetradecane was comparable for beta zeolite, being within ca. 0.0007 to 0.001 mol/L while the desilicated H-Beta-300 showed the highest concentration of tetradecane of 0.0033 mol/L followed by desilicated H-Beta-150 giving 0.0025 mol/L. The concentrations of tetradecane and pentadecane were constant during the whole reaction indicating that they were formed already during heating the reactor while the concentration of tetradecane gradually decreased with time, which can be explained by its further transformations into other hydrocarbons. A higher concentration of long-chain hydrocarbons can be related to increased pore volume of the desilicated catalysts along with their decreased Brønsted acidity.

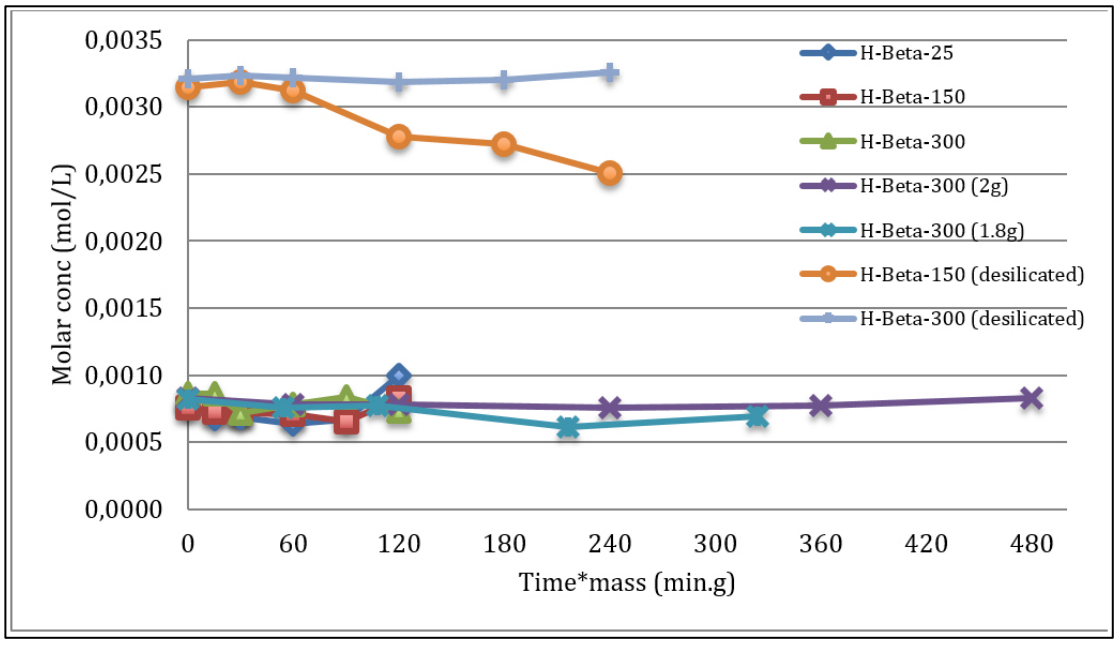

Figure 4.14: Molar concentration of tetradecane over beta zeolites.

The concentration of pentadecane was different for all beta zeolites. The highest concentration was exhibited by H-Beta-300 (1.8 g) and desilicated H-Beta-150 of 0.0130 mol/L while H-Beta-300 (2 g) also showed a comparable concentration of 0.0117 mol/L. The lowest concentration of ca. 0.0024 mol/L was displayed by H-Beta-300. Similar concentrations of pentadecane were obtained by H-Beta-150 and

desilicated H-Beta-300, i.e. 0.0050 mol/L, while H-Beta-25 had a slightly elevated concentration than desilicated H-Beta-300 of 0.0070 mol/L.

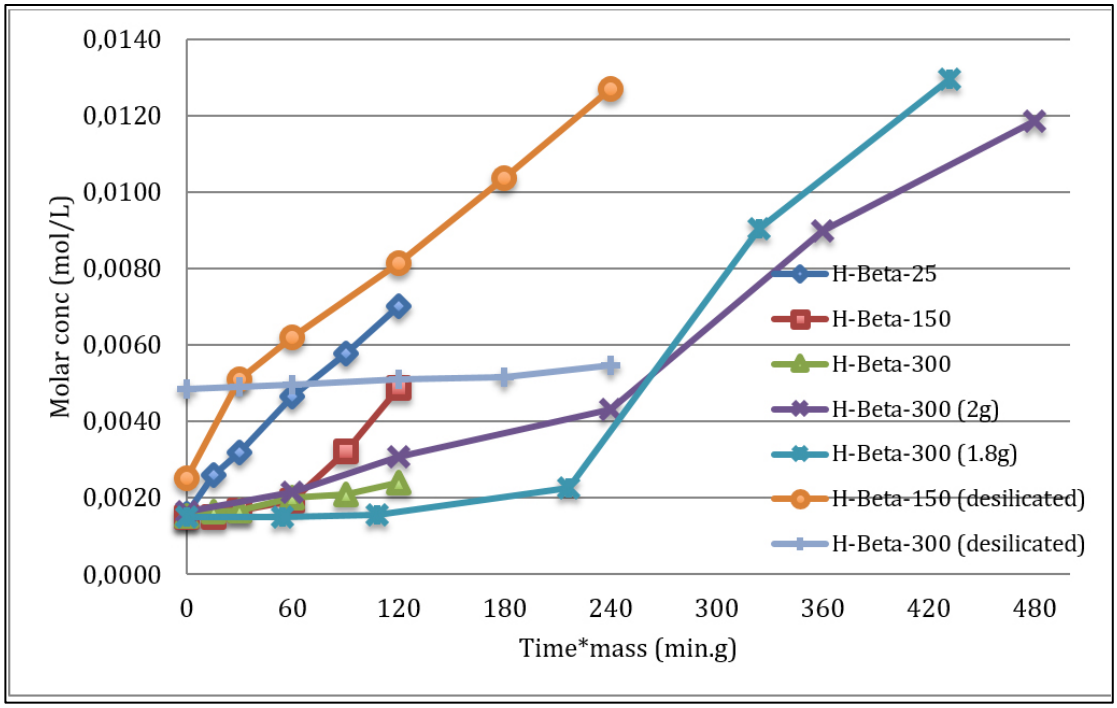

Figure 4.15: Molar concentration of pentadecane over beta zeolites.

4.2.5.3 Isomerized hexadecane (Methyl-pentadecane)

The concentration of isomerized hexadecane is displayed in Figure 4.16 over beta zeolites. The highest concentration was formed by H-Beta-300 (1.8 g) and H-Beta-300 (2 g) with 0.012 and 0.010 mol/, respectively. The desilicated H-Beta-150 also formed significantly more methylpentadecane compared to other catalysts while the desilicated H-Beta-300 had the lowest concentration among all beta zeolites. The reason for a large amount of methyl-pentadecane for the desilicated H-Beta-150 zeolite was a large amount of Brønsted acid sites (Table 4.2) and large micropores as compared to desilicated H-Beta-300 zeolite. At a modified time value of 120 min.g_{cat}, H-Beta-150 exhibited the highest concentration of methyl-pentadecane of all beta zeolites while H-Beta-25 and H-Beta-300 also displayed similar results. A higher concentration of methylpentadecane over H-Beta-150 in comparison to H-Beta-25 was due to a higher acidity of H-Beta-25 (Table 4.2), which leads to a more excessive cracking than isomerization activity. Brønsted acidity of H-Beta-300 is considerably lower than for both H-Beta-25 and H-Beta-150, which was the reason for a lower concentration of methyl-pentadecane.[2,3]

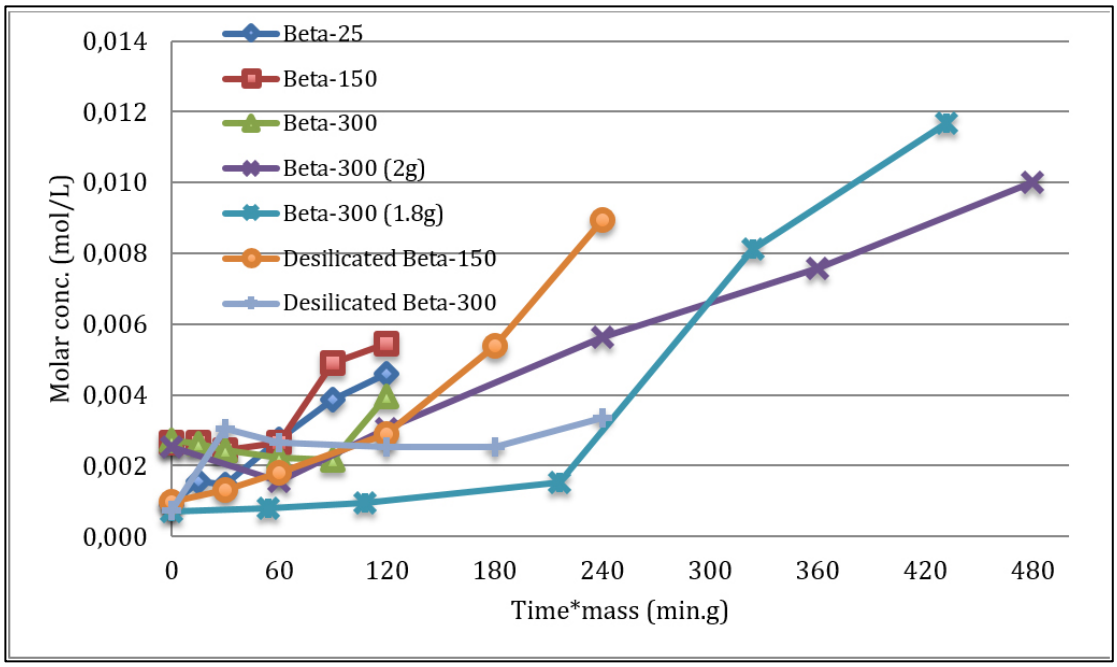

Figure 4.16: Molar concentration of methyl-pentadecane over beta zeolites.

Table 4.14: Molar concentration of methyl-pentadecane over different beta zeolites at 120 min.g_{cat}.

Catalyst	Molar conc. at 120 min.g_{cat} (mol/L)
H-Beta-25a	0.0046
H-Beta-150a	0.0054
H-Beta-300a	0.0040
H-Beta-300b	0.0100
H-Beta-300c	0.0117
Desilicated H-Beta-150d	0.0089
Desilicated H-Beta-300d	0.0033

a. 0.5 g catalyst, b. 2 g catalyst, c. 1.8 g catalyst, d. 1 g catalyst.

4.2.5.4 Alkylated hexadecane

The molar concentrations of alkylated hexadecane, i.e. heptadecane and octadecane, are shown in Figure 4.17 and 4.18, respectively. Heptadecane was obtained in a large quantity over the desilicated H-Beta-150 and H-Beta-300, ca. 0.0023 mol/L, while it was about half of that concentration with all other beta zeolites, ca. 0.0013 mol/L. Moreover, the concentration of heptadecane did not change with time with all other catalysts except desilicated H-Beta-150. An opposite trend was seen in octadecane formation for which desilicated H-Beta-150 and H-Beta-300 generated less

octadecane, ca. 0.006 mol/L, than beta zeolite catalysts, which resulted in an excessive octadecane concentration of ca. 0.0005 mol/L. This decreasing trend in its concentration confirms that the catalyst keeps its activity during the reaction in line with this the concentration of cracked products also increased with time.

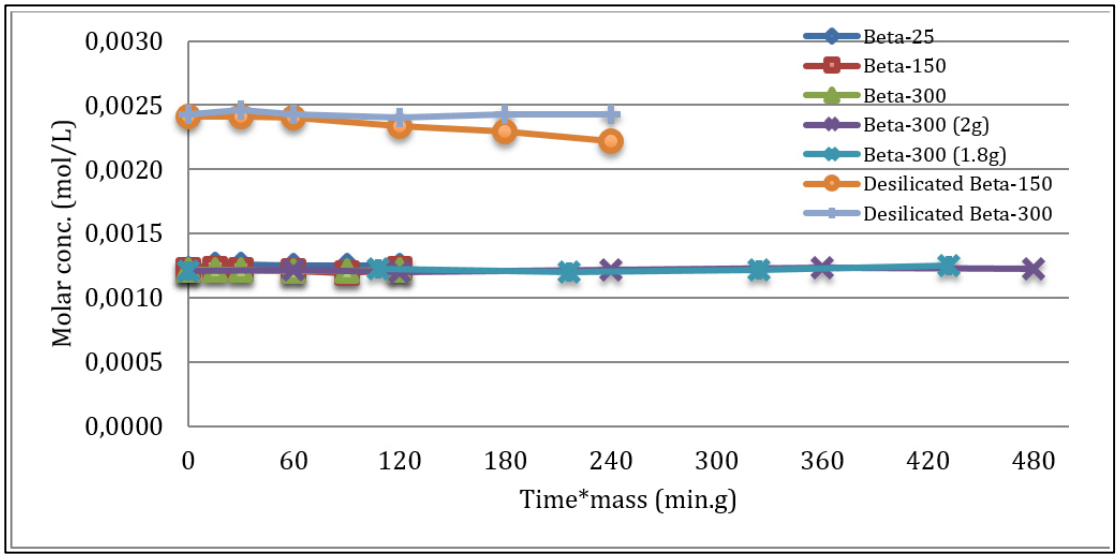

Figure 4.17: Molar concentration of heptadecane over beta zeolites.

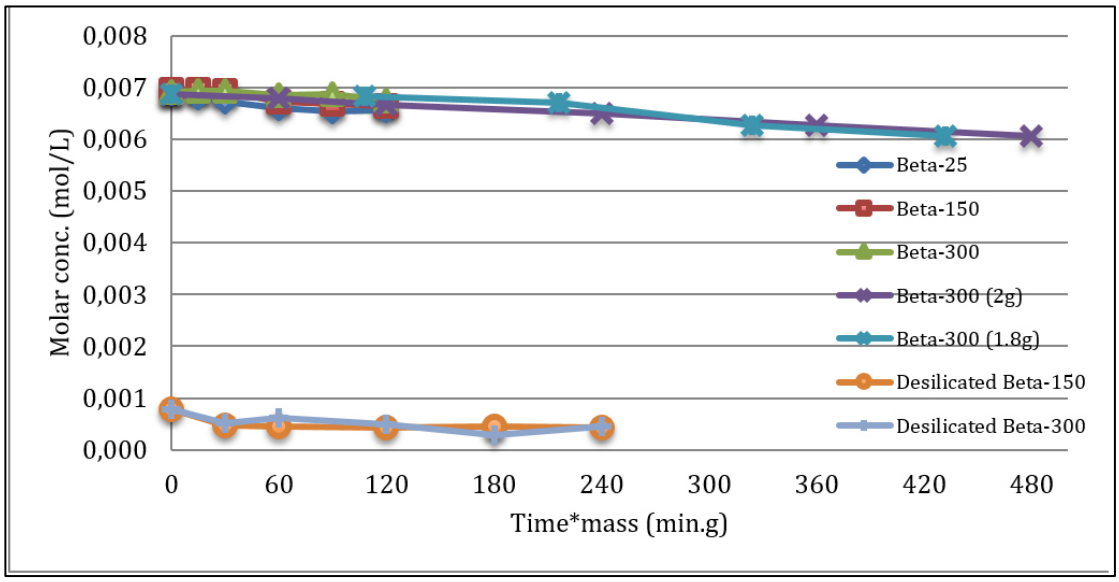

Figure 4.18: Molar concentration of octadecane over beta zeolites.

4.2.6 Product formation in hexadecane hydroisomerization over platinum catalysts

Hydroisomerization of hexadecane was tested over several bifunctional platinum catalysts giving a variety of products including cracked, branched and alkylated

hexadecane. There were no clear trends in the products distribution due to secondary cracking reported by Park et al.[3]

4.2.6.1 Cracked hydrocarbons

All bifunctional platinum catalysts catalyzed the formation of cracked products, however, lower amounts than with the metal free catalysts. Moreover, there were more isomerized cracked products than obtained with other catalysts (Figure 4.19). Analogous results were also reported by Park et al.[3] for platinum beta bifunctional catalysts.[3] With all bifunctional catalysts, the cracking products were essentially linear and branched C_3-C_{12}, in line with the literature.[2,3]

The highest concentrations of cracked products were formed over a mechanical mixture of Pt/A: H-Beta-300, giving iso-hexane, n-octane and n-dodecane. While the molar concentration of dodecane remained almost constant, two other compounds were increasing with time. The concentration of all cracked hydrocarbons increased was leveling off at 120 min.g_{cat} except Pt/A: H-Beta-300b mixture (Figure 4.19).

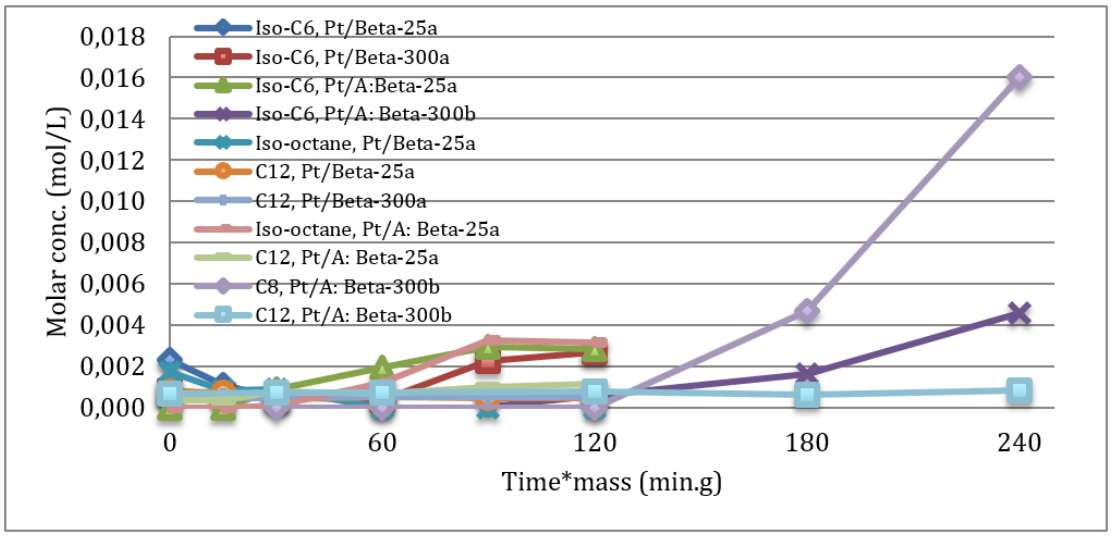

Figure: 4.19: Molar concentration of cracked products over platinum catalysts.

Notation: a. 0.5 g catalyst, b. 1 g catalyst.

4.2.6.2 Long-chain hydrocarbons

All platinum catalysts promoted the formation of long-chain hydrocarbons (Figure 4.20). Tridecane was, however, absent in all catalysts. The concentration of tetradecane started on the same level and was comparable for all catalysts being ca. 0.0012 to 0.0014 mol/L. The concentration of pentadecane started from 0.0015 mol/L

in all catalysts and remained the same for Pt/H-Beta-300 and for the mechanical mixture of platinum on alumina and H-Beta-300 increasing for other catalysts. The highest concentration of pentadecane was displayed by Pt/H-Beta-25, 0.0095 mol/L followed by the mechanical mixture of platinum alumina and H-Beta-25 having 0.0034 mol/L.

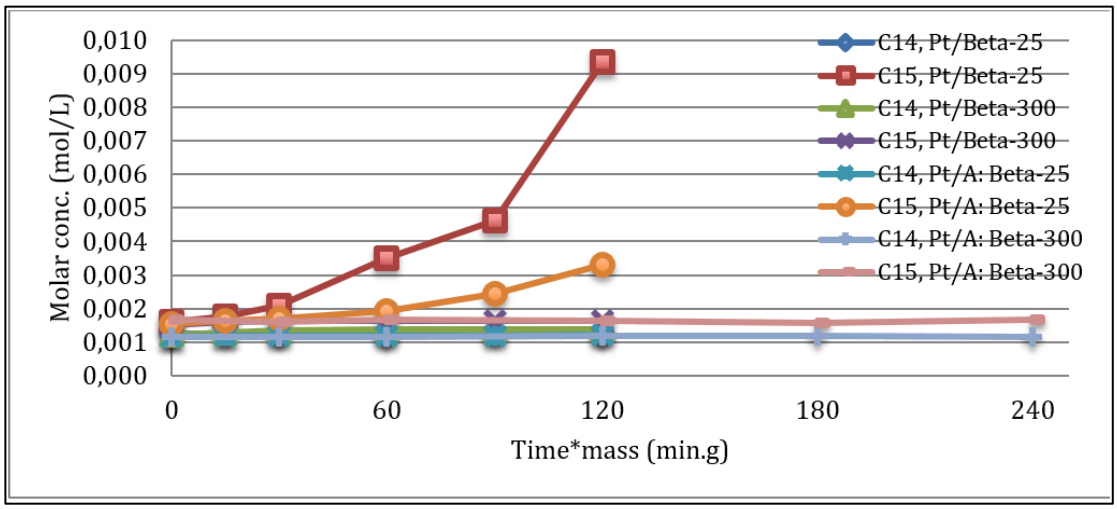

Figure: 4.20: Molar concentration of long-chain hydrocarbons over platinum catalysts.

4.2.6.3 Isomerized hexadecane (methyl-pentadecane)

All platinum catalysts generated methyl-pentadecane (Figure 4.21) with the best result displayed by Pt/H-Beta-25 of 0.067 mol/L being the highest among all tested materials. The results from other platinum catalysts were comparatively the same, 0.003 mol/L. The results obtained with platinum catalysts confirm that a combination of platinum exhibiting hydrogenation/dehydrogenation function with acidic support possessing large amounts of Brønsted acid sites (H-Beta-25) promoted isomerization.

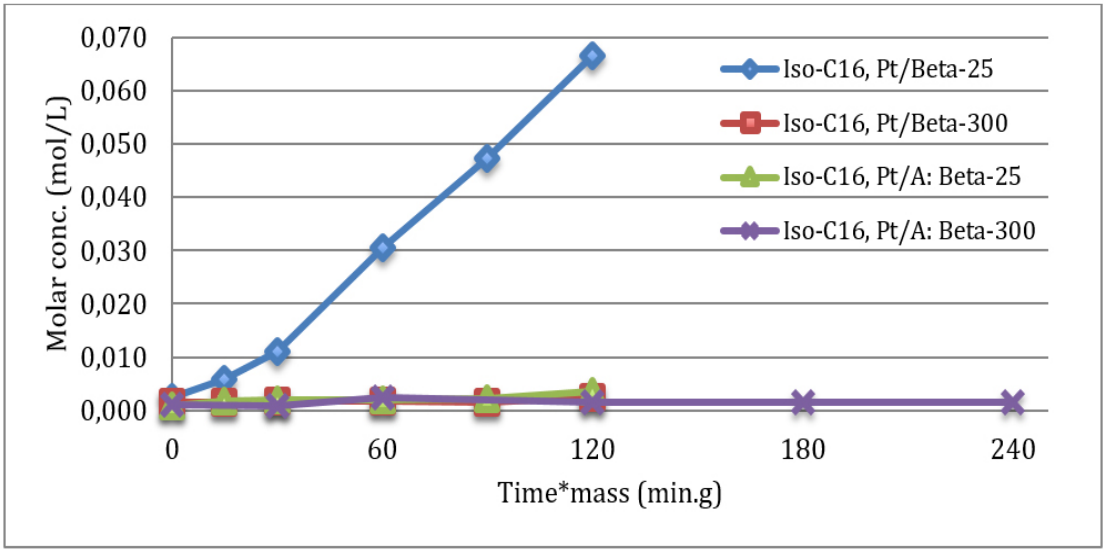

Figure: 4.21: Molar concentration of methyl-pentadecane over platinum catalysts.

Table 4.15: Molar concentration of methyl-pentadecane over platinum beta zeolites at 120 min.g_{cat}.

Catalyst	Molar conc. at 120 min.g_{cat} (mol/L)
Pt/H-Beta-25a	0.0664
Pt/H-Beta-300a	0.0024
Pt/Al_2O_3: H-Beta-25a	0.0036
Pt/Al_2O_3: H-Beta-25b	0.0015

a. 0.5 g catalyst, b. 1 g catalyst.

4.2.6.4 Alkylated hexadecane

All platinum catalysts displayed formation of alkylated hexadecane containing heptadecane and octadecane (Figure 4.22). The concentrations of heptadecane and octadecane did not change during the reaction. Only Pt/H-Beta-25 showed a slight decrease in heptadecane concentration of 0.0003 mol/L with time. The concentration of heptadecane and octadecane was 0.0011 mol/L and 0.007 mol/L, respectively. These results indicate that alkylated hexadecane was formed already during heating of the initial reaction mixture.

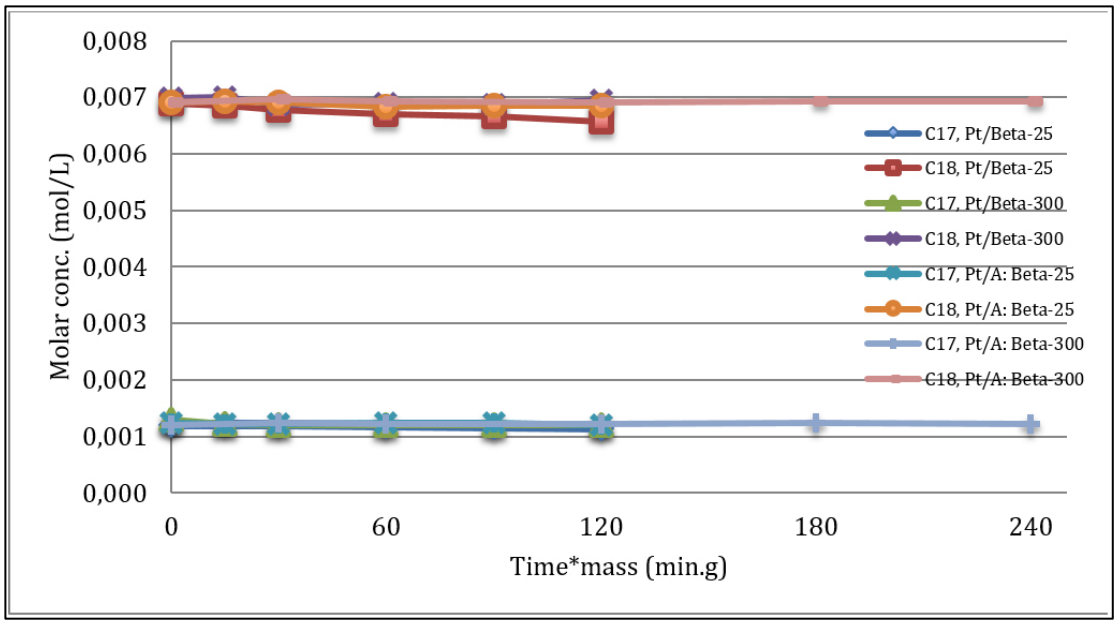

Figure: 4.22: Molar concentration of alkylated hexadecane over platinum catalysts.

4.2.7 Product formation in hexadecane hydroisomerization over nickel and ruthenium catalysts

Hydroisomerization of hexadecane was tested over a several of nickel and ruthenium catalysts, giving cracked products, branched and alkylated hexadecane. There were no clear trends in the products distribution due to secondary cracking reported by Park et al.[3]

4.2.7.1 Cracked hydrocarbons

Most of the studied catalysts formed mainly cracked hydrocarbons. Some hydrocarbons which nature has to be further confirmed were also formed. With all bifunctional catalysts, cracking products were essentially linear and branched C_3-C_{12} compounds, similar to the literature.[2,3]

Over 5 wt.% Ni/H-Beta-25 at a higher temperature, 250 °C, many cracked hydrocarbons were formed comprising both linear and branched products (Figure 4.23). The highest molar concentration, ca. 0.014 mol/L, was obtained for iso-hexane (methylpentane). Other products have lower molar concentration values of ca. 0.002 mol/L. The molar concentration of iso-decane and decane was 0.0023 and 0.0014 mol/L, respectively. Over other nickel catalysts except for 5 wt.% Ni/H-Beta-25 (250 °C), no cracked products were seen apart from traces of dodecane (Figure 4.25).

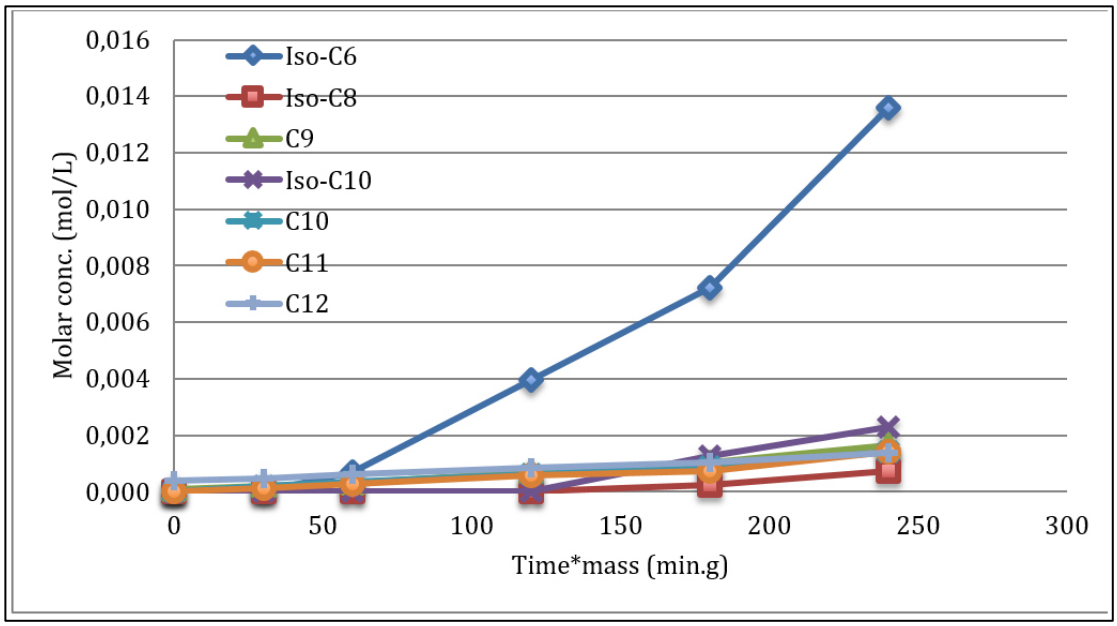

Figure: 4.23: Molar concentration of cracked hydrocarbons over 5 wt.% Ni/H-Beta-25 (250 °C).

There was no lower molecular weight cracked hydrocarbons formed except n-nonane to dodecane in the case of 1 wt. Ru/H-Beta-150 (Figure 4.24). The highest molar concentration for n-dodecane of ca. 0.0013 mol/L was observed over this catalyst. Other hydrocarbons had lower concentrations of ca. 0.0009 mol/L.

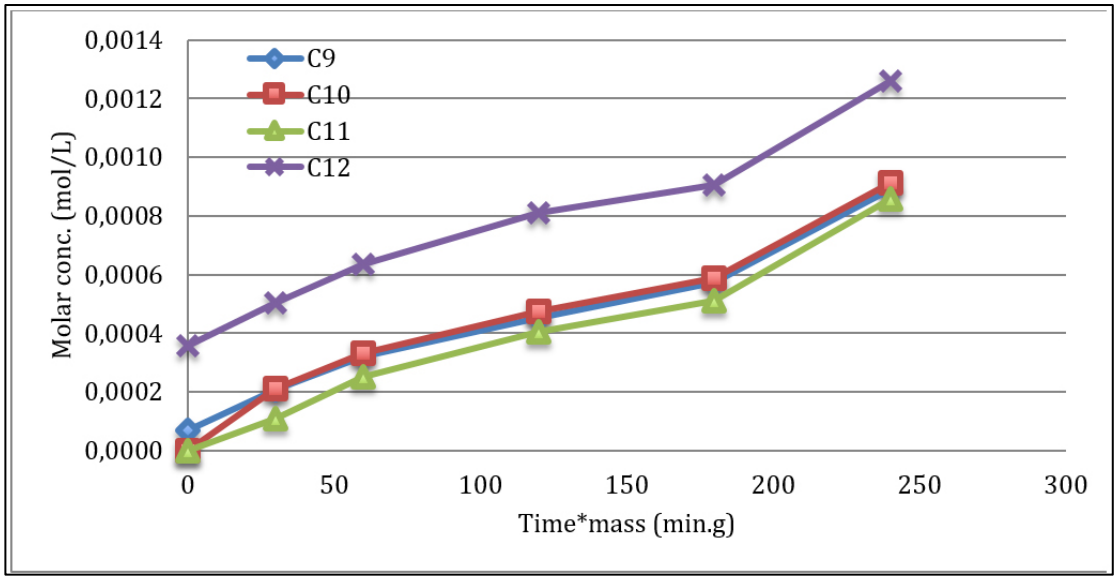

Figure: 4.24: Molar concentration of cracked hydrocarbons over 1 wt.% Ru/H-Beta-150 catalyst.

Dodecane was found in all catalysts displaying a higher molar concentration for ruthenium on Y-zeolites compared to nickel and ruthenium on beta zeolite (Figure 4.25). The highest molar concentration was found on 5 wt.% Ru/USY-15 and 2.5 wt.% Ru/USY-30 having values of 0.018 and 0.0041 mol/L. Other dodecane molar concentration values were from 0.0008 to 0.0015 mol/L.

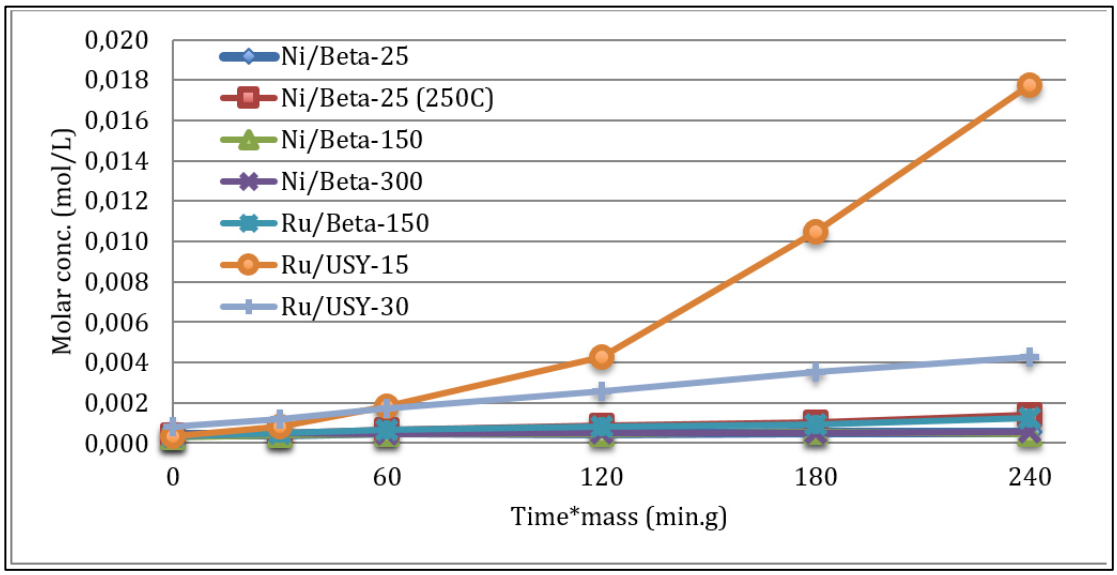

Figure: 4.25: Molar concentration of dodecane over nickel and ruthenium catalysts.

For ruthenium supported on Y-zeolites, more cracked products were found on 5 wt.% Ru/USY-15, comprising both linear and branched hydrocarbons (Figure 4.26). Among these cracked hydrocarbons, n-hexane, n-nonane, n-decane and n-undecane had the highest molar concentration over 5 wt.% Ru/USY-15 of 0.018 mol/L. Isomerized hexane and normal octane also displayed higher concentration along with isomerized octane, ca. 0.0014 and 0.001 mol/L, respectively, on 5 wt.% Ru/USY-15. Other hydrocarbons were present in lower molar concentrations in the range between 0.01 to 0.02 mol/L. Furthermore, in comparison to 5 wt.% Ru/USY-15, 2.5 wt.% Ru/USY-30 had a lower acidity (Table 4.2) giving only traces of cracked isomerized hydrocarbons.

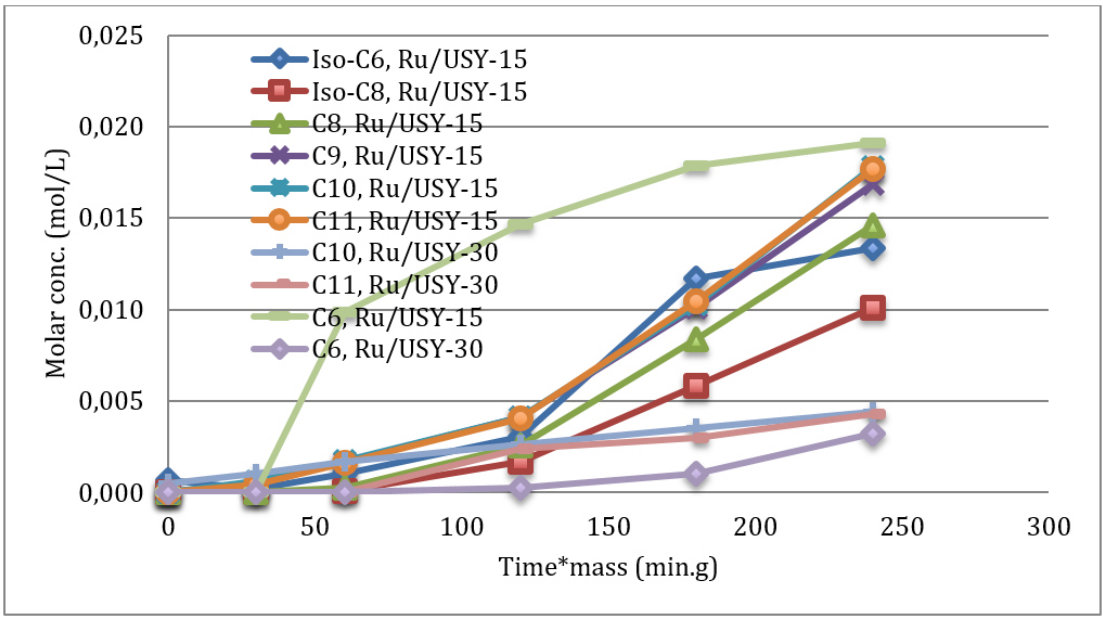

Figure: 4.26: Molar concentration of cracked hydrocarbons on ruthenium over Y-zeolites.

4.2.7.2 Long-chain hydrocarbons

All catalysts formed the long-chain hydrocarbons including tridecane, tetradecane and pentadecane. For tridecane, the highest molar concentration was found in 5 wt.% Ru/USY-15 and 2.5 wt.% Ru/USY-30 of 0.023 and 0.006 mol/L while ruthenium on beta zeolite gave a lower molar concentration of 0.002 mol/L. Tetradecane and pentadecane also displayed the same pattern. Ruthenium on Y-zeolite resulted in a higher concentration of long-chain hydrocarbons than other catalysts containing nickel and ruthenium on the beta zeolite. 5 wt.% Ru/USY-15 showed a concentration of 0.044 and 0.112 mol/L for tetradecane and pentadecane. 2.5 wt.% Ru/USY-30 displayed concentration of 0.013 and 0.030 mol/L for tetradecane and pentadecane.

All nickel catalysts apart from 5 wt.% Ni/H-Beta-25 at 250 °C did not exhibit any tridecane formation. The molar concentrations for tetradecane remained the same for all other nickel and ruthenium on beta zeolite catalysts during the whole reaction. The molar concentration for pentadecane was constant apart of 5 wt.% Ni/H-Beta-25 at 250 °C when the molar concentration increased with time.

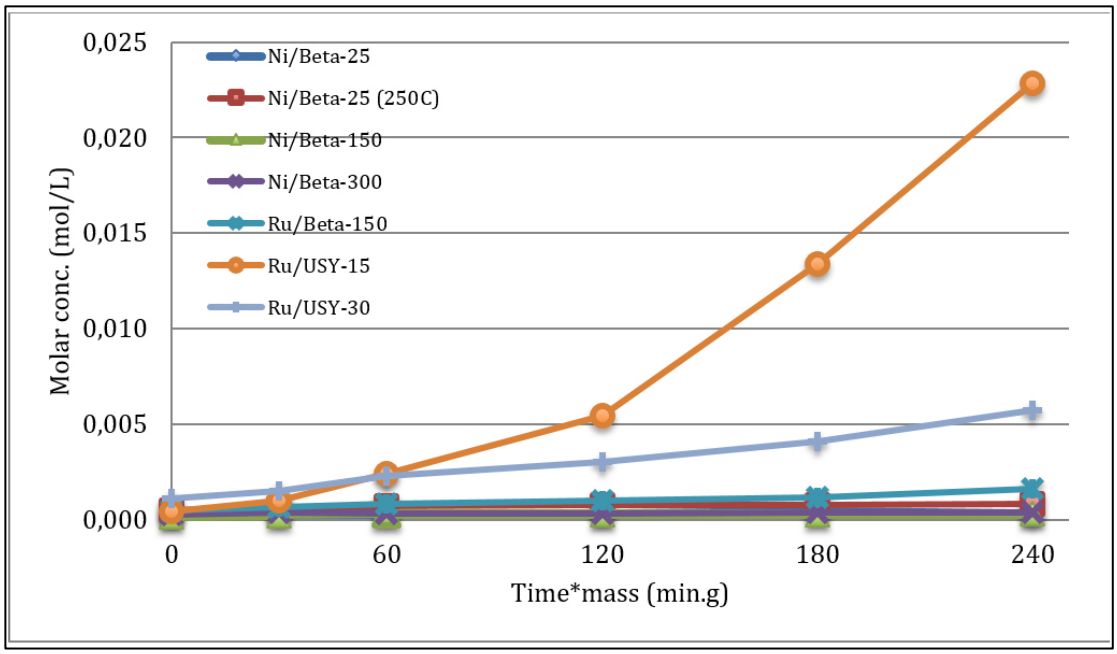

Figure: 4.27: Molar concentration of tridecane over nickel and ruthenium catalysts.

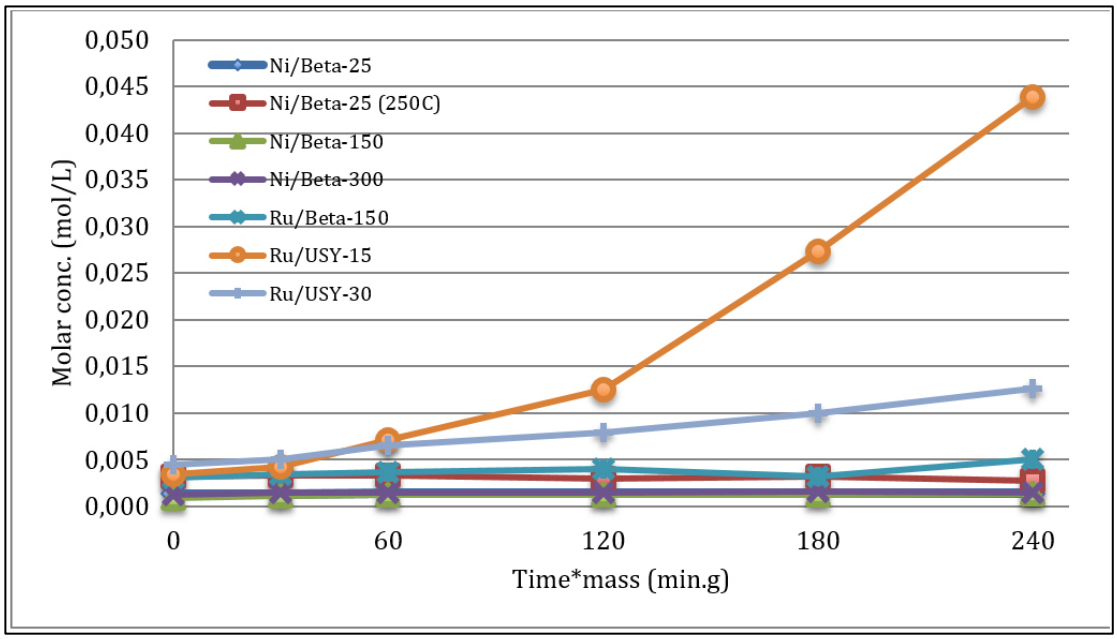

Figure: 4.28: Molar concentration of tetradecane over nickel and ruthenium catalysts.

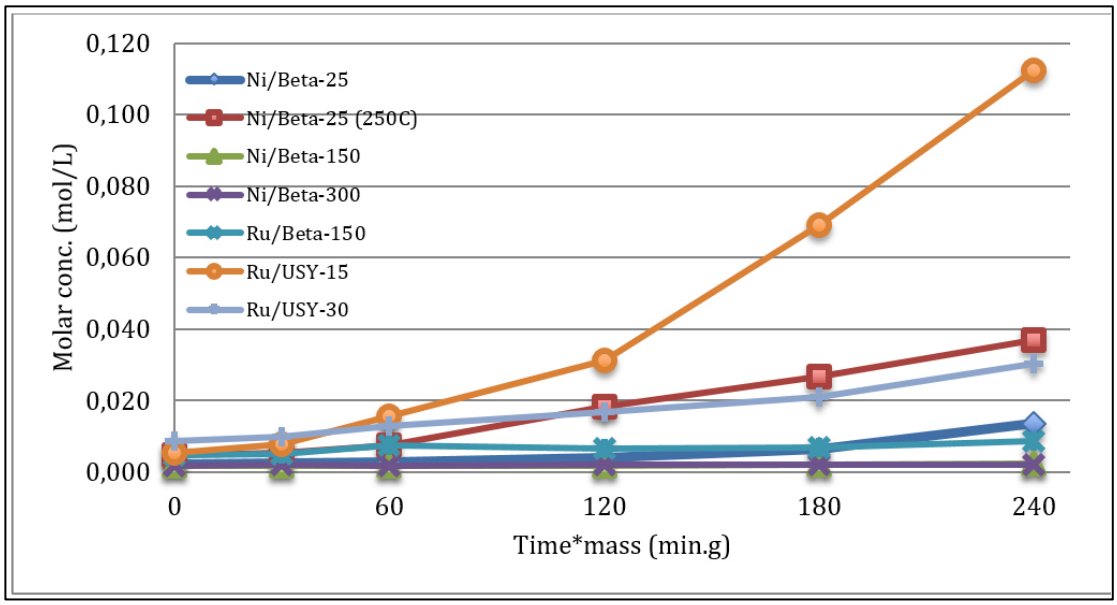

Figure: 4.29: Molar concentration of pentadecane over nickel and ruthenium catalysts.

4.2.7.3 Isomerized hexadecane (methyl-pentadecane)

All nickel and ruthenium catalysts formed methyl-pentadecane (Figure 4.30). The highest molar concentration was shown by Ni/H-Beta-25 (250 °C) and Ru/USY-15, 0.052 and 0.048 mol/L, respectively. This result was interesting as at elevated temperature, 250 °C, nickel produced a higher amount of methylpentadecane than the noble metal ruthenium supported on Y-zeolite catalyst at 210 °C. 5 wt.% Ni/H-Beta-25 and 5 wt.% Ni/H-Beta-150 displayed the same molar concentration of 0.018 mol/L, while 1 wt.% Ru/H-Beta-150 and 2.5 wt.% Ru/USY-30 exhibited the same molar concentration of 0.013 mol/L, although their acidity is different (Table 4.2). The lowest molar concentration of methyl-pentadecane was shown by 5 wt.% Ni/H-Beta-300, ca. 0.0026 mol/L.

Table 4.16: Molar concentration of methyl-pentadecane over platinum beta zeolites at 240 min.g_{cat}.

Catalyst	Molar conc. at 120 min.g_{cat} (mol/L)
Ni/H-Beta-25	0.0178
Ni/H-Beta-25 (250 °C)	0.0521
Ni/H-Beta-150	0.0190
Ni/H-Beta-300	0.0026
Ru/H-Beta-150	0.0129

Ru/USY-15	0.0479
Ru/USY-30	0.0131

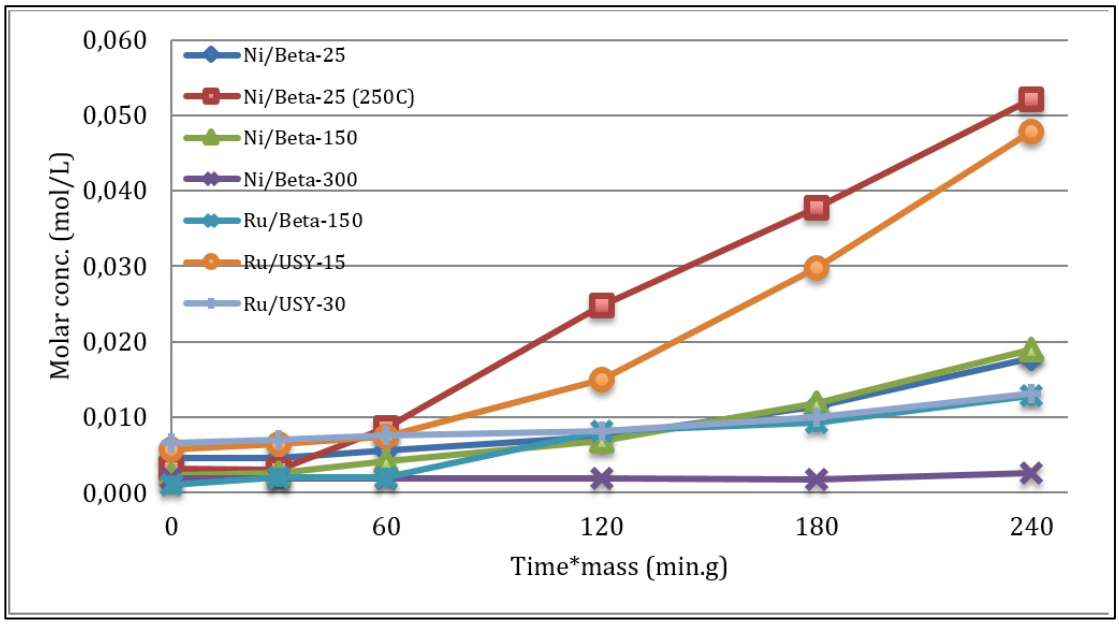

Figure: 4.30: Molar concentration of methylpentadecane over nickel and ruthenium catalysts.

4.2.7.4 Alkylated hexadecane

All nickel and ruthenium catalysts displayed alkylated hexadecane, i.e. heptadecane and octadecane (Figure 4.31 and 4.32). The concentrations of heptadecane were constant for 5 wt.% Ni/H-Beta-25, 5 wt.% Ni/H-Beta-150 and 5 wt.% Ni/H-Beta-300 with increasing time, being 0.0013 mol/L. The molar concentration remained the same for 1 wt.% Ru/H-Beta-150 (0.0023 mol/L). The molar concentration for 5 wt.% Ni/H-Beta-25 (250 °C), 5 wt.% Ru/USY-15 and 2.5 wt.% Ru/USY-30 decreased with time by 10%.

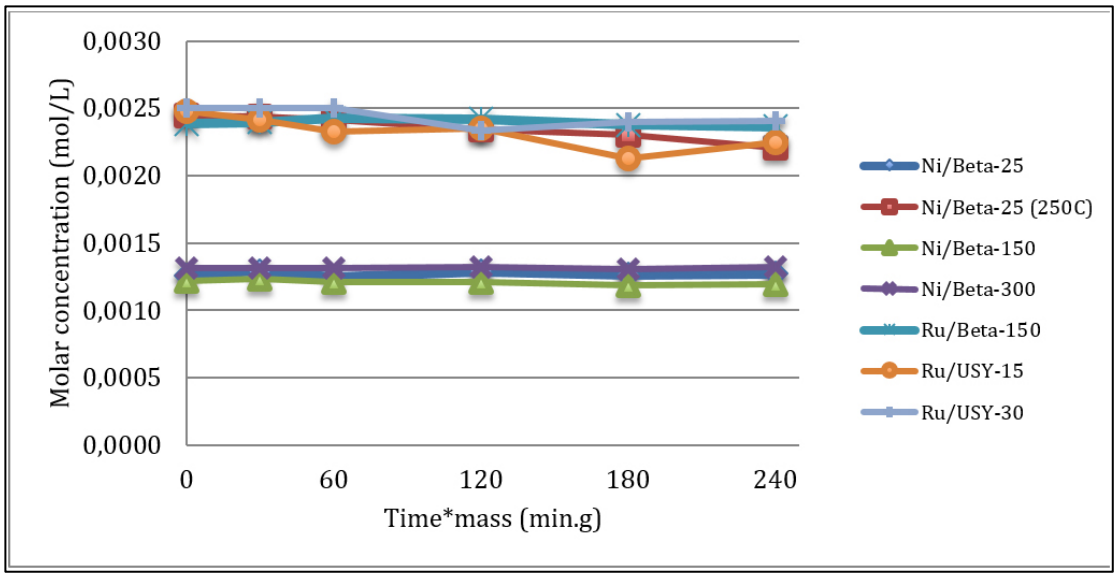

Figure: 4.31: Molar concentration of heptadecane over nickel and ruthenium catalysts.

The molar concentrations for octadecane remained constant except for 1 wt.% Ru/H-Beta-150, which showed a slight decrease in concentration in the beginning and then remained constant at 0.0004 mol/L. The highest concentration of octadecane, 0.007 mol/L was displayed by 5 wt.% Ni/H-Beta-150 and wt.% Ni/H-Beta-300. All other catalysts exhibited a constant molar concentration of 0.0005 mol/L.

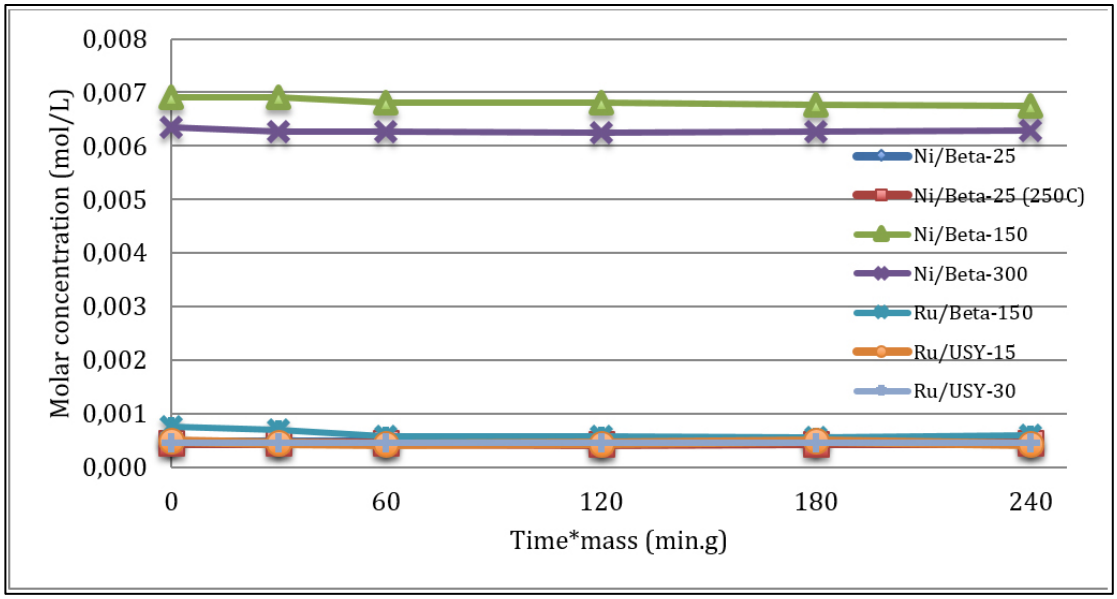

Figure: 4.32: Molar concentration of octadecane over nickel and ruthenium catalysts.

The results from the alkylated hexadecane product indicate that alkylation is very fast and occurs already during heating. Gaseous light hydrocarbons were formed very

rapidly during heating (Section 4.2.2). Moreover, alkylation of alkanes with alkanes is very low while the alkylation of olefins can be faster. Thus, the mechanism of heptadecane and octadecane formation is not that simple.

4.2.8 Product yield over H-Beta and Pt, Ru and Ni bifunctional catalysts

The product yields over beta and metal-acid bifunctional catalysts after 4 hours are displayed in Figure 4.33, while the corresponding table can be found in Appendix 8. The list of experiments is shown in Table 4.13.

All beta catalysts showed feasible product yields in line with their acidity. Higher yields of cracking products and long-chain hydrocarbons were shown by H-Beta-25, while H-Beta-300 displayed the lowest cracking yield. H-Beta-25 and H-Beta-150 exhibited comparable yields of methyl-pentadecane, 0.14% and 0.16% respectively; a lower yield, 0.12% was observed for H-Beta-300. Higher yields were obtained over H-beta-300 in TR8 and TR10, 0.29% and 0.34%, respectively. Desilicated H-Beta-150 showed higher cracking, long-chain hydrocarbons and methyl-pentadecane yields than neat H-Beta-150 and displayed a much lower alkylated hexadecane yield than other catalysts. Desilicated H-Beta-300 did not display any cracking products giving a long-chain hydrocarbon yield higher than H-Beta-300 and a lower yield of methyl-pentadecane. Alkylated hexadecane yields were similar in all beta catalysts, 0.23% for beta catalysts and 0.08% for desilicated beta catalysts.

Platinum beta bifunctional catalysts showed the same trend as beta catalysts and elaborated the role of acidity in hexadecane hydroisomerization; 2 wt.% Pt/H-Beta-25 showed the highest yield of methyl-pentadecane, 1.94%, 2 wt.% Pt/H-Beta-300 displayed a low yield of 0.07%, which was lower compared to the proton form of beta catalysts. The mechanical mixtures of platinum/alumina and beta zeolites showed lower yields than platinum beta bifunctional catalysts. Alkylated hexadecane yield was similar over all platinum catalysts, 0.24%.

Nickel beta bifunctional catalysts displayed lower cracking yields; 5 wt.% Ni/H-Beta-25 had higher yields of long-chain hydrocarbons, while other nickel catalysts gave lower yields; 5 wt.% Ni/H-Beta-25 and 5 wt.% Ni/H-Beta-150 displayed similar methyl-pentadecane yields, while 5 wt.% Ni/H-Beta-300 showed a lower yield. The alkylated hexadecane yield decreased with an increase of beta zeolite acidity. Overall, yields comparable to beta and platinum beta zeolites were shown for nickel containing materials. 5 wt.% Ni/H-Beta-25 at 250 °C displayed higher yields of

cracking products, long-chain hydrocarbons and methyl-pentadecane except alkylated hexadecane yield showed that product activity of nickel catalysts increased with elevated temperature. Alkylated hexadecane yields were similar compared to platinum catalysts, 0.24%.

1 wt.% ruthenium beta catalysts showed lower yields of cracked hydrocarbons and comparable yields of long-chain hydrocarbons as 5 wt.% Ni/H-Beta-25. Methyl-pentadecane yield was higher than for beta, a mechanical mixture of platinum on alumina and beta zeolites but lower than 5 wt.% Ni/H-Beta-25. Ruthenium Y-zeolites showed the highest cracking and long-chain hydrocarbons yields. Highly acidic 5 wt.% Ru/USY-15 displayed the highest cracked and long-chain hydrocarbon yield among all catalysts, 3.55 and 4.56%, respectively. It showed a high methyl-pentadecane yield following 2 wt.% Pt/H-Beta-25. 2.5 wt.% Ru/USY-30 exhibited a similar yield trend but lower yields of cracked products, long-chain hydrocarbons and methyl-pentadecane due to its lower acidity. The yields of alkylated hexadecane were similar in both catalysts, 0.08%.

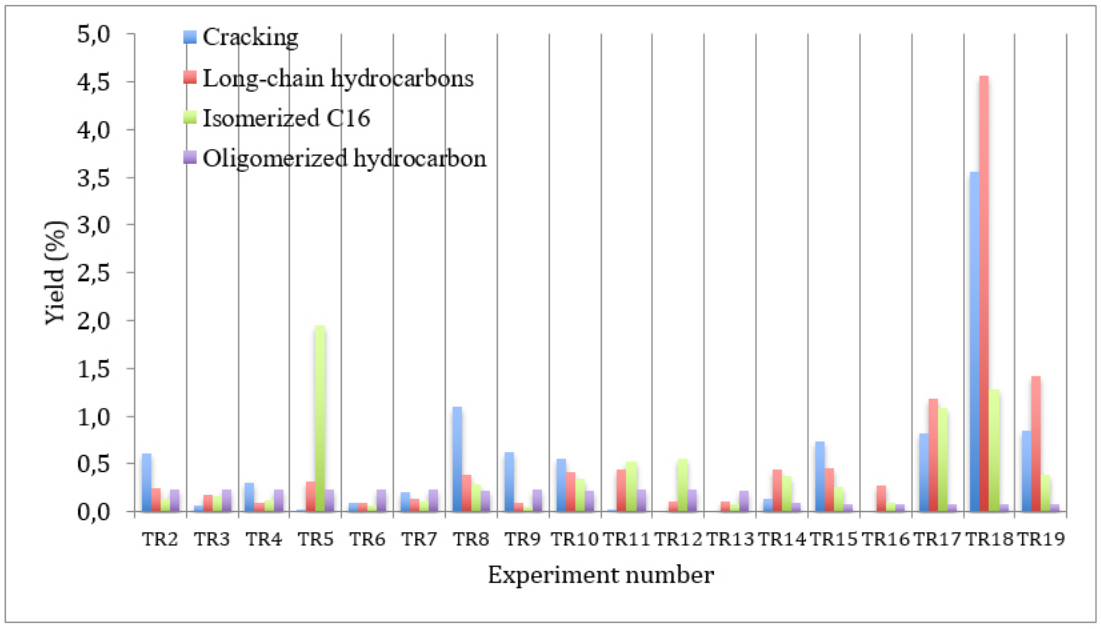

Figure 4.33: Product yields over beta and metal-acid bifunctional catalysts.

A list of experiments is displayed in Table 4.13.

4.3 Influence of metal and zeolite support on hydroisomerization

4.3.1 Influence of metals on hydroisomerization

Most of the studies on hydroisomerization of hexadecane or other long-chain hydrocarbons have been carried out with noble metals while only a few experiments have been performed on transition metal catalysts. Conversion for all catalysts is shown in Figure 4.34a. The list of experimental data is presented in Table 4.13.

In comparison to other metals, platinum beta bifunctional catalysts showed the best results for the gas phase (Figure 4.7, Table 4.9) and liquid phase cracked hydrocarbons (Figure 4.19), giving low amounts of these products. The concentration of methyl-pentadecane (Figure 4.21) was the highest with 2 wt.% Pt/H-Beta-25 among all tested catalysts. These catalysts also formed lower amounts of alkylated hexadecane (Figure 4.22) in comparison to other catalysts. These results can be related to the superior hydrogenating ability of platinum, which was also confirmed by a lower hydrogen content in organic elemental analysis. The amount of hydrogen was comparable in all catalysts except Pt-H-Beta-25, i.e. 7.1-9.4 wt.% and 1.8 wt.%, respectively. Additionally, less coke, which has a lighter character, was formed on platinum bifunctional catalysts ca. 7 wt.% compared to other catalysts, as shown from thermogravimetric analysis and size exclusion chromatography. Such coke analysis agrees with the hypothesis of a higher platinum hydrogenation ability, preventing coke formation and giving thus a lighter coke.

Nickel beta bifunctional catalysts showed the highest amount of gas-phase (Figure 4.7, Table 4.9) and the liquid phase cracking products (Figure 4.23, 4.25, 4.27, 4.28, 4.29). These catalysts gave a lower methyl-pentadecane amount at 210 °C, while the concentration increased when the experiment was conducted at 250 °C. Higher concentrations of alkylated hexadecane was also noticed for bifunctional catalysts containing nickel.

Ruthenium beta catalysts gave a higher amount of amount gas-phase products compared to platinum still lower than nickel catalysts (Figure 4.7, Table 4.9). The liquid phase cracked hydrocarbons were comparable with the nickel catalysts (Figure 4.24). These catalysts formed lower methyl-pentadecane and alkylated hexadecane yields (Figure 4.30, 4.31, 4.32).

Ruthenium Y-zeolite had the lowest amount of gas-phase products (Figure 4.7, Table 4.9) and the highest liquid phase cracked hydrocarbons yields (Figure 4.26, 4.27, 4.28, 4.29). 5 wt.% Ru/USY-15 gave the same methyl-pentadecane yield as formed by 5 wt.% Ni/H-Beta-25 (250 °C) (Figure 4.30) and formed comparable amounts of alkylated hexadecane products (Figure 4.31, 4.32).

4.3.2 Effect of acidic supports on hydroisomerization

The acidity of catalysts is presented in Table 4.2 while conversion data is presented in Figure 4.34a. The list of experimental data is presented in Table 4.13. Figure 4.34b shows a trend, with high acidity, there was more conversion. Among beta zeolite catalysts, H-Beta-25 (TR2) exhibited the highest conversion while H-Beta-300 (TR4) gave the lowest one. The same trend continues with platinum-beta, nickel-beta and ruthenium-Y-zeolite catalysts. H-Beta-300 (TR8, TR10) showed a higher conversion when a higher mass of catalysts was used in these experiments.

Beta zeolites showed high amounts of cracked hydrocarbons along with long-chain hydrocarbons. The isomerized methylpentadecane was formed in higher amounts over beta zeolites compared to other catalysts. They also gave higher amounts of heptadecane and less octadecane.

Platinum-beta bifunctional zeolites formed low amounts of cracked hydrocarbons and long-chain hydrocarbons. 2 wt.% Pt/H-Beta-25 had the highest methyl-pentadecane production among all catalysts. The concentrations of heptadecane and octadecane were comparable to beta zeolites.

Nickel and ruthenium over beta and Y-zeolites gave low amounts of formed cracked hydrocarbons with the lowest content given by 1 wt.% Ru/H-Beta-150. Some of these catalysts displayed comparable yields of methyl-pentadecane while for other lower concentrations of methyl-pentadecane were formed. Nickel and ruthenium catalysts exhibited higher heptadecane and comparable octadecane concentrations.

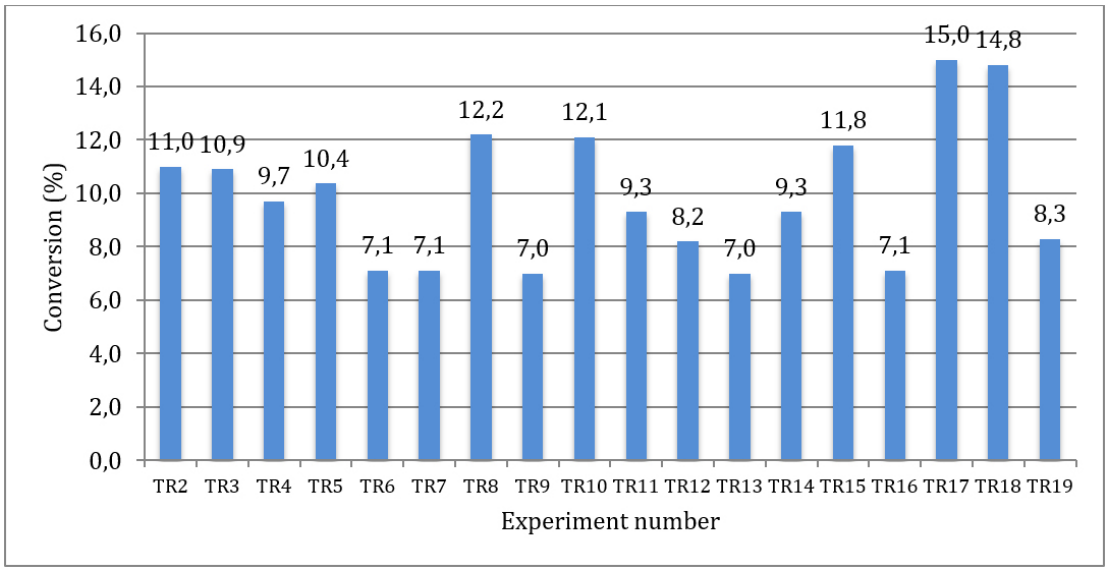

Figure 4.34a: Conversion of hexadecane for all experiments. The list of experiments is given in Table 4.13.

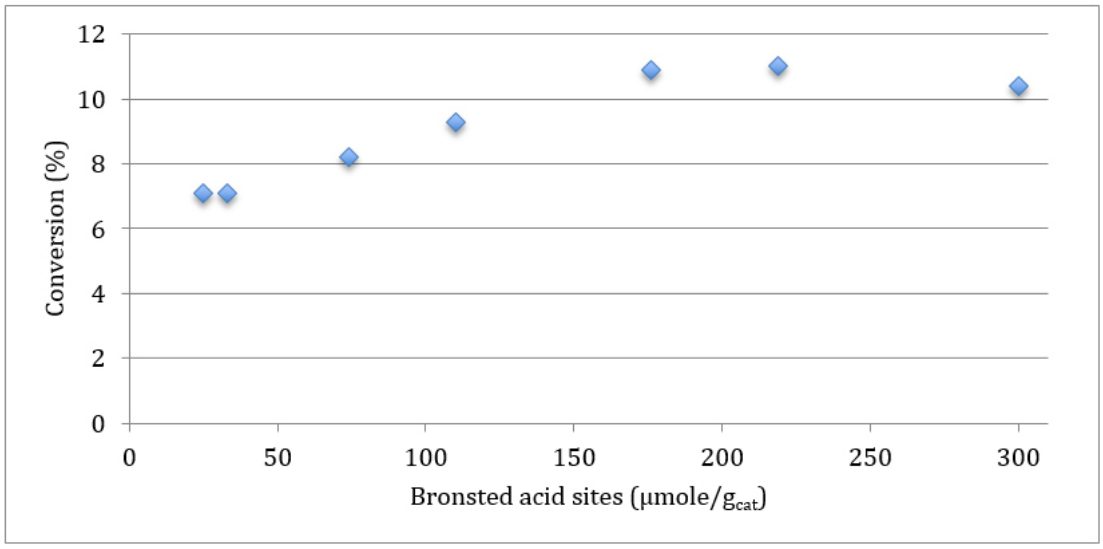

Figure 4.34b: Conversion of hexadecane as a function of Brønsted acid sites.

4.4 Influence of reaction conditions

4.4.1 Effect of temperature and pressure

To study the influence of temperature and pressure, hydroisomerization of hexadecane was carried out at three different temperatures, i.e. 240, 250 and 270 °C over 1 wt.% Ru/H-Beta-300 at an elevated pressure of 45 bar. The concentrations of the cracked products as a function of time at three different temperatures are displayed in Figure 4.35a, 4.35b and 4.35c, respectively.

The concentration of all cracked hydrocarbons is comparable to each other and showed the same trend at 240 °C and 250 °C but at a higher temperature of 270 °C, the concentration of iso-hexane had increased more than other hydrocarbons. In comparison to 1 wt.% Ru/H-Beta-150 (Figure 4.24), high concentrations of cracked hydrocarbons are formed at higher temperatures and with higher concentration in comparison to the concentrations obtained at 210 °C. With all bifunctional catalysts, cracking products were essentially C_3-C_{12}, both linear and branched as also reported in the literature.[2,3]

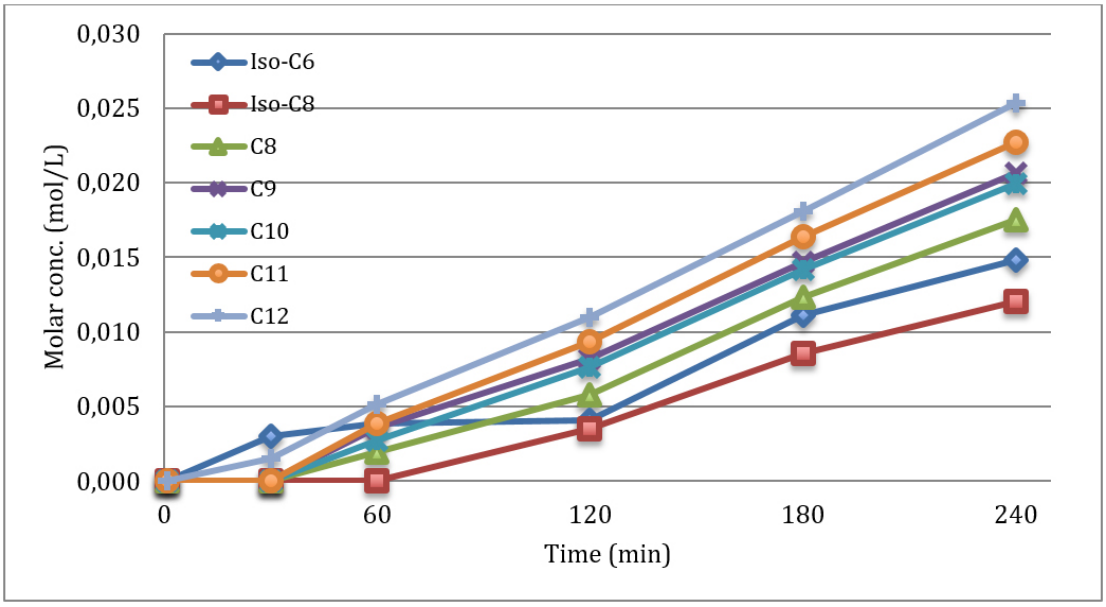

Figure 4.35a: Molar concentration of the cracked products over 1 wt.% Ru/H-Beta-300 at 240 °C.

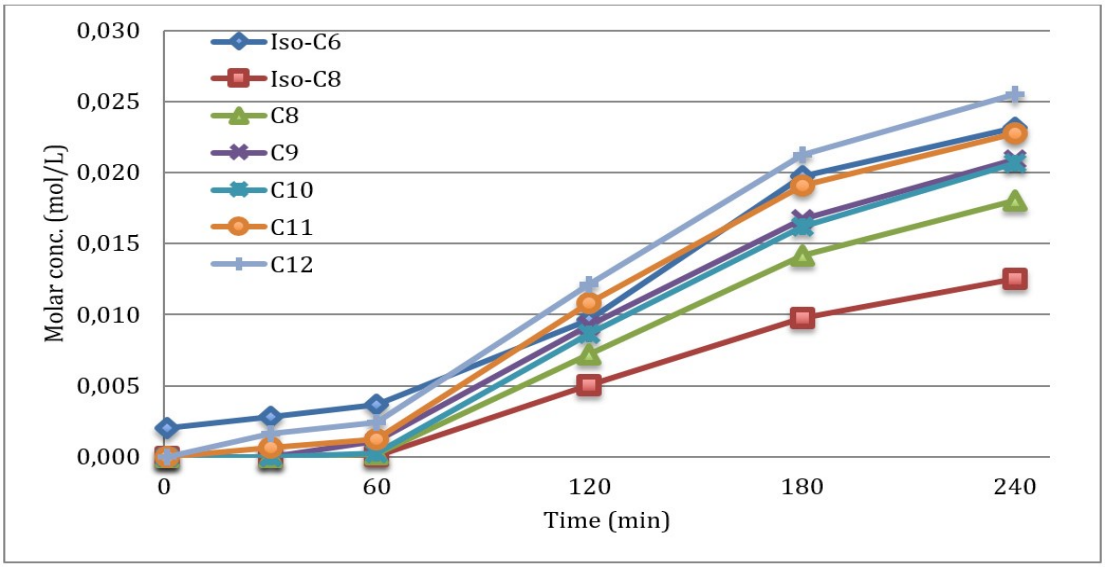

Figure 4.35b: Molar concentration of the cracked products over 1 wt.% Ru/H-Beta-300 at 250 °C.

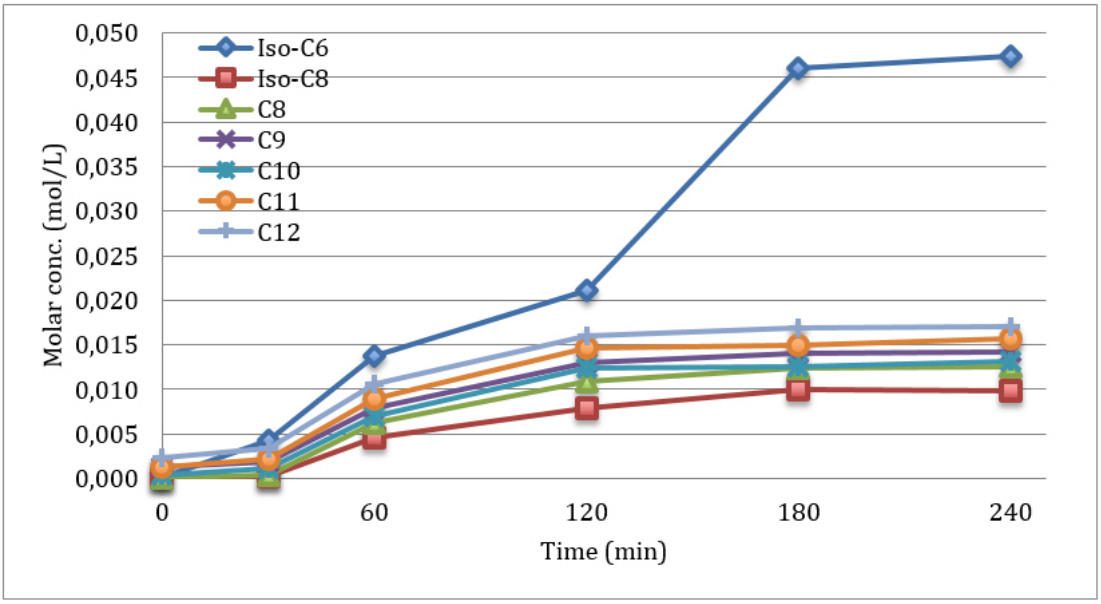

Figure 4.35c: Molar concentration of the cracked products over 1 wt.% Ru/H-Beta-300 at 270 °C.

Long-chain hydrocarbons also exhibited the same molar concentration at 240 °C and 250 °C while at a higher temperature of 270 °C, their concentration decreased for all three long-chain hydrocarbons. This trend can be seen for normal pentadecane in Figure 4.36. In comparison to 1 wt.% Ru/H-Beta-150 (Figure 4.27, 4.28 and 4.29), more long-chain hydrocarbons were formed with 1 wt.% Ru/H-Beta-300. This decrease in concentration may be due to higher secondary cracking at a higher temperature.

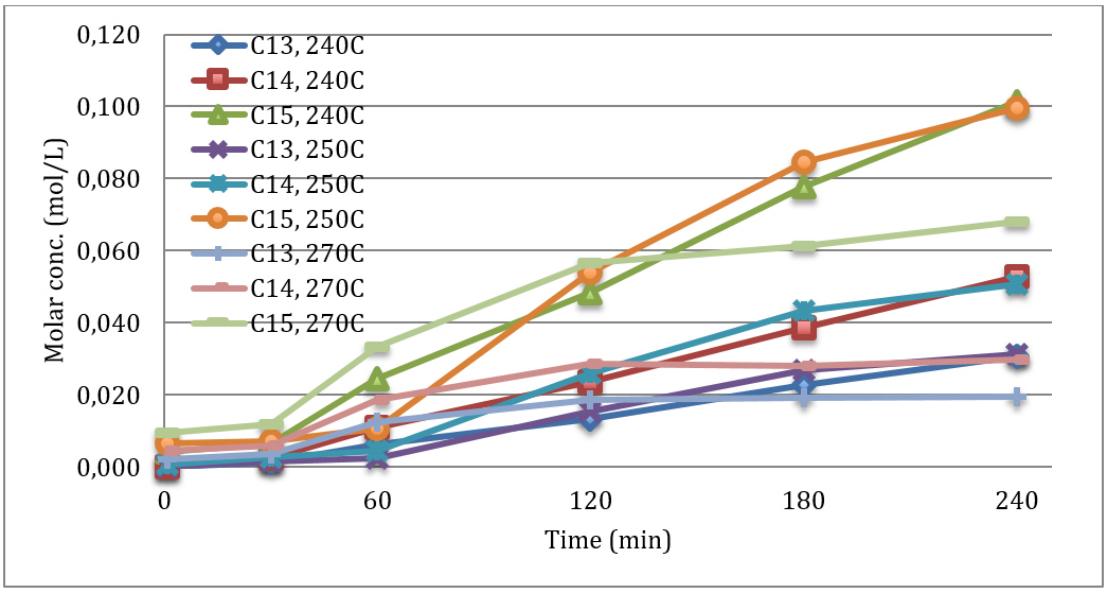

Figure 4.36: Molar concentration of long-chain hydrocarbons over 1 wt.% Ru/H-Beta-300 at different temperatures.

The most interesting results are presented in Figure 4.37 displaying a direct increase of methyl-pentadecane with temperature elevation. The concentration of methylpentadecane had clearly increased over 1 wt.% Ru/H-Beta-300 compared to 1 wt.% Ru/H-Beta-150 despite lower acidity of H-Beta-300. This would rather say that limiting steps are dehydrogenation (metal sites) than skeletal isomerization (acid sites).

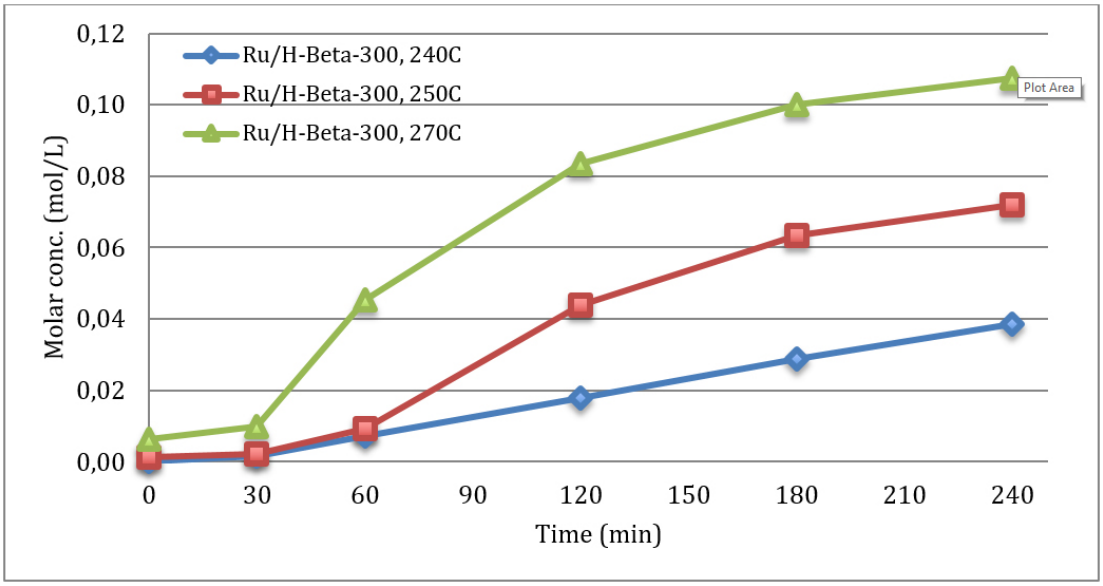

Figure 4.37:Molar concentration of methylpentadecane over 1 wt.% Ru/H-Beta-300 at different temperatures.

Table 4.17: Molar concentration of methyl-pentadecane over platinum beta zeolites at 240 min.

Catalyst	Molar conc. at 240 min (mol/L)
1 wt.% Ru/H-Beta-300 (240 °C)	0.0385
1 wt.% Ru/H-Beta-300 (250 °C)	0.0720
1 wt.% Ru/H-Beta-300 (270 °C)	0.0108

Concentrations of alkylated hexadecane products are displayed in Figure 4.38, revealing comparable values at all temperatures with minor differences. In comparison to 1 wt.% Ru/H-Beta-150 (Figure 4.31 and 4.32), the concentrations of heptadecane increased slightly over 1 wt.% Ru/H-Beta-300 at elevated temperatures. In the case of octadecane, the concentration had increased from 0.0006 mol/L to 0.0036 mol/L.

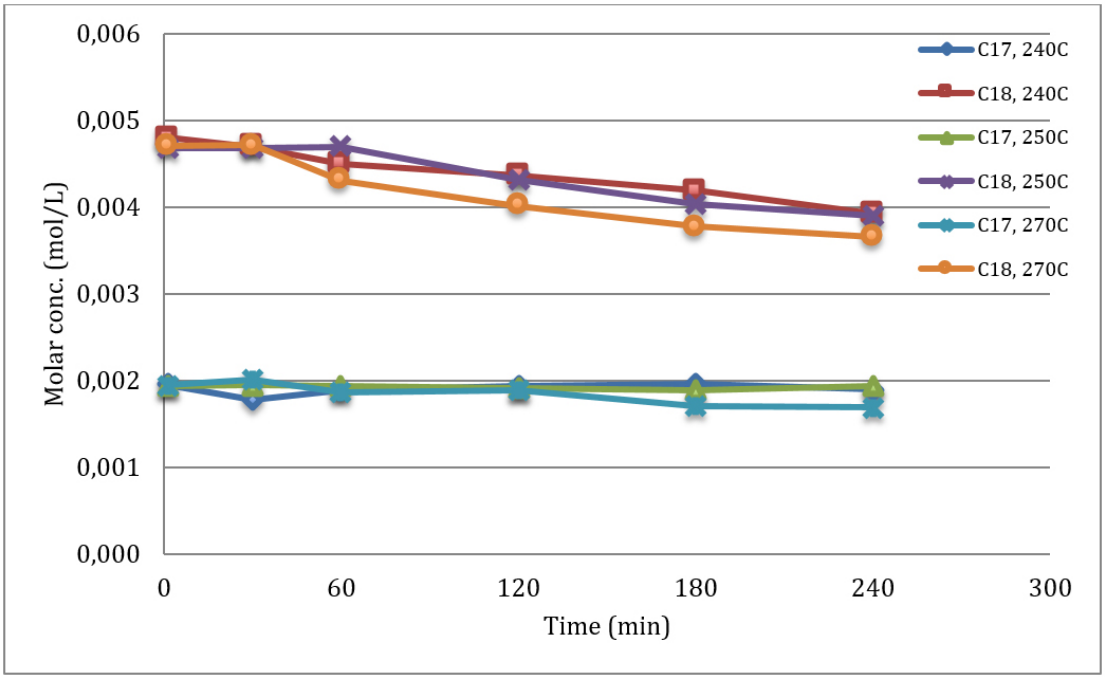

Figure 4.38:Molar concentration of alkylated hexadecane products over 1 wt.% Ru/H-Beta-300 at different temperatures.

From Figure 4.38 it can be concluded that at elevated temperature, the alkylated hexadecane products are more reactive as their concentrations are decreasing. This effect can be seen from the molar concentrations of normal octadecane, which was more reactive in comparison to heptadecane.

The yield of 1 wt.% Ru/H-Beta-300 is displayed in Table 4.18, and in comparison, the yields of 2 wt.% Pt/H-Beta-25 and 1 wt.% Ru/H-Beta-150 are shown in Table 4.19. It was evident that at elevated temperatures, the yield of methyl-pentadecane was increasing while other yields of cracking; long-chain hydrocarbons and alkylated hexadecane products were decreasing. From these results, it can be concluded that at higher temperature the ruthenium catalyst was more active.

Table 4.18: Yield of 1 wt.% Ru/H-Beta-300 at different temperatures, i.e. 240, 250 and 270 °C.

Temperature (°C) (45 bar)	**Cracked hydrocarbons**	**Long-chain hydrocarbons**	**Isomerized methyl-pentadecane**	**Alkylated hexadecane**
240	4.83	5.41	1.13	0.17
250	4.53	5.32	2.11	0.17
270	4.26	3.43	3.15	0.16

Table 4.19: Yield of 2 wt.% Pt/H-Beta-25 and 1 wt.% Ru/H-Beta-150 at 210°C and 40 bar.

Catalyst	Cracked hydrocarbons	Long-chain hydrocarbons	Isomerized methyl-pentadecane	Alkylated hexadecane
2 wt.% Pt/H-Beta-25	0.03	0.32	1.94	0.23
1 wt.% Ru/H-Beta-150	0.13	0.44	0.38	0.09

4.5 Role of metal dispersion and crystalline size of zeolites on hydroisomerization of hexadecane

4.5.1 Role of metal dispersion

From the literature [50] it can be concluded that a high metal dispersion promotes hydroisomerization. The role of metal dispersion can be seen in 2 wt.% Pt/H-Beta-25, which exhibited the highest dispersion of 30% (Table 4.4) among all bifunctional catalysts. A high dispersion of platinum, combined with superior hydrogenation ability of platinum aided hydroisomerization of hexadecane to methyl-pentadecane, with the conversion of 10.4%. In comparison, 2 wt.% Pt/H-Beta-300 had only 6.75% dispersion and displayed very a low methyl-pentadecane yield (Figure 4.21), with the conversion of 7%. Lower conversion and isomerization to methyl-pentadecane of 2 wt.% Pt/H-Beta-300 can be correlated to a lower metal dispersion and lower acidity.
Nickel and ruthenium catalysts also exhibited lower metal dispersion, which explains their poor hydroisomerization results. The metal dispersion of 5 wt.% Ni/H-Beta-25 and 1 wt.% Ru/H-Beta-150 were almost the same, 10% and they displayed almost similar molar concentrations of methyl-pentadecane Figure 4.30, although their acidity was different.

4.5.2 Role of the crystalline size of the zeolite

The crystalline size plays an important role in hydroisomerization reaction along with pore size of zeolites.[4] The optimal size of pores ensures the access of reactants to acid sites, which is vital for the catalytic reaction and thus formation of the desired product, methyl-pentadecane. The pore size of beta zeolite is 6.4 to 7.6 Å whereas the pore size of Y-zeolite is 7.4 Å. The cavities generated from the intersections have dimensions of 12 Å in both zeolites.[12] The crystalline sizes of H-Beta-25, 150 and

300 are 10 nm, 18 nm and 450 nm, respectively, measured by transmission electron microscopy.

Influence of the crystalline size can be directly seen in the results for TR2, 3 and 4. Conversion decreases as the crystalline size increases from H-Beta-25, 150 and 300. A similar trend can be seen with platinum and nickel catalysts. The conversion results can be seen in Table 4.13. Small crystalline size of H-Beta-25 allows better diffusion of reactants into the zeolite channels in comparison to H-Beta-300.[4] H-Beta-300 had a much higher crystalline size, hence slower diffusion compared to H-Beta-25 and lower acidity gave the lowest conversions in both parent and bifunctional metal modified zeolites.

4.6 Reaction pathways

Hydroisomerization and hydrocracking reactions proceed on bifunctional metal-acid catalysts containing hydrogenating/dehydrogenation sites provided by the noble or transition metals, with isomerization via carbenium ions occurring on the following acidic sites.[1] Hydroisomerization is accompanied by hydrocracking reaction, which is happening after skeletal isomerization of normal paraffins. Furthermore, multibranched are more prone towards cracking than the monobranched counterparts.[1] The isomerization mechanism comprises consecutive steps, [3,49]

i. Dehydrogenation on metallic sites
ii. Diffusion of the formed olefin to a Brønsted acid site
iii. Protonation of olefin on a Brønsted acid site with the formation of a secondary alkylcarbenium ion
iv. Addition of proton to form alkylcarbenium ion on the Brønsted acid site
v. Rearrangement of the alkylcarbenium ion
vi. Deprotonation on the Brønsted acid site
vii. Diffusion of the rearranged alkylcarbenium ion to metallic site
viii. Hydrogenation on the metallic site

Hexadecane can go undergo different reactions, i.e. cracking, hydroisomerization and alkylation. Reaction pathways of hexadecane transformation depend on the amount and strength of Brønsted acid sites and metal promoters. The reactions routes are demonstrated in Figure 4.39. All beta zeolites and bifunctional metal-zeolite catalysts catalyze hexadecane transformation under the reaction conditions, but they result in

different product distributions depending on the zeolite and metal promoter. Highly acidic supports, e.g. H-Beta-25 were prone to form high amounts of cracking products and formed methyl-pentadecane while low acidic zeolites like desilicated H-Beta-300 performed poorly. All the reactions, mentioned above, occur simultaneously. The gas-phase hydrocarbons are formed by cracking giving alkanes and alkenes. These alkenes then react with alkanes to form the alkylated hydrocarbons, i.e. heptadecane and octadecane. Liquid phase cracking products contain linear hydrocarbons, ranging from n-hexane to n-pentadecane, and single or double substituted branched hydrocarbons. Methyl-pentadecane is transformed directly from hexadecane via an alkylcarbenium ion.

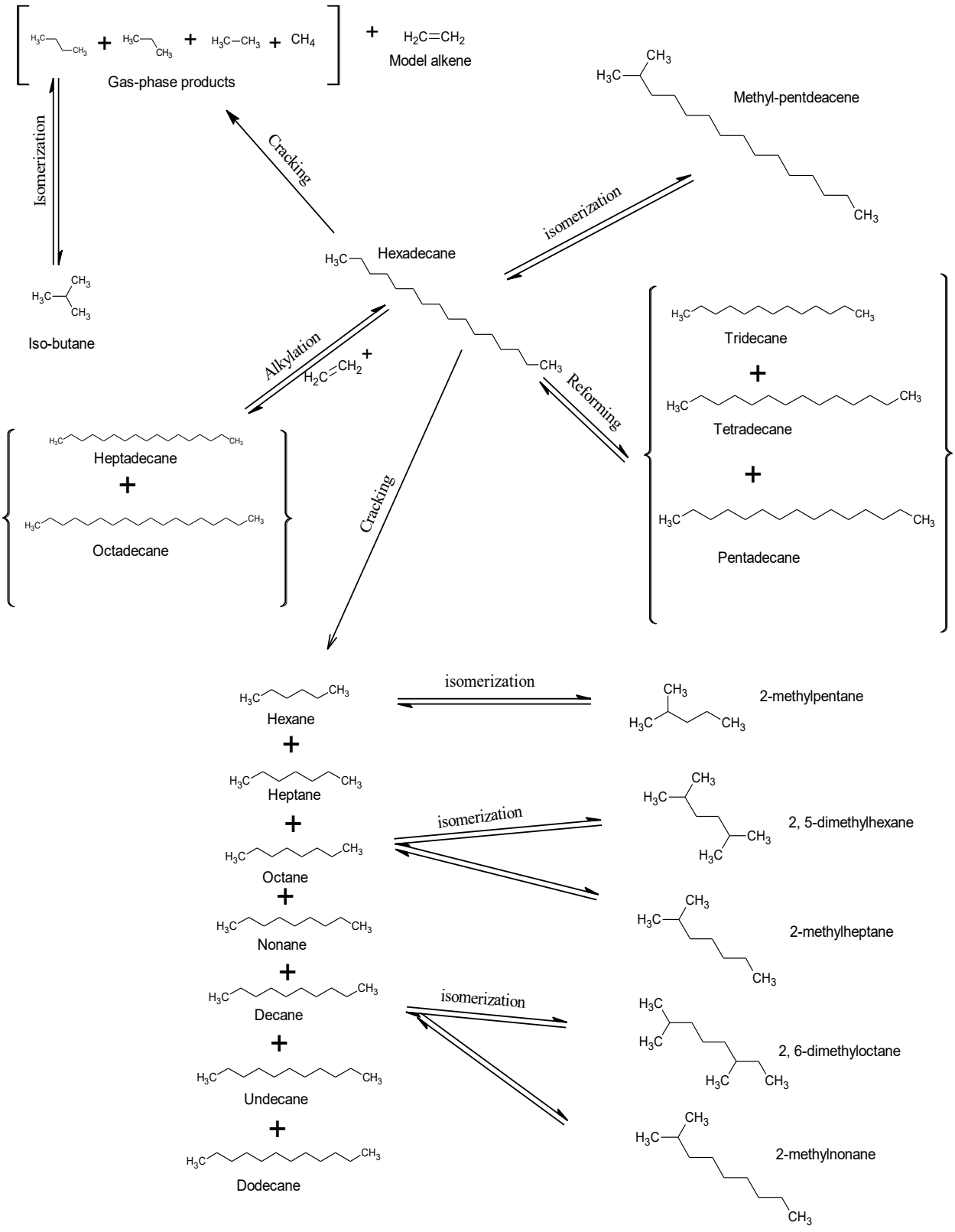

Figure 4.39: Reaction pathways for hydroisomerization of hexadecane over different catalysts.

5 Conclusions

The aim of this work was to improve the fuel properties of long-chain hydrocarbons, using hexadecane (n-C_{16}) as a model compound, under 210 °C and 40 bar of overall pressure. The experiments were performed over different acidic catalysts for hydroconversion of normal hexadecane to products. A broad range of acidic catalysts was tested for hydroisomerization of hexadecane, namely beta zeolite, desilicated beta zeolites, bifunctional platinum beta zeolites, bifunctional nickel beta zeolites, bifunctional ruthenium beta zeolites and bifunctional ruthenium Y-zeolite catalysts. Different product distribution was obtained as a result of hydroisomerization and hydrocracking reactions including gaseous hydrocarbons, cracked hydrocarbons, long-chain hydrocarbons, isomerized hexadecane (methyl-pentadecane) and alkylated hexadecane products.

Beta zeolites obtained from Zeolite International were transformed into proton forms by the step calcination method. The desilicated beta zeolites were formed by desilication using 0.1 M NaOH solution. Platinum and nickel catalysts were impregnated using hexachloroplatinic and nickel-nitrate as metal precursors by the evaporation impregnation method, respectively. Furthermore, ruthenium catalysts were prepared using ruthenium chloride as a metal precursor by an ion exchange method. The mechanical mixture (1:1 mass ratio) of platinum on alumina and H-Beta catalysts was physically mixed for the experiments. Ruthenium USY zeolites were obtained from ETH, Switzerland.

A preliminary experiment was performed at 210 °C and 40 bar total pressure with H-Beta-150, the reaction products in gas-phase and liquid phase were run in GC-MS for possible hydroisomerization products. The obtained products were calibrated for GC analysis to identify and quantify the reaction products.

The fresh and spent catalysts were characterized by different techniques to correlate their catalytic properties with their performance. Each of these fresh catalysts were characterized by nitrogen physisorption for the specific surface area and pore volume, Fourier-transform infrared spectroscopy (FTIR) with pyridine adsorption/desorption for Brønsted and Lewis acid sites, scanning electron microscopy for the catalyst morphology and elemental composition of catalysts, transmission electron microscopy for the catalyst structure and to determine the metal cluster size on the catalyst surface.

The spent catalysts were characterized by thermogravimetric analysis and organic elemental analysis for coke quantification. The molecular weight of the organic residue on the catalyst surface was determined by size exclusion chromatography. The results from the spent catalysts confirmed excessive coking on all bifunctional metal-beta zeolites except platinum-beta zeolites, which exhibited 4 times lower coke determined by the thermogravimetric method compared to other catalyst counterparts. The size exclusion chromatography confirmed the presence of lighter coke on platinum-beta zeolites, while other catalysts exhibited heavier coke.

The most prominent results were obtained by 2 wt.% Pt/H-Beta-25, 5 wt.% Ni/H-Beta-25 (250 °C) and 5 wt.% Ru/USY-15. These catalysts displayed the highest hydroisomerization yields among all catalysts. Among these catalysts, 2 wt.% Pt/H-Beta-25 showed the highest selectivity for methyl-pentadecane and a low amount of gas-phase and cracking products and long-chain hydrocarbons. 5 wt.% Ni/H-Beta-25 resulted in the highest formation of gas-phase products, a high amount of cracking products and long-chain hydrocarbons and displayed a lower yield of methyl-pentadecane compared to 2 wt.% Pt/H-Beta-25. 5 wt.% Ru/USY-15 exhibited the lowest amount of gas-phase products, and the highest amounts of cracked and long-chain hydrocarbons and formed the highest amount of methyl-pentadecane after 2 wt.% Pt/H-Beta-25. Moreover, the product distribution indicates that methyl-pentadecane was the primary reaction product on 2 wt.% Pt/H-Beta-25, while on nickel and ruthenium catalysts, hydrocracking reactions were the main ones.

The methyl-pentadecane yield decreased in the following order: 2 wt.% Pt/H-Beta-25 > 5 wt.% Ru/USY-15 > 5 wt.% Ni/H-Beta-25. The cracking yield decreased as follows: 5 wt.% Ru/USY-15 > 5 wt.% Ni/H-Beta-25, 2.5 wt.% Ru/USY-30 > 2 wt.% Pt/H-Beta-25. The long-chain hydrocarbons decreased as follows: 5 wt.% Ru/USY-15 > 5 wt.% Ni/H-Beta-25 > 2.5 wt.% Ru/USY-30 > 2 wt.% Pt/H-Beta-25. The yields of alkylated hexadecane products, i.e. heptadecane and octadecane, were mostly the same in all experiments. The gas-phase analysis after 4 h hydroisomerization reaction indicated the presence of methane in all catalysts. Other light hydrocarbons, such as ethane, propane and butane, were present along with isomerized iso-butane formed via hydrogenolysis.

The kinetic experiments with 1 wt.% Ru/H-Beta-300 at 240 °C, 250 °C and 270 °C indicated that at elevated temperature and pressure, the methyl-pentadecane yield was

significantly increased and the yields of cracking products and long-chain hydrocarbons along with alkylated hexadecane products decreased.

The results from the experimental work implied that hydroisomerization reactivity of hexadecane depends on two parameters: hydrogenation activity of the metal and acidity. These parameters are equally important to obtain hydroisomerization of hexadecane. The hydrogenation activity of different metals in bifunctional catalysts indicated superiority of platinum over other metals; Brønsted acid sites provided efficient acidity, which is a key for better hydroisomerization. In addition to their high acidity, H-Beta-25 exhibits large channels together with a small crystalline size, which enables efficient diffusion of reactants. Subsequently, 2 wt.% Pt/H-Beta-25 showed the best hydroisomerization results in n-hexadecane transformation and formed the highest yield of methyl-pentadecane with lower yields of cracking products and long-chain hydrocarbons.

The kinetic experiments with 1 wt.% Ru/H-Beta-300 suggested that elevated temperature and total pressure can increase the methyl-pentadecane yield with a lower yield of cracking products. Thus,appen this catalyst can be considered as an efficient candidate for dewaxing of hexadecane at 270 °C and 45 bar total pressure for improved fuel properties. In the future, research work with these catalysts for the hydroisomerization of hexadecane could be carried out in a continuous reactor, i.e. a trickle bed reactor.

References

[1] Deldari, H. **(2005)**. Suitable catalysts for hydroisomerization of long-chain normal paraffins. *Applied Catalysis A: General*, 293, pp.1-10.

[2] Batalha, N., Pinard, L., Bouchy, C., Guillon E., Guisnet, M. **(2013)**. n-Hexadecane hydroisomerization over Pt-H-BETA catalysts. Quantification and effect of the intimacy between metal and protonic sites. *Journal of Catalysis*, 307, pp.122-131.

[3] Park, K. Ihm, S. **(2000)**. Comparison of Pt/zeolite catalysts for n-hexadecane hydroisomerization. *Applied Catalysis A: General*, 203(2), pp.201-209.

[4] Soualah, A., Lemberton, J., Pinard, L., Chater, M., Magnoux, P. Moljord, K. **(2008)**. Hydroisomerization of long-chain n-alkanes on bifunctional Pt/zeolite catalysts: Effect of the zeolite structure on the product selectivity and on the reaction mechanism. *Applied Catalysis A: General*, 336(1-2), pp.23-28.

[5] Gomes, L., de Oliveira Rosas, D., Chistone, R., Zotin, F., de Araujo, L. Zotin, J. **(2017)**. Hydroisomerization of n-hexadecane using Pt/alumina-Beta zeolite catalysts for producing renewable diesel with low pour point. *Fuel*, 209, pp.521-528.

[6] Mériaudeau, P., Tuan, V., Nghiem, V., Lai, S., Hung, L. Naccache, C. **(1997)**. SAPO-11, SAPO-31, and SAPO-41 molecular sieves: synthesis, characterization, and catalytic properties inn-octane hydroisomerization. *Journal of Catalysis*, 169(1), pp.55-66.

[7] Martens, J., Vanbutsele, G., Jacobs, P., Denayer, J., Ocakoglu, R., Baron, G., Muñoz Arroyo, J., Thybaut, J. Marin, G. **(2001)**. Evidences for pore mouth and key–lock catalysis in hydroisomerization of long n-alkanes over 10-ring tubular pore bifunctional zeolites. *Catalysis Today*, 65(2-4), pp.111-116.

[8] Mériaudeau, P., Tuan, V., Nghiem, V., Lai, S., Hung, L. Naccache, C. **(1997)**. SAPO-11, SAPO-31, and SAPO-41 molecular sieves: synthesis, characterization, and catalytic properties inn-octane hydroisomerization. *Journal of Catalysis*, 169(1), pp.55-66.

[9] Chao, K., Wu, H. Leu, L. **(1996)**. Hydroisomerization of light normal paraffins over series of platinum-loaded mordenite and beta catalysts. *Applied Catalysis A: General*, 143(2), pp.223-243.

[10] Martens, J., Parton, R., Uytterhoeven, L., Jacobs, P. Froment, G. **(1991)**. Selective conversion of decane into branched isomers: A comparison of

platinum/ZSM-22, platinum/ZSM-5 and platinum/USY zeolite catalysts. *Applied Catalysis*, 76(1), pp.95-116.

[11] Claude, M., Vanbutsele, G. Martens, J. **(2001)**. Dimethyl branching of long n-alkanes in the range from decane to tetracosane on Pt/H–ZSM-22 bifunctional catalyst. *Journal of Catalysis*, 203(1), pp.213-231.

[12] Meier, W. M., Olson, D. H., Baerlocher, Ch. **(1996)**. Atlas of zeolites structure types. *Zeolites- international Journal of Molecular sieves*, 5th edition, 405.

[13] Camblor, M. A., Pérez-Pariente, J. **(1991)**. Crystallization of zeolite beta–effect of Na and K–ions, *Zeolites*, 11(3), pp.202-210.

[14] http://www.iza-online.org [Accessed July 31, 2018]

[15] García-Martínez, J., Li, K. Krishnaiah, G. **(2012)**. A mesostructured Y zeolite as a superior FCC catalyst – from lab to refinery. *Chemical Communications*, 48(97), pp.11841.

[16] Kortunov, P., Vasenkov, S., Kärger, J., Valiullin, R., Gottschalk, P., Fé Elía, M., Perez, M., Stöcker, M., Drescher, B., McElhiney, G., Berger, C., Gläser, R. Weitkamp, J. **(2005)**. The role of mesopores in intracrystalline transport in US-Y zeolite: PFG NMR diffusion study on various length scales. *Journal of the American Chemical Society*, 127(37), pp.13055-13059.

[17] Leofanti, G., Padovan, M., Tozzola, G. Venturelli, B. **(1998)**. Surface area and pore texture of catalysts. *Catalysis Today*, 41(1-3), pp.207-219.

[18] Belskaya, O., Danilova, I., Kazakov, M., Mironenko, R., Lavrenov, A. Likholobov, V. **(2013)**. ChemInform Abstract: FTIR spectroscopy of adsorbed probe molecules for analyzing the surface properties of supported Pt (Pd) catalysts. *ChemInform*, 44(51). Available at: <http://cdn.intechopen.com/pdfs-wm/36172.pdf> [Accessed July 19, 2018].

[19] Swapp, S. **(2017)** Scanning Electron Microscopy (SEM). [online] Available at: <https://serc.carleton.edu/research_education/geochemsheets/techniques/SEM.html> [Accessed July 21, 2018].

[20] Murzin, D. **(2013)** Engineering Catalysis. [e-book] Available at: <http://ebookcentral.proquest.com/lib/aboebooks/reader.action?Docid=912966&ppg=1>

[21] Anderson Materials Evaluation, Inc. **(2018)** TGA Analysis or Thermogravimetric Analysis. Available at: <http://www.andersonmaterials.com/tga.html> [Accessed July 22, 2018].

[22] Abdullah, H.A., Hauser, A., Ali, F.A. Al-Adwani. **(2006)**. Optimal conditions for coke extraction of spent catalyst by accelerated solvent extraction compared to soxhlet. *Energy Fuels*, 20(1), pp.320-323.

[23] Duca, D. Deganello, G. **(1996).** Analysis by size exclusion chromatography (SEC) of catalytic materials: The fractal properties and the pore size distribution of pumice. *Journal of Molecular Catalysis A: Chemical*, 112(3), pp.413-421.

[24] Thompson, M. **(2008).** CHNS Elemental Analysers. Available at: <http://www.rsc.org/images/CHNS-elemental-analysers-technical-brief-29_tcm18-214833.pdf> [Accessed July 11, 2018]

[25] Guisnet, M. Magnoux, P. **(1989)**. Coking and deactivation of zeolites. *Applied Catalysis*, 54(1), pp.1-27.

[26] Thet, K. Woo, N. **(2015)**. Gas Chromatography [online] Available at: <https://chem.libretexts.org/Core/Analytical_Chemistry/Instrumental_Analysis/Chromatography/Gas_Chromatography> [Accessed July 15, 2018].

[27] Johnsen, L. G., Skou, P. B., Khakimov, B. **(2017)**. Gas chromatography – mass spectrometry data processing made easy. Journal of Chromatography, 1503, pp.57-64.

[28] Wilson, I.D. Poole, C.F. **(2009)**. Handbook of Methods and Instrumentation in Separation Science. 1st edition, London: Elsevier.

[29] https://clu-in.org/characterization/technologies/mspec.cfm
[Accessed August 8, 2018].

[30] Rodríguez, E., Félix, G., Ancheyta, J, Trejo, F. **(2018)**. Modeling of hydrotreating catalyst deactivation for heavy oil hydrocarbons. *Fuel*, 225, 118-133

[31] Bartholomew, C. **(2001)**. Mechanism of catalyst deactivation. *Applied Catalysis A: General*, 212(1-2), pp.17-60.

[32] Thakur, D., Thomas, M. **(1985)**. Catalyst deactivation in heavy petroleum and synthetic crude processing: *a review*, 15(2), pp.197-225.

[33] Tamm, P., Harnsberger, H., Bridge, A. **(1981)**. Effects of feed metals on catalyst aging in hydroprocessing residuum. *Industrial and Engineering Chemistry, Process Design and Development*. 20(2), pp.262-273.

[34] Menon, P. **(1990)**. Coke on catalysts-harmful, harmless, invisible and beneficial types. *Journal of Molecular Catalysis*, 59(2), pp.201-220.

[35] Emeis, C. **(1993)**. Determination of integrated molar extinction coefficients for infrared absorption bands of pyridine adsorbed on solid acid catalysts. *Journal of Catalysis*, 141(2), pp.347-354.

[36] Patterson, R. **(1973)**. Automated Pregl-Dumas technique for determining total carbon, hydrogen, and nitrogen in atmospheric aerosols. *Analytical Chemistry*, 45(3), pp.605-609.

[37] Halász, I., Martin, K. **(1978)**. Pore sizes of solids. *Angewandte Chemie International Edition*, 17(12), pp.901-908.

[38] Mori, S., Barth, H. **(2011)**. Size exclusion chromatography. Berlin: Springer.

[39] Stekrova, M., Kumar, N., Díaz, S., Mäki-Arvela, P., Murzin, D. (2015). H- and Fe-modified zeolite beta catalysts for preparation of trans-carveol from α-pinene oxide. *Catalysis Today*, 241, pp.237-245.

[40] Schmidt, S., Kumar, N., Shchukarev, A., Eränen, K., Mikkola, J., Murzin, D. Salmi, T. **(2013)**. Preparation and characterization of neat and $ZnCl_2$ modified zeolites and alumina for methyl chloride synthesis. *Applied Catalysis A: General*, 468, pp.120-134.

[41] Groen, J., Abelló, S., Villaescusa, L, Pérez-Ramírez, J. **(2008)**. Mesoporous beta zeolite obtained by desilication. *microporous and Mesoporous materials*, 114(1-3), pp.93-102.

[42] Dewajani, H., Purwono, S, and Budiman A. **(2016)**. Effect of modification ZSM-5 catalyst in upgrading quality of organic liquid product derived from catalytic cracking of Indonesian nyamplung oil (Calophyllum inophyllum), AIP conference proceedings, 1755-1, 050002.

[43]Guisnet, M. and Magnoux, P. **(1994)**. Fundamental description of deactivation and regeneration of acid catalysts. *Elsevier Science B. V*., (88), pp. 53-67.

[44] Guisnet, M., Magnoux, P. **(1989)**. Coking and deactivation of zeolites. *Applied Catalysis*, 54(1), pp.1-27.

[45] Moljord, K., Magnoux, P., Guisnet, M. **(1995)**. Coking, aging and regeneration of zeolites XV. Influence of the composition of HY zeolites on the mode of formation of coke from propene at 450°C. *Applied Catalysis A: General*, 122(1), pp.21-32.

[46] Guisnet, M., Magnoux, P. **(1997)**. Deactivation by coking of zeolite catalysts. Prevention of deactivation. Optimal conditions for regeneration. *Catalysis Today*, 36(4), pp.477-483.

[47] Froment, G., Figueiredo, J. **(1982)**. Progress in catalyst deactivation, NATO ASI Series E, *Catalysis Today*, 36, pp.477-483.

[48] Liu, X., Mäki-Arvela, P., Aho, A., Vajglova, Z., Gun'ko, V., Heinmaa, I., Kumar, N., Eränen, K., Salmi, T., Murzin, D. **(2018)**. Zeta potential of beta zeolites: influence of structure, acidity, pH, temperature and concentration. *Molecules*, 23(4), pp.946.

[49] Regali, F., Boutonnet, M., and Järås, S. **(2013)**. Hydrocracking of n-hexadecane on noble metal/silica–alumina catalysts. *Catalysis Today*, 214, p.12-18.

[50] Wang, Y.; Tao, Z.; Wu, B.; Xu, J.; Huo, C.; Li, K.; Chen, H.; Yang, Y.; Li, Y. **(2015)**. Effect of metal precursors on the performance of Pt/ZSM-22 catalysts for n-hexadecane hydroisomerization. *J. Catalysis*, *322*, pp.1–13.

[51] Kubička, D., Kumar, N., Venäläinen, T., Karhu, H., Kubičková, I., Österholm, H. and Murzin, D. **(2006)**. Metal−Support Interactions in Zeolite-Supported Noble Metals: Influence of Metal Crystallites on the Support Acidity. *The Journal of Physical Chemistry B*, 110(10), pp.4937-4946.

Appendix 1

Catalyst preparation, properties and product distributions found in [2,3,4].

1.1 Hydroisomerization of hexadecane in a batch reactor [Park et al. 2000]

The experimental work was carried in a batch reactor (EZE-Seal, Autoclave Engineers, 300 ml) and 50 ml of hexadecane was used in the reactor with 0.5 grams of the catalyst. The catalyst was reduced at 350 °C for 2 h with 50 ml/min hydrogen flow. The experimental work was carried at 350 °C, 103 bars and 1000 rpm of stirring. The liquid products were analyzed by gas chromatograph (HP 6890A) equipped with a flame ionization detector and 50 m HP-1 capillary column. [3]

Catalyst preparation conditions are listed in Table 1, while the surface area, dispersion and pore structure are presented in Table A1.2. The respective conversion over Pt/zeolite catalysts can be seen in Figure A1.1. The product distributions over hexadecane conversion and cracking product distribution over carbons numbers are given in Figure A1.2 and Figure A1.3 respectively.[3]

Table A1.1: Conditions for catalyst preparation.

Supports	Hydrogel composition	Temperature (°C)	Time (h)	Si/Al (mole ratio)
ZSM-5	$0.2TPABr–0.1Na_2O–SiO_2–0.0143Al_2O_3–40H_2O$	170	72	35
ZSM-22	$0.22HMDA–0.12K_2O–SiO_2–0.008Al_2O_3–30H_2O$	160	72	63
SAPO-11	$1.0DPA–0.1SiO_2–Al_2O_3–0.9P_2O_5–40H_2O$	200	48	0.05
MCM-41	$1.0HTACl–1.0Na_2O–4.0SiO_2–400H_2O$	100	144	∞
Al-MCM-41	–	–	–	20

Table A1.2: Properties of zeolite catalysts.

Catalysts	S_{BET} (m^2/g)	Dispersion		Pore structure of zeolite support (Å)
		%[b]	Å[c]	
Pt/ZSM-5	408	59	50	5.3×5.6, 5.1×5.5
Pt/ZSM-22	200	41	230	4.4×5.5
Pt/SAPO-11	169	35	80	3.9×6.3
Pt/Al-MCM-41	1180	55	30	26
Pt/H-Y	520	45	210	7.4
Pt/H-β	612	37	240	5.6×6.5, 5.7×7.5

a. All catalysts have the nominal Pt content of 0.5wt.%.
b. Dispersion (%) was characterized by CO chemisorption.
c. Average Pt size was estimated from the transmission electron micrograph.

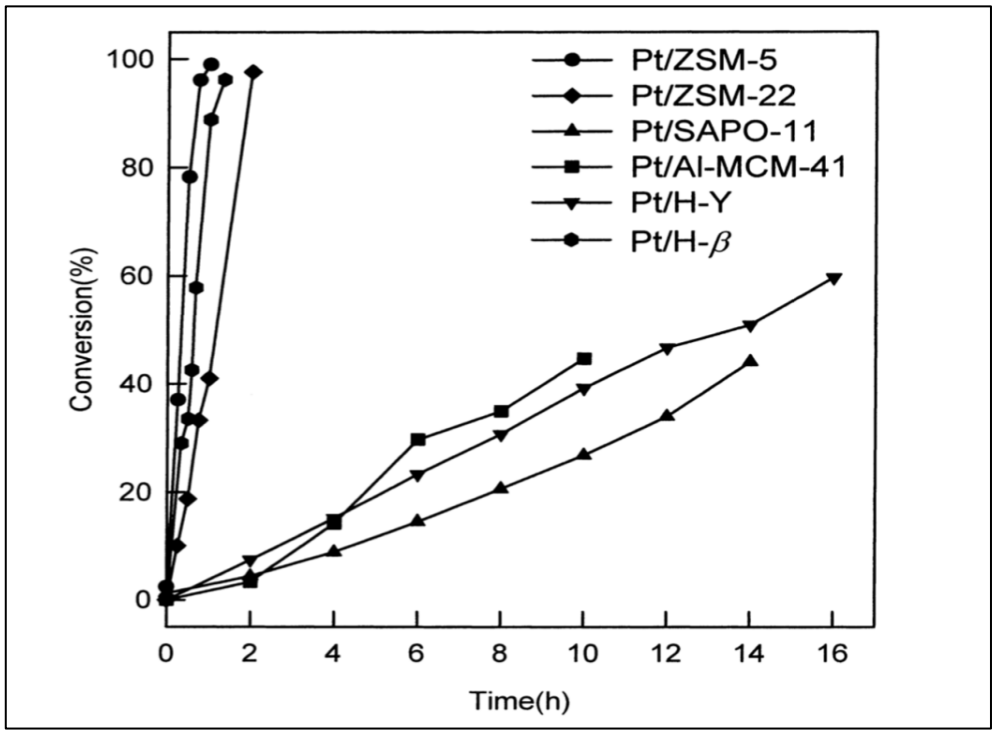

Figure A1.1: Conversion of n-hexadecane at 350 °C and 103 bar over Pt/zeolite catalysts.[3]

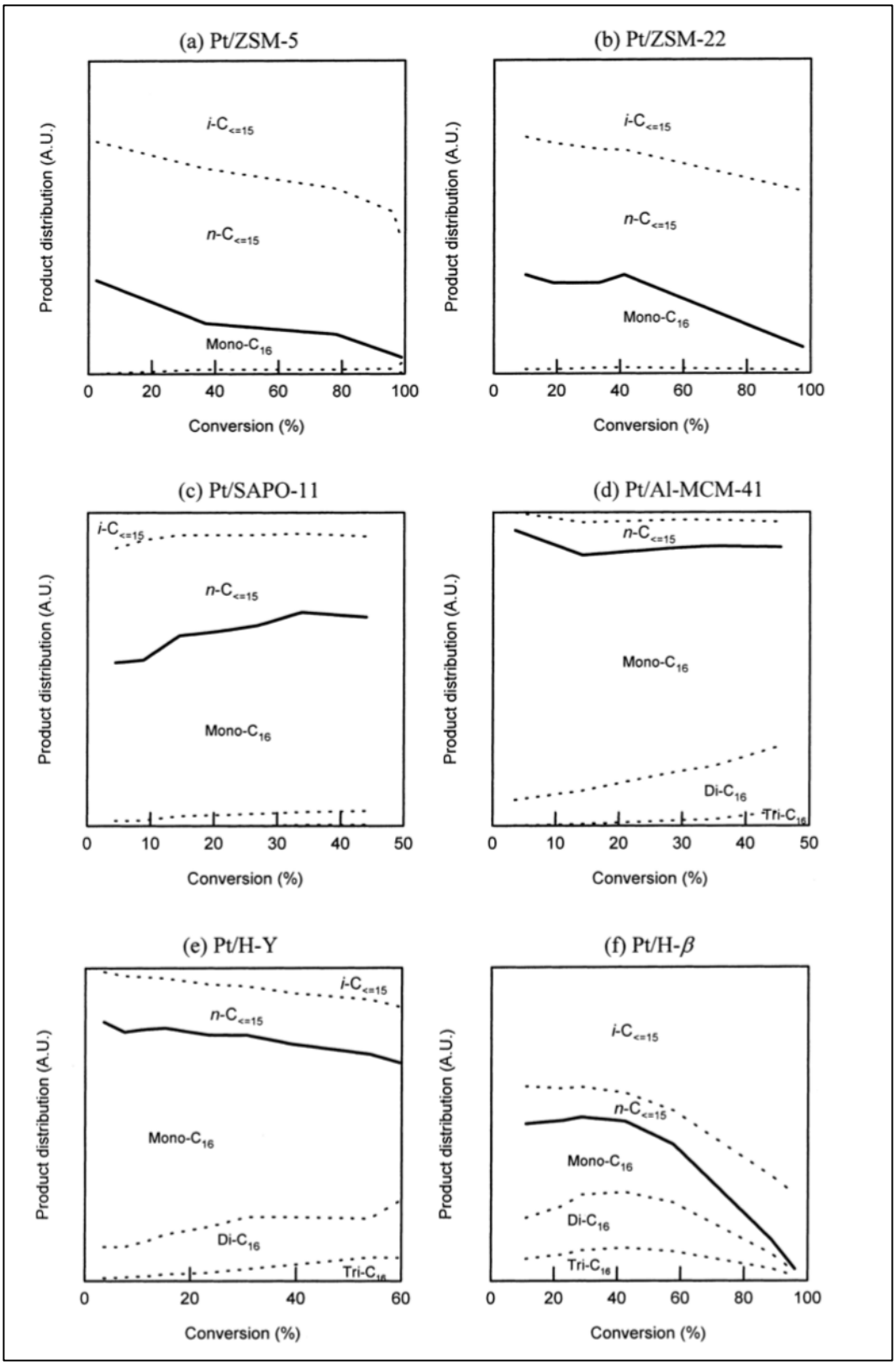

Figure A1.2: Product distribution as a function of conversion (%) for the isomerization of n-hexadecane. [3]

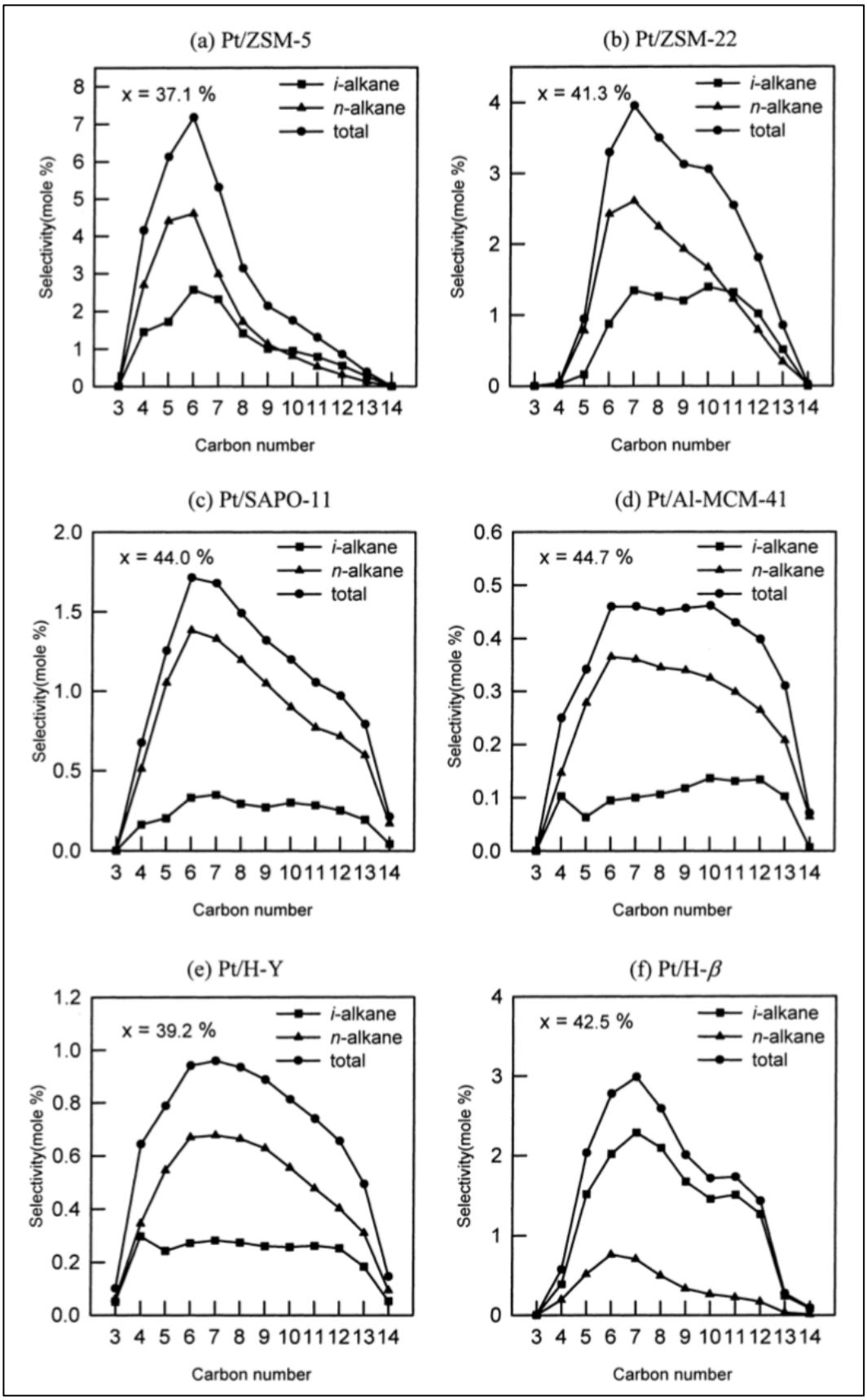

Figure A1.3: Molar concentration of cracked products for n-hexadecane isomerization. [3]

1.2 Hydroisomerization of n-hexadecane over Pt/H-BETA catalyst [Batalha et al. 2013]

The physiochemical characteristics of the bifunctional catalysts are listed in Table A1.3. The yield of isomers over three series of catalysts are presented in Figure A1.4 while the product distribution as a function of their carbon atoms is displayed in Figure A1.5. [2]

Table A1.3: Physicochemical characteristics of the bifunctional catalysts: Pt dispersion (D) estimated by CO chemisorption, concentrations of accessible Pt atoms (C_{Pt}), of protonic sites (C_{H+}), and balance between metal and acid functions (C_{Pt}/C_{H+}).

	Catalyst	D^a (%)	C_{Pt} (µmol g^{-1})	C_{H+} (µmol g^{-1})	C_{Pt}/C_{H+}
	HBEA	–	–	440[b]	0
	0.7Pt/(HBEA/A)	18	4.7	86[b]	0.055
Series S1	0.2Pt/HBEA	2	0.1	394[b]	0.0003
	0.5Pt/HBEA	6	1.7	406[b]	0.0040
	1.0Pt/HBEA	17	8.3	425[b]	0.0200
	1.5Pt/HBEA	16	12.7	396[b]	0.0320
	PtA	40	19.7	0	∞
Series S2 and S3	PtA-HBEA(5-95)	40	1.0	418[c]	0.002
	PtA-HBEA(25-75)	40	4.9	330[c]	0.015
	PtA-HBEA(50-50)	40	9.9	220[c]	0.045
	PtA-HBEA(75-25)	40	14.8	110[c]	0.130

a. Measured by CO chemisorption at 25 °C.

b. Measured by pyridine adsorption at 150 °C.

c. Calculated from the amount of zeolite in the composite catalysts.

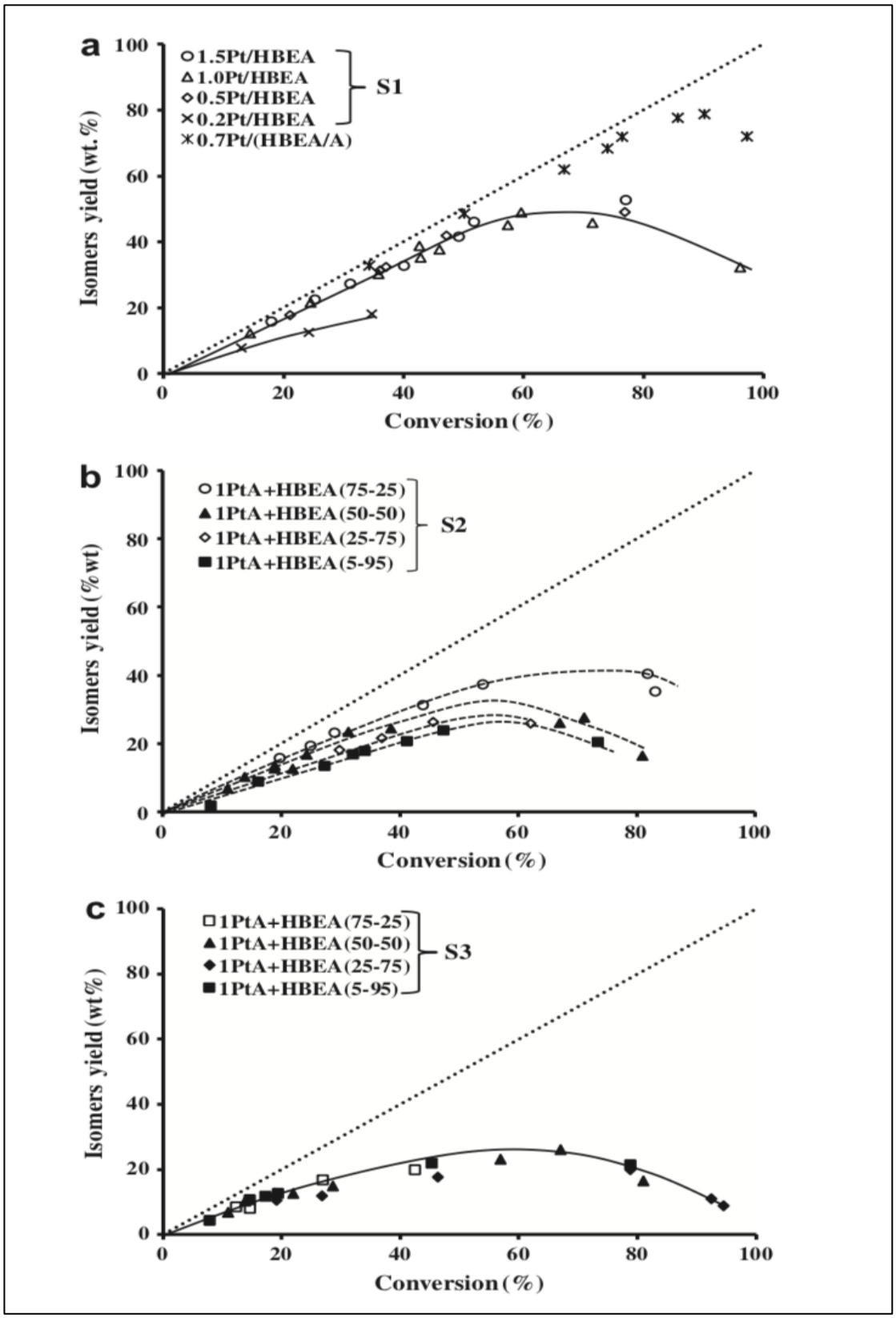

Figure A1.4: Yield of isomer vs n-C_{16} conversion for the three series of bifunctional catalysts: (a) Pt/H-BETA (S1) and 0.7 Pt/H-BETA/A) catalysts, (b) S2: an intimate mixture of PtA and H-BETA, (c) S3: a physical mixture of PtA and H-BETA.[2]

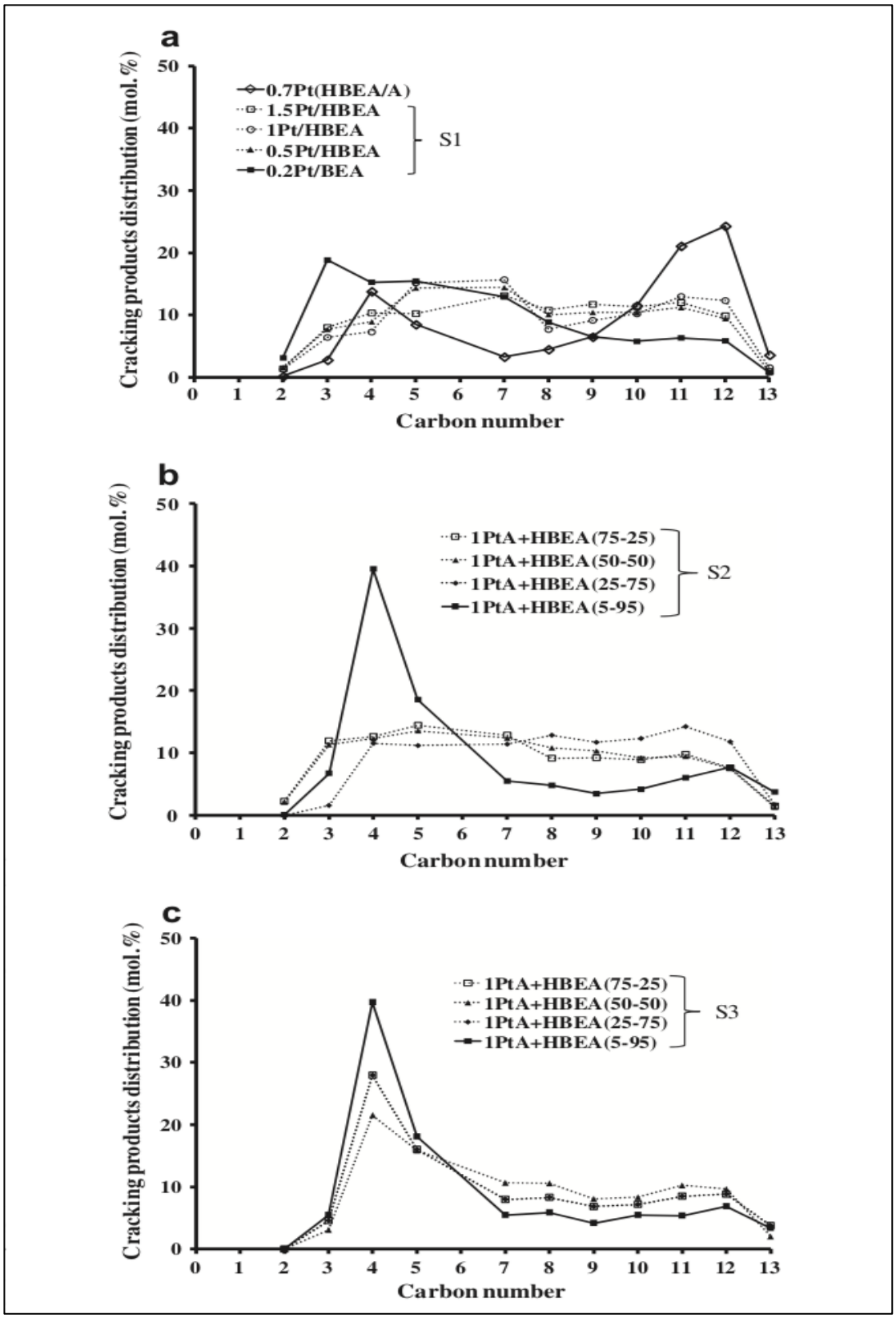

Figure A1.5: Cracking product distribution (mol.%): percentage of cracking products as a function of the number of carbon atoms. (a) Pt/H-BETA (S1) and 0.7 Pt/H-BETA/A) catalysts, (b) S2: an intimate mixture of PtA and H-BETA, (c) S3: a physical mixture of PtA and H-BETA.[2]

1.3. Hydroisomerization of long-chain alkanes over Pt/zeolite catalyst [Soualah et al. 2008]

The catalysts were reduced in-situ before the reaction under hydrogen flow for 6 hours at 450 °C. To facilitate product analysis, n-alkanes were diluted with n-hexane, which is inert at reaction conditions, n-Tetradecane and n-hexadecane were also diluted while n-decane can be used without dilution. The feed compositions of diluted components were 20 mol.% n-C_{14}- 80 mol.% n-C_6 and 10 mol.% n-C_{16}- 90 mol.% n-C_6. The reaction products were analyzed online by gas liquid chromatograph (Varian 3400) with 50 m CPSil-5 capillary column from Chrompack under hydrogen as a carrier gas. [4]

The characteristics of the zeolite catalysts are listed in Table A1.4. The product distributions (mol.%) over carbon number are listed in Figure A1.6. Transformations of the three reactants over Pt/zeolite catalysts into three categorized groups are listed in Figure A1.7. Isomerization of the three reactants on Pt/zeolite catalysts as a function of n-alkane conversion is shown in Figure A1.8. [4]

Table 4: Zeolite catalyst characteristics.

Zeolite	Framework Si/Al ratio	Crystallite size (nm)	Specific surface area ($m^2\ g^{-1}$)	Pore volume ($cm^3\ g^{-1}$)		Brönsted acidic sites (mmol g^{-1})	
				Micro	Meso	Total[a]	Strong[b]
HBEA	11	20	640	0.21	0.51	0.444	0.142
HMCM-22	17	100–150	575	0.22	0.26	0.589	0.451
HZSM-5	25	150–300	415	0.16	0.03	0.456	0.259

a. Number of pyridine molecules retained on the zeolite after desorption at 150 °C.
b. Number of pyridine molecules retained on the zeolite after desorption at 450 °C.

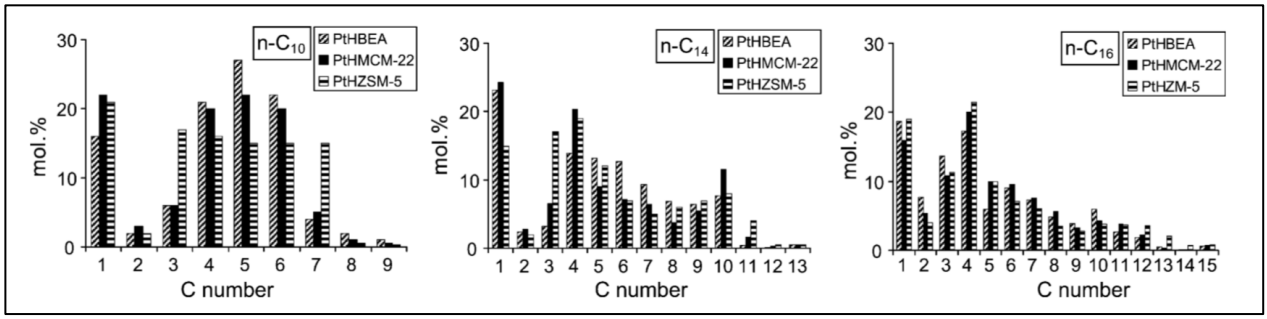

Figure A1.6: Cracking product distribution for 20 wt.% n-C_{10}, n-C_{14} and n-C_{16} on Pt/zeolite catalysts [4].

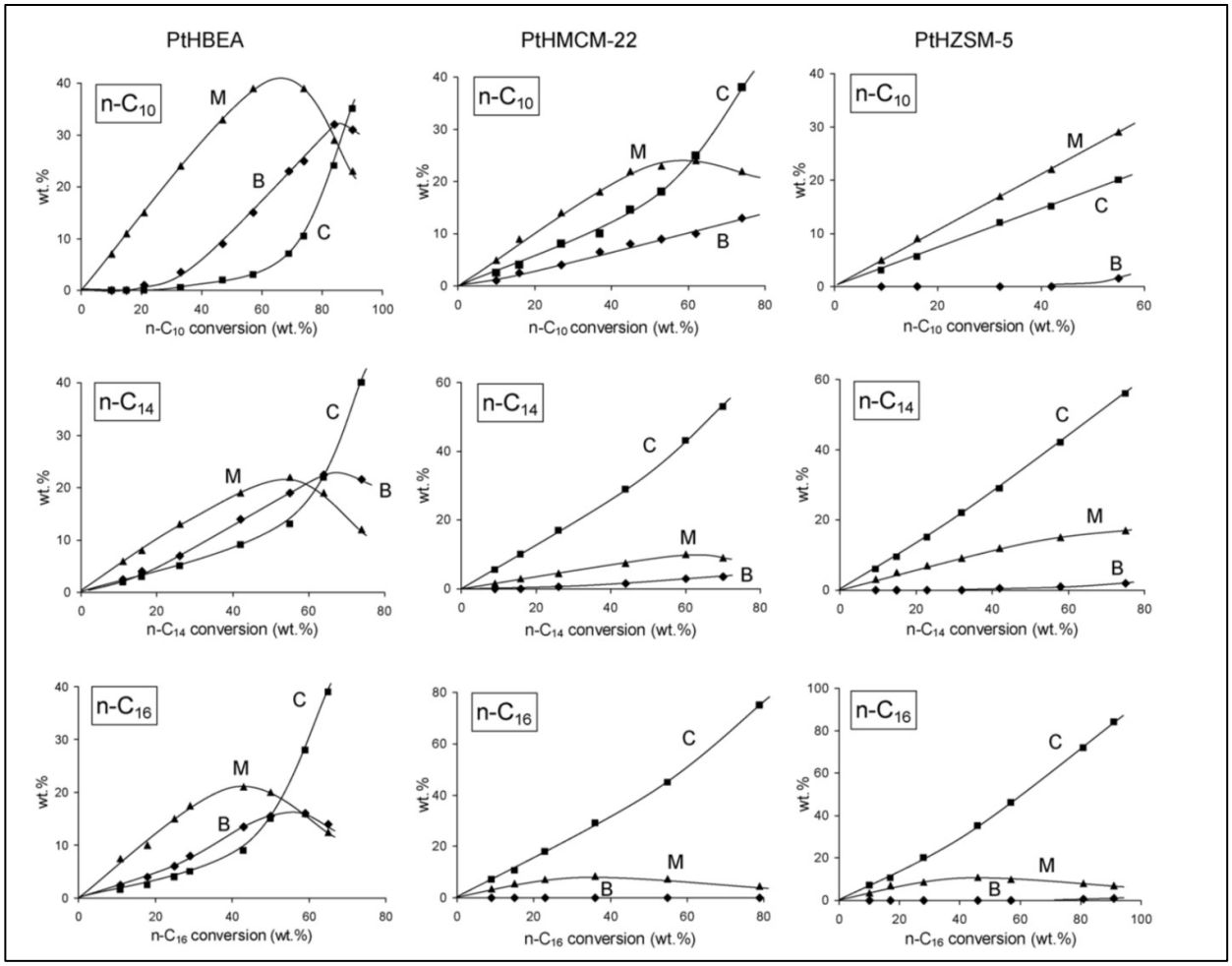

Figure 7: Product distribution of n-C_{10}, n-C_{14} and n-C_{16} on Pt/zeolites in Mono-branched (M), multi-branched (B), and cracking products (C) as a function of n-alkane conversion. [4]

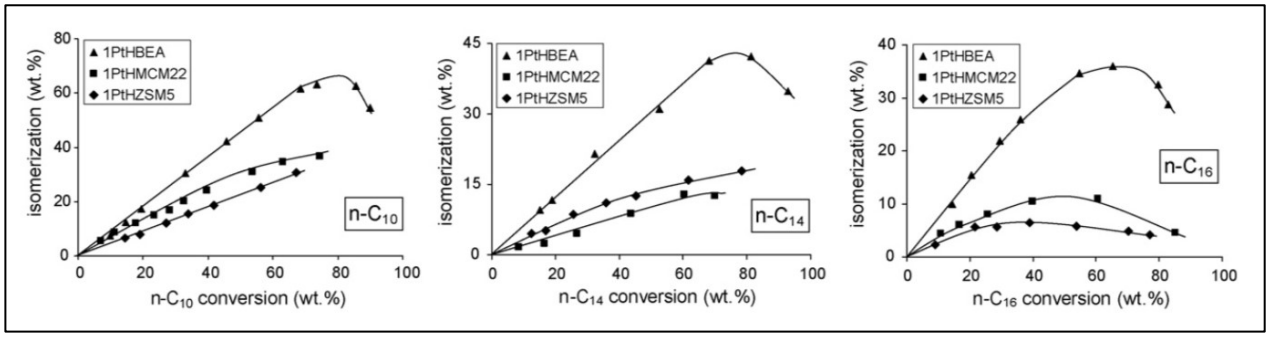

Figure A1.8: Transformation of n-C_{10}, n-C_{14} and n-C_{16} on Pt/zeolites as a function of n-alkane conversion. [4]

Appendix 2

Scanning electron microscopy.

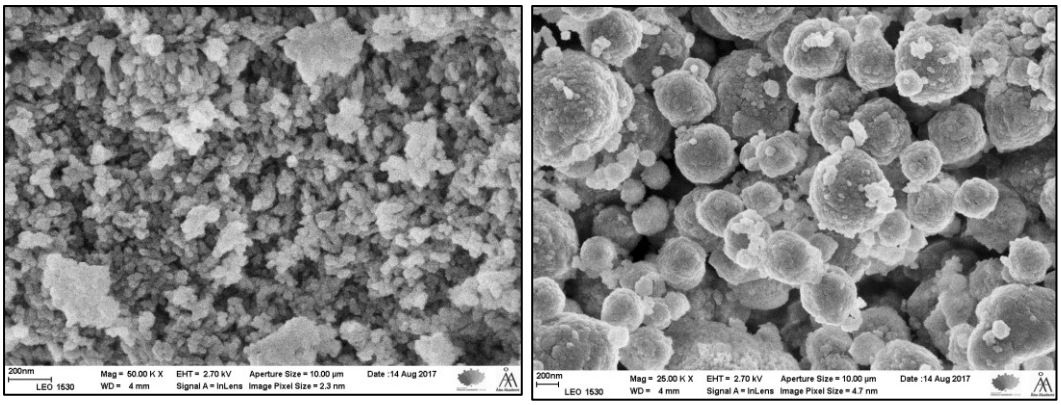

a b

Figure A2.1: Scanning electron micrographs for a. H-Beta-150 and b. H-Beta-300.

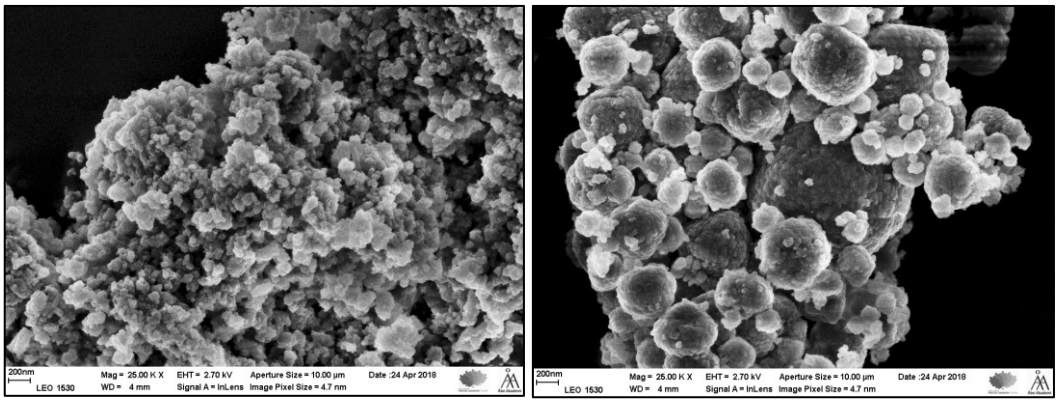

a b

Figure A2.2: Scanning electron micrographs for desilicated a. H-Beta-150 and b. H-Beta-300.

Appendix 3

Transmission electron microscopy for measurement of metal particle size.

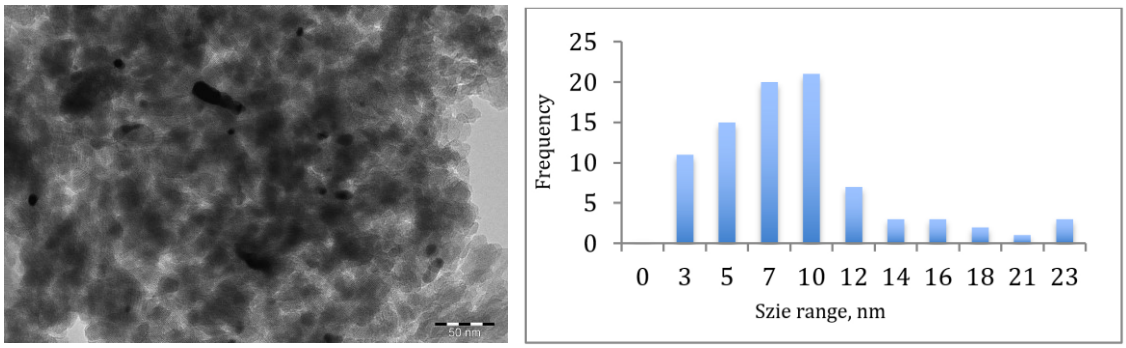

a b

Figure A3.1 (a): TEM image and

(b) Metal particle size distribution using histogram for 1 wt.% Ru/H-Beta-150.

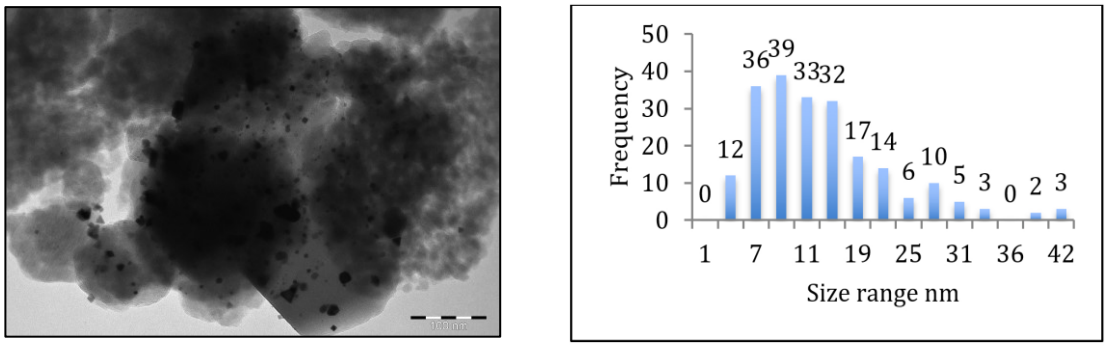

a b

Figure A3.2 (a): TEM image and

(b) Metal particle size distribution using histogram for 2 wt.% Pt-H-Beta-300.

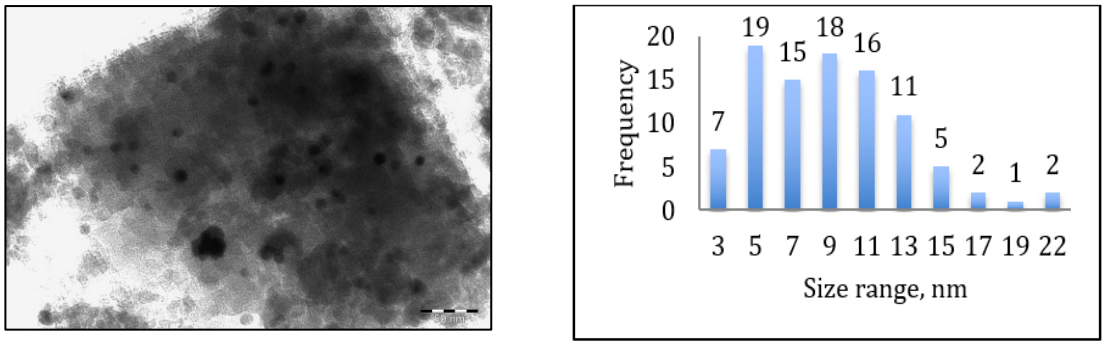

a b

Figure A3.3 (a): TEM image and

(b) Metal particle size distribution using histogram for 2.5 wt.% Ni-H-Beta-25.

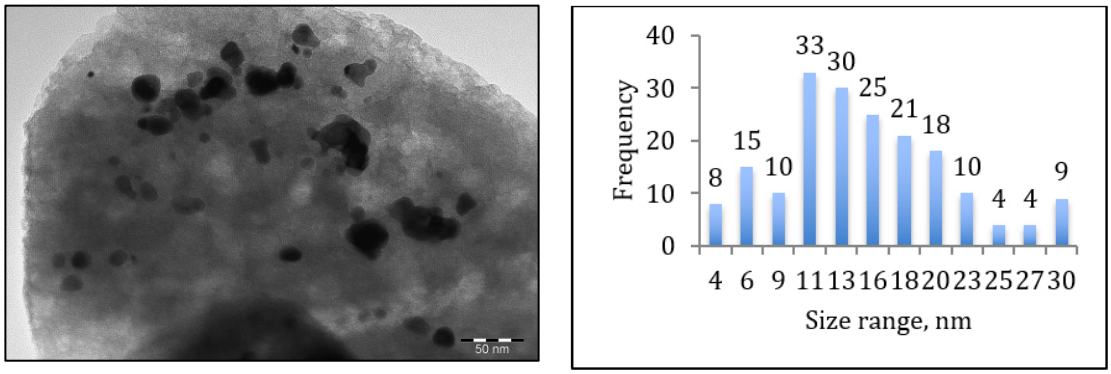

a b

Figure A3.4 (a): TEM image and

(b) Metal particle size distribution using histogram for 2.5 wt.% Ru-USY-15.

Appendix 4

Thermogravimetric analysis for determination of coke.

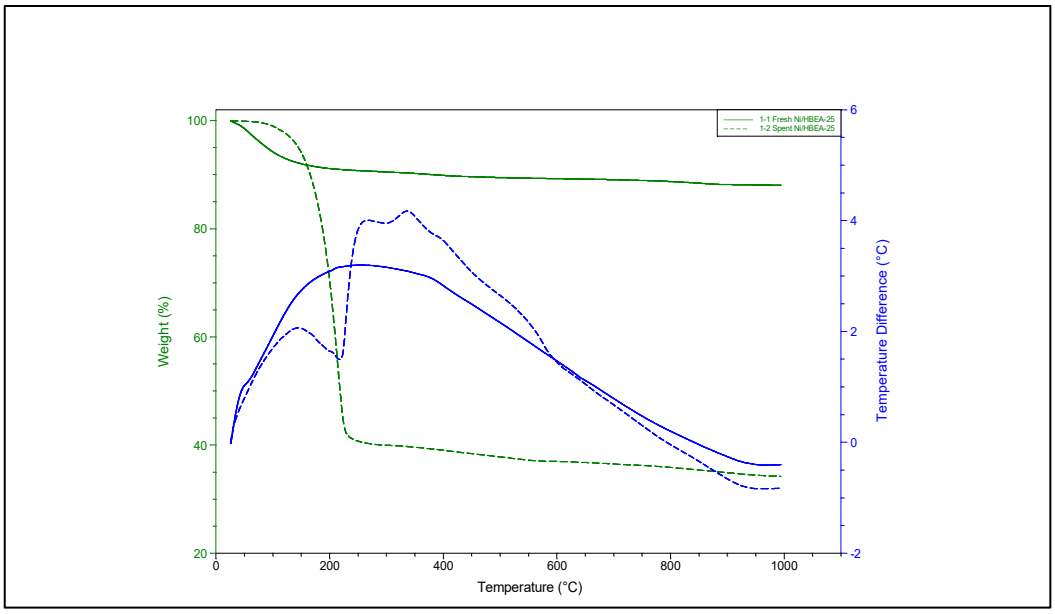

Figure A4.1: Derivative temperature difference (DTD) and weight loss for fresh and spent 5 wt.% Ni/H-Beta-25 catalyst.

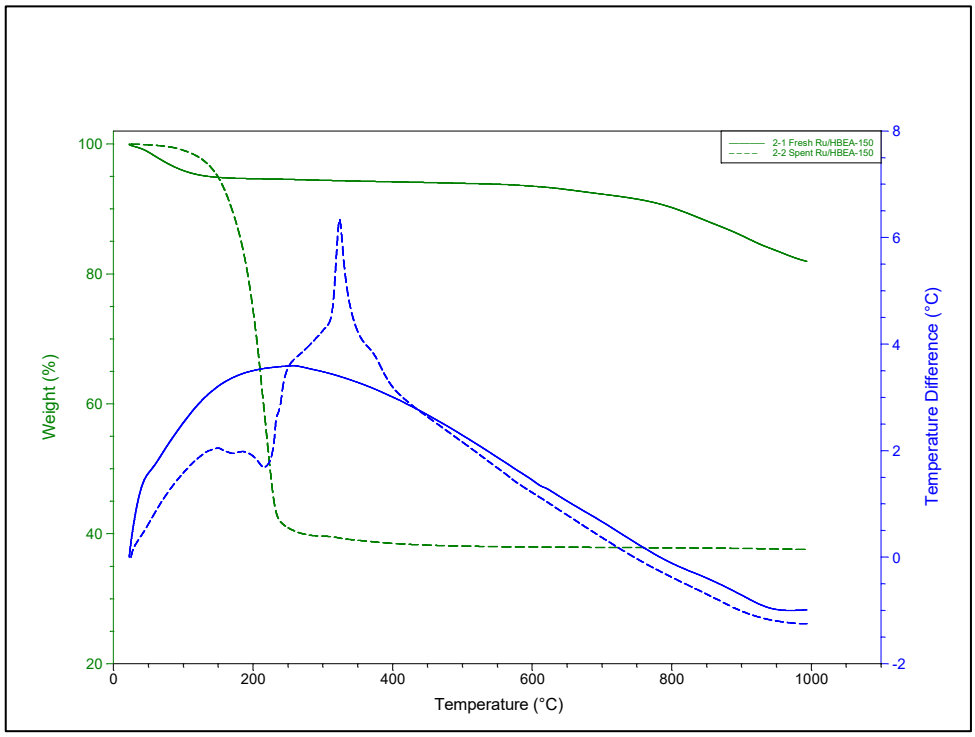

Figure A4.2: Derivative temperature difference (DTD) and weight loss for fresh and spent 1 wt.% Ru/H-Beta-150 catalyst.

Appendix 5

Size exclusion chromatography.

Calibration Curve and calibration curve table are displayed below.

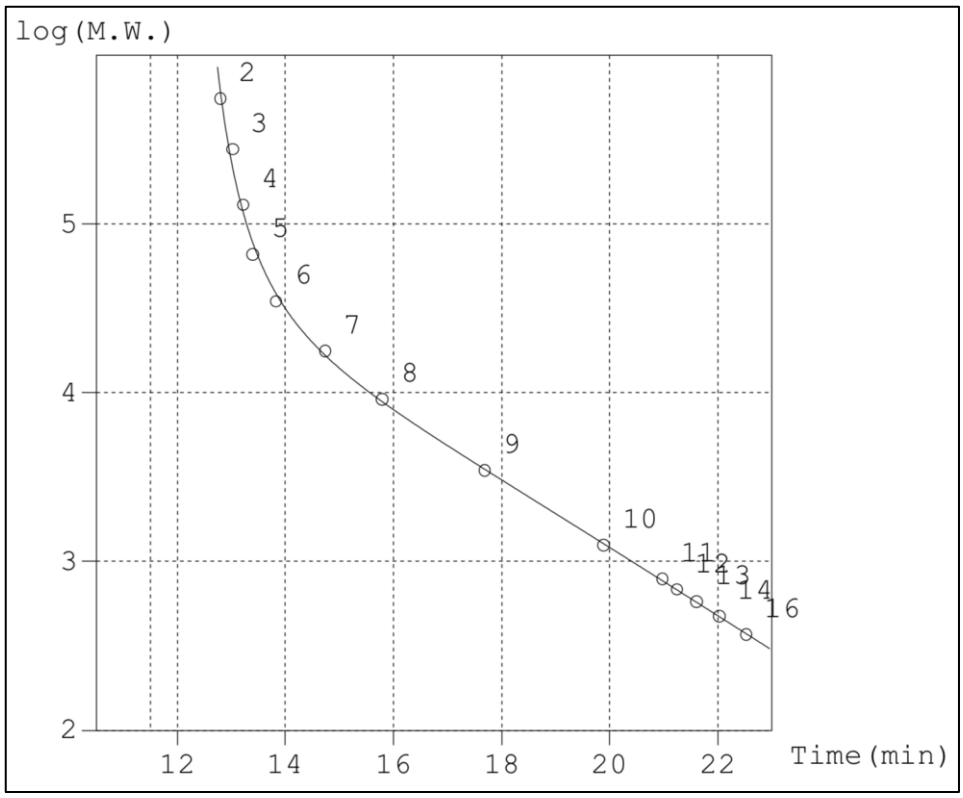

Figure A5.1: Standard curve of log molecular weight versus time.

Table A5.1: Calibration curve table.

	R.T(min)	Molecular Weight	Active	Virtual
1	11,980	2 520 000	OFF	OFF
2	12,790	552 000	ON	OFF
3	13,018	277 000	ON	OFF
4	13,221	130 000	ON	OFF
5	13,396	66 000	ON	OFF
6	13,825	34 800	ON	OFF
7	14,740	17 600	ON	OFF
8	15,792	9 130	ON	OFF
9	17,689	3 470	ON	OFF
10	19,893	1 250	ON	OFF
11	20,983	786	ON	OFF
12	21,250	682	ON	OFF
13	21,616	578	ON	OFF
14	22,032	474	ON	OFF
15	22,523	370	OFF	OFF
16	22,535	370	ON	OFF

Table A5.2: Retention times with molecular weight of coke via SEC for Desilicated H-Beta-150.

Desilicated-H-BETA-150		
Ret. time	**Molecular weight (g/mol)**	**Area (%)**
12.71	N.a.	39.2
19.2	1400	1.3
19.57	1300	1.6
19.91	1250	1.3
20.82	786	34.9
21.8	578	21.7

Table A5.3: Retention times with molecular weight of coke via SEC for Pt/alumina: H-Beta-300.

5 wt.% Pt/Alumina:H-BETA-300		
Ret. time	**Molecular weight (g/mol)**	**Area (%)**
14.33	N.a.	48.9
16.05	N.a.	3.2
20.32	900	2.7
21.06	682	5.7
21.85	500	39.5

Table A5.4: Retention times with molecular weight of coke via SEC for Ni/H-Beta-300.

5 wt.% Ni-H-BETA-25		
Ret. time	**Molecular weight (g/mol)**	**Area (%)**
13.39	N.a.	18.4
15.08	N.a.	3.6
19.74	1280	4.4
20.68	815	14.2
21.6	578	18.8
22	474	40.7

Table A5.5: Retention times with molecular weight of coke via SEC for Ru/USY-15.

5 wt.% Ru/USY-15		
Ret. time	**Molecular weight (g/mol)**	**Area (%)**
14.28	N.a.	49.1
19.2	1400	3.1
20.52	870	4.7
21.06	682	6.5
21.83	500	36.6

Appendix 6

Mass balance.

Table A7.1: Mass balance for all experiments.

Exp. no.	Reactant mass (g)	Reactant left after reaction (g)	Total samples (g)	Coke (CHNS) (g)*	Total reactant after exp.	Mass balance (%)
TR2	46.38	28.6	10.33	0.11	39.04	84.19
TR3	46.38	29.37	9.81	0.11	39.29	84.73
TR4	46.38	30.92	10.35	0.11	41.38	89.24
TR5	46.38	31.62	10.26	0.11	41.99	90.55
TR6	46.38	33.62	9.92	0.11	43.65	94.13
TR7	46.38	28.98	10.82	0.38	40.18	86.65
TR8	46.38	27.8	9.01	0.11	36.92	79.62
TR9	46.38	29.37	7.83	0.38	37.58	81.04
TR10	30.92	13.91	7.53	0.11	21.55	69.72
TR11	46.38	28.61	7.29	1.21	37.11	80.02
TR12	46.38	28.6	7.91	1.21	37.72	81.33
TR13	46.38	29.37	8.84	1.21	39.42	85.00
TR14	46.38	29.36	9.21	1.23	39.80	85.82
TR15	46.38	26.26	10.56	0.72	37.54	80.95
TR16	46.38	25.5	12.86	0.72	39.08	84.27
TR17	46.38	27.08	12.37	1.21	40.66	87.67
TR18	46.38	25.5	14.3	1.17	40.97	88.35
TR19	21.64	11.59	5.86	1.17	18.62	86.08

*The amount of coke was taken from the organic elemental analysis (Table 4.7), 6 samples were analyzed and results were interpolated for the other catalysts.

Appendix 7

Product yield.

Table A8.1: Yield of products over beta and bifunctional metal catalysts.

Exp. no.	Catalyst	Cracking HC* Yield (%)	Long-chain HC* yield (%)	Iso-C16 Yield (%)	Alkylated hexadecane yield (%)
TR2	H-BETA-25	0.61	0.25	0.14	0.23
TR3	H-BETA-150	0.06	0.17	0.16	0.23
TR4	H-BETA-300	0.30	0.10	0.12	0.23
TR5	2 wt.% Pt/H-BETA-25	0.03	0.32	1.94	0.23
TR6	1 wt.% Pt/H-BETA-300	0.09	0.10	0.07	0.24
TR7	5 wt.% Pt/Al2O3, H-BETA-25 (1:1)	0.21	0.14	0.11	0.24
TR8	H-BETA-300	1.10	0.38	0.29	0.21
TR9	5 wt.% Pt/Al2O3, H-BETA-300 (1:1)	0.63	0.09	0.04	0.24
TR10	H-BETA-300	0.56	0.41	0.34	0.21
TR11	5 wt.% Ni/H-BETA-25	0.02	0.45	0.52	0.24
TR12	5 wt.% Ni/H-BETA-150	0.00	0.11	0.55	0.23
TR13	5 wt.% Ni/H-BETA-300	0.02	0.11	0.08	0.22
TR14	1 wt.% Ru/H-BETA-150	0.13	0.44	0.38	0.09
TR15	H-BETA-150 (desilicated)	0.73	0.46	0.26	0.08
TR16	H-BETA-300 (desilicated)	0.00	0.27	0.10	2.47
TR17	5 wt.% Ni/H-BETA-25	0.82	1.18	1.08	0.08
TR18	5 wt.% Ru/USY-15	3.55	4.56	1.29	0.08
TR19	2,5 wt.% Ru/USY-30	0.84	1.43	0.38	0.08

*HC: Hydrocarbon

Appendix 8

Gas-phase analysis

The gas-phase analysis for the experiments, not mentioned in section 4.2, is displayed in Table A9.2.

Table A9.1. Retention times for the calibrated gas-phase products.

Compound	Retention time (min)
Methane	2
Carbon dioxide	2.5
Ethylene	3.6
Ethane	4.5
Propane	12.01
Iso-butane	14.60
n-butane	15.17

Table A9.2: Number of unidentified gas-phase hydrocarbons and total GC area percentage.

Catalyst	Number of unidentified peaks	The total area of in the GC analysis of the formed gaseous products normalized by catalyst mass
H-Beta-150	3	3722
H-Beta-300	6	26947
2 wt.% Pt/H-Beta-25	5	2670
5 wt.% Pt/Al2O3, H-Beta-300 (1:1 mass ratio)	5	3183
5 wt.% Ni/H-Beta-300	3	5204
5 wt.% Ni/H-Beta-25 (250 °C)	12	57241